Statistical Vibro-Acoustic Modelling of Nonlinear Systems with Applications in Vehicles

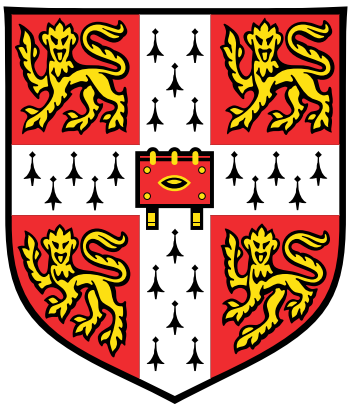

Luis Gilmour Andrade Acosta

Supervisor: Prof. Robin Langley

Advisor: Dr. Tore Butlin

Department of Engineering
University of Cambridge

This dissertation is submitted for the degree of
Doctor of Philosophy

Wolfson College

November 2019

Declaration

I hereby declare that except where specific reference is made to the work of others, the contents of this report are original and have not been submitted in whole or in part for consideration for any other degree or qualification in this, or any other university. This dissertation is my own work and contains nothing which is the outcome of work done in collaboration with others, except as specified in the text and Acknowledgements. Professor Langley supervised the entirety of this thesis and provided guidance at every stage. The work presented here is my own, although Profesor Langley played an integral part. This dissertation contains fewer than 65000 words including appendices, bibliography, footnotes, tables and equations and has fewer than 150 figures.

Luis Gilmour Andrade Acosta
November 2019

Abstract

Statistical Vibro-Acoustic Modelling of Nonlinear Systems with Applications in Vehicles

Designing quiet cars has become an important issue in the automotive industry, where passive and active noise control techniques can be employed to improve the acoustic comfort without compromising the vehicle performance. At the design stage of a noise control system, the estimation of the structure-borne sound pressure levels in the car cabin is a challenging problem, as uncertainties in a physical structural-acoustic system have an impact on the vehicle dynamics at high frequencies. Additionally, the response of the system can be affected by nonlinearities in the vibrations transmission path. Therefore, this research has been focused in developing computationally efficient vibro-acoustic models to predict the statistical structural-acoustic response of a system to random inputs, as well as analysing the degree of dependency of the response to nonlinear behaviour in the interface between the excitation and the structure.

Key aspects of the impact that a nonlinear transmission path might have in the response of a statistical structural-acoustic system, were investigated from an equivalent damper model of the structural vibrating subsystem, under the assumption of weak acoustic coupling and the infinite plate theory. Numerical data in the time domain were generated from the simplified nonlinear system excited by random inputs with known power spectral density. The effects of nonlinearities were observed and quantified in the power spectral density of the response, as well as in the reduction of coherence between the input and output. Additionally, the Wiener theory in the frequency domain has been explored to estimate the degree of contribution of a nonlinearity of second order to the total response of the system.

Finally, an extended hybrid Finite Element-Statistical Energy Analysis (FE-SEA) model was proposed to analyse the response of a deterministic-statistic structural-acoustic system, where the nonlinear transmission path is considered as a deterministic structure. The equations of an existing FE-SEA approach, based on the diffuse field reciprocity, have been generalised to include prescribed displacements as inputs, in addition to external forces. The nonlinear analysis with the FE-SEA approach has been carried out by adopting the concept of equivalent linearisation of the deterministic dynamic stiffness matrix, and the capability of the approach has been validated against experimental data from a physical nonlinear structural-acoustic setup.

Luis Gilmour Andrade Acosta

Acknowledgements

I am deeply indebted to my supervisor and mentor Professor Robin Langley, who has provided an immeasurable impact on my academic development as an early stage researcher. Many thanks also to Dr Tore Butlin, Matt de Brett and especial thanks to Dr Ole Nielsen from Bose Corporation, for the valuable discussions and advice during the development of this research project.

I would also like to express my gratitude to friends and fellows of Wolfson college where I felt at home and lived the full Cambridge experience, as well as to colleagues and friends of the Dynamics and Vibration Research Group for the valuable shared experiences during the tea and beer-time talks.

Finally, I would like to gratefully acknowledge the financial support from the National Secretariat of Higher Education, Science, Technology and Innovation of Ecuador (SENESCYT); under the scholarship programme "Universidades de Excelencia 2015" for doctoral studies at this prestigious institution as is the University of Cambridge.

To my darling, siblings, mum and particularly dad, whose motivation has made me dream with this goal since I was a kid. . . It is finally done!

Table of contents

List of figures

List of tables

Chapter 1

Introduction and Literature Review

1.1 Introduction

The noise levels inside of a car cabin has become an important concern for vehicle manufacturers, as passenger acoustic comfort is a demanding issue that has to be addressed without affecting the vehicle performance. Interior noise can arise from several sources that excite the structure and panels of the vehicle, and the vibrations are transmitted to the components that enclose the acoustic cavity, ultimately radiating acoustic energy to the cabin. Musser et al. (2011) have pointed out that low frequency noise is generated by the vibrations transmitted to the structure from the engine and the suspension system, whereas sources as wind noise are mostly related to higher frequency noise. Figure 1.1 illustrates the major noise sources in a vehicle.

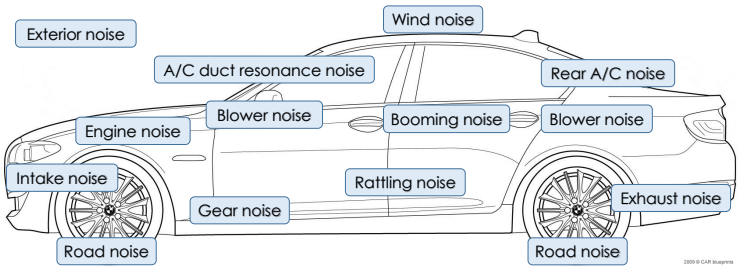

Fig. 1.1 Noise sources in a vehicle. [Blueprint taken from http://carblueprints.info]

In this matter, modelling techniques to understand the noise generation and transmission paths have been developed and improved over the years, with the purpose of addressing the acoustic comfort at the design stage (Genuit, 2004). The development of new materials and manufacturing techniques have been applied to attenuate the vibration levels by employing damped structures, sound barriers and absorbers (Fraser, 1998), intended to reduce the overall

interior noise to produce more quiet vehicles, improving the acoustic comfort of the driver and occupants (Steel et al., 2000). Nevertheless, it is notorious that an excessive effort to reduce the noise levels would increase the production costs, and might affect other aspects such as safety, economy and performance. Fraser (1998), for example, points out that the use of damping and sound absorbing materials has a direct impact in the increment of the vehicle weight. In fact, according to Ver and Beranek (2006), highly damped structures are needed to reduce noise from low frequency sources since the acoustic wavelengths are large, and therefore, the initial cost due to the material and fuel consumption is increased as well.

Hansen et al. (2012) suggest that acceptable noise reduction can be achieved for high frequency noise, above 500 Hz, with passive noise control (PNC), such as employing noise-isolating materials, however it may not be feasible to achieve an ideal acoustic comfort at lower frequencies below this range without compromising vehicle performance. Hence, other noise cancelling techniques have been subject of development over recent years. This is the case of the active noise control (ANC) that is intended to address the sound pressure levels (SPL) in the environment, rather than modifying the structure or the original design. The term "active" is referred to techniques that make use of a power source.

Active control requires information of the sound pressure levels and frequencies in the environment that is being controlled. In principle, this information can be obtained from measurements in the enclosed volume, however, a large number of sensors might be required to adequately reduce the noise levels (Nelson and Elliott, 1991). In addition, although current signal processors have a great capability for feed-back and feed-forward control applications, there is a limitation on the structural and acoustics characteristics of the problem.

The aim of this study is to develop a vibro-acoustic framework to explore the dynamics of the structural-acoustic system, i.e. the vehicle structure and the car cabin, in the noise generation due to external excitations, and the implications of the nature of transmission paths in the acoustic response of the system.

1.2 Methods in Vibro-Acoustic Modelling

Structure-borne noise inside the car cabin arises from the interaction between the acoustic medium and the structure that conforms the cabin. As a vehicle can be represented as a structural-acoustic dynamic system, it is expected that excitation forces arising from the engine, the interaction of the wind with the exterior panels or the contact of the wheels with the road; generate vibrations that are transmitted to all of the structural components of the vehicle, and ultimately radiate sound to the interior. Modal analysis and wave mechanics are

concepts in mechanical vibrations that allows to describe and model a structure-borne noise problem.

Analytical models can be developed to describe the dynamics of a single structural element or a built-up system from the equations of motion. The dynamic response can then be determined in the time or frequency domain, where the main task is to solve the eigenvalue problem in order to get information of the resonant frequencies in a modal analysis. Unfortunately, as Meirovitch (1975) points out, although the equations of motion can be derived, it might be usually impossible or not feasible to obtain solutions for the eigenvalues in vibro-acoustic analysis, since the vast majority of systems can have complex geometries or nonuniform mass or stiffness distributions. Therefore, several methods can be found in the literature to approximately estimate the response of continuous or discrete systems. The choice of the method to analyse a particular system depends mainly on its complexity, boundary conditions and range of frequencies. Common methods used for vibro-acoustics analysis are summarised in figure 1.2.

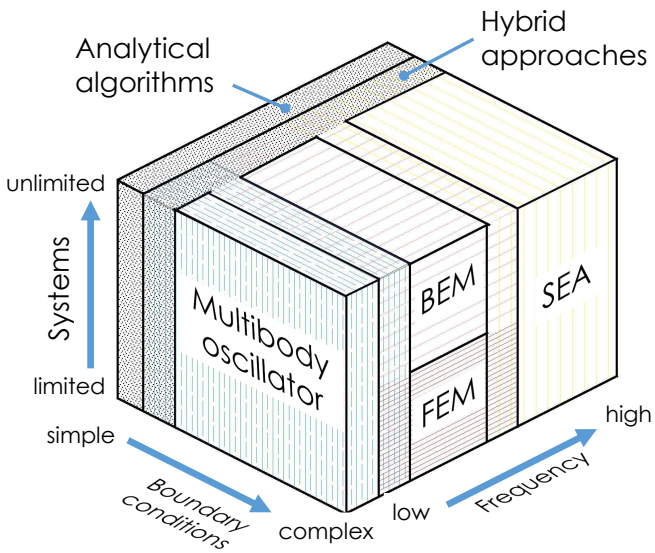

Fig. 1.2 Methods for Vibro-acoustic analysis. [Adapted from Fischer, M. (2006). Statistical energy analysis. Seminar: Vibrations and Structure-Borne Sound. TU München.]

Hambric et al. (2016) discuss the use of numerical techniques that can be employed in order to study the vibro-acoustics of complex systems, such as a vehicle, to predict the SPL in the car cabin. There are certain advantages and disadvantages in the use of one technique over another, depending on the frequency range of interest, but, as it can be appreciated in figure 1.2, the Finite Element (FE), Boundary Element (BE) and the Statistical Energy Analysis (SEA) are the most commonly used methods in vibro-acoustics as they perform with good accuracy in the acoustic frequency range for complex systems. The FE and BE

methods, for example, can be used to deal with interior and exterior structural-acoustic problems respectively, and are suitable tools to determine impedances or to model acoustic absorption of materials. However, these methods are deterministic and detailed information about the geometry and properties are required. In addition, Langley (1989) indicates that they are limited to the analysis at low frequencies, as for high frequencies they turn out to be prohibitively expensive, in terms of computing resources, due to the large number of degrees of freedom required to model the motion of short-wavelength acoustic waves.

As limitations are encountered in the use of the FE method to model the acoustic response of a large complex system as a vehicle, several authors have emphasized the importance of the use of the Statistical Energy Analysis (SEA) (see for example Lyon and DeJong (1995). SEA is a statistical standard tool that addresses the prediction of averaged vibrating energy in coupled structural and/or acoustic systems, being more applicable at higher frequencies (Musser et al., 2011). However, due to the deterministic nature of systems at low frequencies and the statistical behaviour at higher frequencies, inaccuracies are encountered when analysing a mid-range frequency problem. Shorter and Langley (2005a) have developed a general approach that combine the FE and SEA concepts into an hybrid method to analyse complex built-up systems, that are comprised by deterministic and statistical structures, and numerical, as well as experimental evidence has demonstrated the capability to implement this method in a vibro-acoustic model of a complex system.

1.2.1 Deterministic Methods for Vibro-Acoustics

As the performance of modern computers has been continuously increased, the use of the Finite Element method (FE) has been extended to analyse complex structures at a relatively high degree of accuracy. This is a displacement-based method that requires the internal forces to be in equilibrium and compatible with the displacements at each location in a discretised structure or system. These locations are known as nodes which have a certain number of degrees of freedom (DOF), up to six for a 3D system (Liu and Quek, 2013). If the boundary conditions and the excitation forces are known, the discretisation of the system can be performed by dividing the system into a finite number of small elements that are connected to each other through their nodes. The vector of static displacements $\mathbf{q}$ of a linear conservative systems due to an excitation force $\mathbf{F}$ can be found by the relation

$$\mathbf{Kq} = \mathbf{f} \tag{1.1}$$

where the stiffness matrix $\mathbf{K}$ has a dimension of $N \times N$, being N the number of DOF of the whole system, i.e. the number of nodes times the DOF of each node. On other hand,

for the dynamic response of linear systems, the matrix that relates the vector of forces and displacements is complex and is a function of the mass **M**, stiffness **K** and damping **B** matrices in the form.

$$\left[\mathbf{K} - \omega^2\mathbf{M} + i\omega\mathbf{B}\right]\mathbf{q} = \mathbf{f}, \tag{1.2}$$

where the terms in the brackets conform the dynamic stiffness matrix $\mathbf{D}_{\mathrm{d}}$. The FE method, therefore, can solve the eigenvalue problem arising from the matrix form of the equations that describe the motion of the system. It can be inferred then, that the higher the number of degrees of freedom, the more computer resources are needed to solve the eigenvalue problem.

The FE method is also applicable to analyse interior structure-borne due to the coupling between structural systems and acoustic cavities (Zienkiewicz et al., 2000), where both systems are discretised, however, the approach is not usually suitable for large room acoustic analysis. The Boundary Element method (BE) is an alternative approach to the the FE method for the analysis of dynamic acoustic responses, which is often applicable for large scale problems with unbounded domains. Both the FE and BE methods address to the numerical solution of partial differential equations, as is the case of the acoustic wave propagation problem.

It is known that the propagation of acoustic waves are due to the change of pressure of the medium at a frequency of the wave transmission. The frequency is associated to the "timbre" (the human hearing is normally in the range of 16 Hz to 16 kHz), whereas the "loudness" is characterised by the pressure level (Möser, 2009). As the rms sound pressure, p_{rms}, that the human hearing can stand is in the range of 2×10^{-5} to 200 Pa, a logarithm scale is commonly used to measure the sound pressure level SPL defined as

$$\mathrm{SPL} = 20\log_{10}\frac{p_{\mathrm{rms}}}{p_{\mathrm{ref}}}\ \mathrm{dB} \tag{1.3}$$

where p_{ref} is the hearing threshold, i.e. 2×10^{-5} Pa. For example, the interior sound pressure level inside a cabin of a sedan can vary from 45 dB at idle, to 75 dB at 140 km/h (www.auto-decibel-db.com). In a three dimensional acoustic volume, the wave equation of the fluctuating pressure, that can be numerically solved by an FE or BE approach,is given by

$$\nabla^2 p = \frac{1}{c_o}\frac{\partial^2 p}{\partial t^2} \tag{1.4}$$

where c_o is the wave speed in the medium. Considering the pressure as a complex function of time $p(x,y,z,t) = p(x,y,z)\exp(i\omega t)$, and defining the wave number as the ratio $\mathrm{k} = \omega/c_o$,

the wave equation yields

$$\left(\nabla^2 + \mathrm{k}^2\right) p(x,y,z) = 0 \tag{1.5}$$

which is known as the Helmholtz equation. A similar expression can be developed for wave motion in elastic solids. Atalla and Sgard (2015) indicates that the integral equations of problems associated with Helmoltz equation, constitute the basis of the BE method.

It is worth noting that range of pressure levels p are small compared to the average pressure of an acoustic volume of interest (for example, the atmospheric pressure at the sea level is 101.33 kPa). Other quantities, such as the variation of the medium density or the speed of particles are also small compared to the air density and speed of the acoustic wave (about 1.22 kg/m^3 and 340 m/s at the atmospheric pressure), respectively. Hence, those variations can be regarded as perturbations. In addition, the Helmholtz equation is linear in the pressure fluctuation range, and the operator ∇^2 is also a linear. Nelson and Elliott (1991) conclude that, as result of these linear characteristics, "the net pressure fluctuation in an acoustic medium is a result of the addition of different pressure levels at each position in the space". This is known as the superposition principle, which is the basis of active noise control techniques, that modify the current sound pressure level by "adding" another pressure fluctuation at different phase and/or amplitude.

1.2.2 Statistical Energy Analysis Approach

Despite the effectiveness of the FE and BE method to numerically estimate the response of a system at a relatively high degree of precision, Lyon and DeJong (1995) points out that it is not feasible to employ this approach when a system has been discretised in an extremely large DOF, due to the computational cost, i.e. a large amount of time is needed for the response to converge. In fact, Langley (1989) explains that for the analysis at high frequencies, an excessive number of DOF are required to model the short wavelength response, which is a common problem in structure-borne sound, and the analysis turns out to be time consuming and practically impossible to model real complex structures that might need hundreds or thousands of million DOF. In addition, experiments carried out by Bernhard (1996), for example, have shown that the frequency response function is sensitive to uncertainties that might arise from measurements, material properties, manufacturing techniques, slightly variation of geometries or environmental conditions, among others. In his work, the author has measured the pressure levels in a car cabin after an excitation force was applied in one of the front wheels of a vehicle. The experiment has been repeated 12 times in one particular

vehicle. Additionally, the same test has been performed in 98 nominally identical vehicles. Results of the measured acoustic pressure in the frequency domain are plotted in figure 1.3.

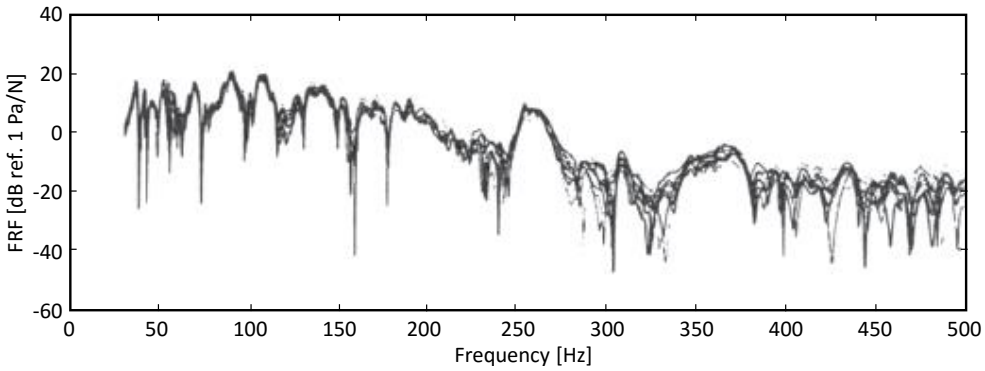

(a) FRF for 12 nominally identical tests in the same vehicle.

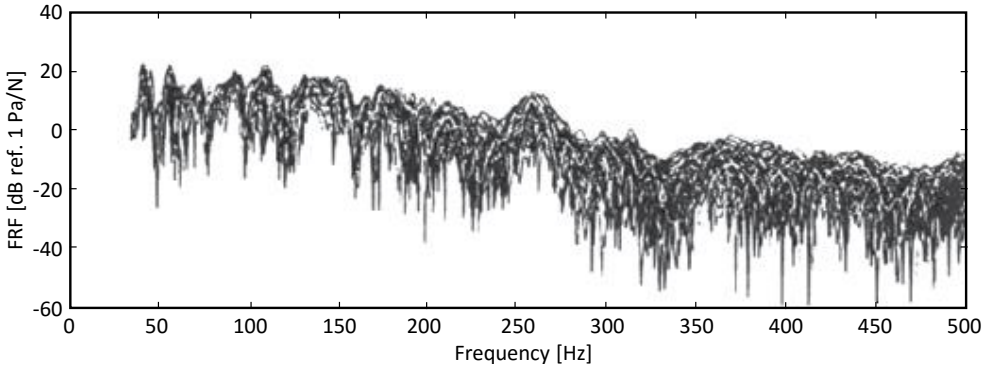

(b) FRF for a test repeated in 98 nominally identical vehicles.

Fig. 1.3 Frequency response function of the pressure levels in a car cabin to a point excitation force applied on the wheel. [Reproduced from Bernhard, R. (1996). The limits of the predictability due to manufacturing and environmentally induced uncertainty. In *Proceedings of InterNOISE*. INCE-USA]

It would have been expected that the same test performed in nominally identical vehicles and conditions would yield the same response, and each plot shown in figure 1.3 would superimpose each other, but it can be clearly seen that this is not true and, in fact, at higher frequencies the mismatch is even more notorious. Therefore, a method such as the FE is clearly not suitable for the analysis of complex systems at high frequencies, as the actual response is statistical rather that deterministic. In principle, a large number of FE simulations can be performed by randomly varying the input parameters and performing a Monte Carlo simulations to compute the statistical quantities such as mean and variance, but this process will be expensive in terms of computing cost and time consumption.

The Statistical Energy Analysis (SEA) overcomes with the impractical issues of deterministic methods, and allows to compute the averaged energy over an ensemble of nominally

identical systems, being particularly applied for random noise and vibration problems that are linked to the prediction of averaged sound pressure levels (Norton and Karczub, 2003).

1.2.3 Hybrid Approaches

A complex dynamic system can be viewed as an assembly of multiple subsystems coupled between each other where, the motion can be transmitted between two coupled subsystems through the coupling interface. Such subsystems can be either relatively rigid structures, flexible panels and/or acoustic cavities. It can be inferred that the nature of a complex system as a whole cannot be regarded as pure deterministic or pure statistic, and therefore it is not viable to adopt either pure FE or SEA approaches to accurately estimate the dynamic response of the system to external excitations. The analysis of complex deterministic-statistical systems is known as the mid-frequency problem, as described by Langley and Bremner (1999), where the response of the system is neither sufficiently random to be accurately modelled by an SEA method nor entirely deterministic to effectively adopt a pure FE approach.

The idea of merging the capability of deterministic and statistical approaches for vibro-acoustic analysis dates from nearly twenty years ago, where numerous works have been published to develop the idea of a hybrid FE-SEA method for analysis in the mid-frequency range. An important contribution to the this hybrid method to reliably estimate the mean response of a complex structure has been done by Shorter and Langley (2005a) and further validated numerically and experimentally by Cotoni et al. (2007). A key concept to combine a displacement-based with an energy-based approaches is the diffuse field reciprocity developed by Shorter and Langley (2005b), where the authors make use of the statistics of the equivalent reverberant force arising from wave reflections at random boundaries within the statistic subsystem. The equations for the FE-SEA method are derived by extending equation 1.2 to include the reverberant forces at the coordinates of the j^{th} statistical subsystem

$$\mathbf{D}_{\text{tot}}\mathbf{q} = \mathbf{f} + \sum_{j} \mathbf{f}_{\text{rev}} \tag{1.6}$$

where the total dynamic matrix is $\mathbf{D}_{\text{tot}}$ is the sum of the deterministic matrix and the direct field matrices of the statistical components. The set of hybrid FE-SEA equations are solved simultaneously for the SEA energy of the system and the displacement response at the deterministic set of coordinates $\mathbf{q}$.

There is a vast number of applications of the FE-SEA approach as it optimises the computation time by largely reducing the number of degrees of freedom. Regarding to the applicability to vibro-acoustics especifically, Chen et al. (2011) for example, have made use of the FE-SEA approach to estimate the noise pressure levels inside a car cabin with a

relatively high degree of accuracy, by defining statistic and deterministic subsystems in the form shown in figure 1.4, where the green areas, such as the roof panel, engine hood, etc.,are

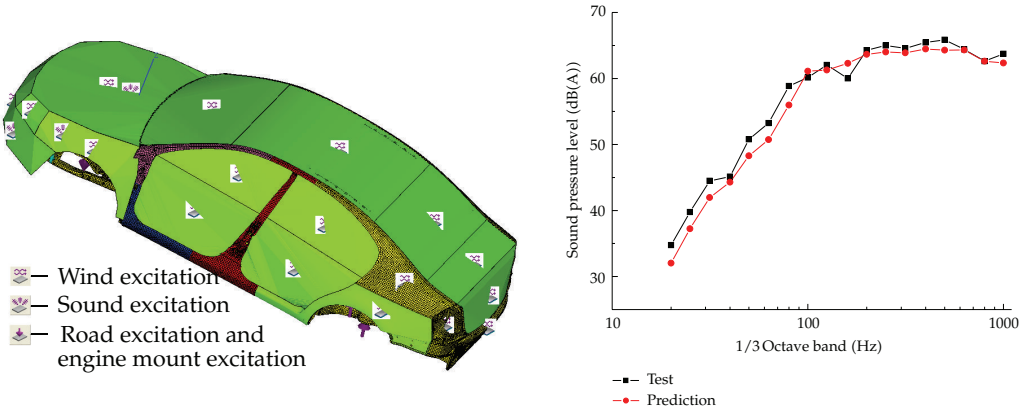

(a) CAD model. (b) Predicted and measured data.

Fig. 1.4 Sound pressure levels predicted by the hybrid FE-SEA approach. [Chen, S., Wang, D., and Zan, J. (2011). Interior noise prediction of the automobile based on hybrid fe-sea method. *Mathematical Problems in Engineering*, 2011.]

considered to be statistical components, whereas the relatively rigid frame is regarded as a deterministic structure.

The described approaches to model a complex vibro-acoustic system to estimate the dynamic response of its components are limited to linear structures, where parameters such as stiffness, damping, mass are assumed as constants and non-dependent on the response of the system. However, one of the aims of the present study is to understand at what degree a nonlinear behaviour in the vibrations transmission path affects, or otherwise, the dynamic response of the system, hence the approaches need to be improved to construct a vibro-acoustic model capable to consider nonlinearities within the components that comprise a complex subsystem.

1.2.4 Nonlinear Analysis

Most of the structure-borne problems are of linear nature, as well as the sound radiation phenomenon, however, invariant or non-constant material properties of the system might result in nonlinearities in the vibrations transmission path, which requires further analysis. Cremer and Heckl (2005) for example, illustrates this nonlinear behaviour linked to the fatigue phenomenon, and points out that long-time cyclic loading conditions produce some irreversible effects in the material, and therefore, it complicates the analysis. Nonlinear

stiffness or damping characteristics in the vibration transmission path might also influence in the response of the system, and the structure-borne noise generation.

Regarding to the road-vehicle interaction problem, nonlinear models of the suspension system, as a vibration transmission path, have been proposed by several authors, however they are addressed to frequencies below the acoustic range. Demir et al. (2012) indicates that nonlinear analysis in vehicle components are addressed to control design for driver and passengers comfort. Yung and Cole (2006) point out that components such as the damper in the suspension system, present a nonlinear behaviour as it has been observed that even low frequency motion can excite high frequency forces due to the nonlinearities, and a numerical model has been proposed to analyse the response of the system up to 500 Hz. Nevertheless, the model is addressed to nonlinear damping only, and very little can be found in the literature regarding to nonlinear analysis in the high frequency range for vibro-acoustic modelling.

As nonlinear damping and/or stiffness characteristics, as well as the dynamic response of a nonlinear system are dependent on the nature of the input, analytical models are not always available as the equations of motion might not have a known solution. The Duffing and the van der Pol oscillators are examples of systems with stiffness and damping nonlinearities, respectively, that have analytical solutions under certain circumstances. (Kovacic and Brennan, 2011).

The Wiener series, initially derived to analyse nonlinear systems in the time domain, have been subject of study for nearly half a century, as they are applicable to decompose the response of a nonlinear system as an orthogonal series expansion of contributions of first order, i.e. linear component, and further orders such as quadratic, cubic, etc., for white-noise inputs Schetzen (2006). Further studies, see Lee and Schetzen (1965) for example, have demonstrated that the Wiener series can be applied in the frequency domain for non-white noise Gaussian inputs. A more detailed study about the application of the Wiener theory is presented in Hawes (2016) thesis, where the author presents a generalised form of the Wiener kernels that allows to estimate the contribution of the power spectral density due to nonlinearities of n^{th} order.

For the analysis of complex systems with a computationally efficient vibro-acoustic model, the equivalent linearisation approach has been initially propossed by Krylov and Bogoliubov (1949) to analyse the response of weak nonlinear systems with harmonic inputs, and further developed by Caughey (1963) for random inputs. The method is based in the idea that a nonlinear system can be linearised by finding a function with constant stiffness and/or damping, provided that the error is minimised. Key nonlinear features such as generation of harmonics are not captured by this method, but it predicts with a high degree of accuracy, the mean square response of the system. In Demetriou (2018) thesis, the author has presented

and enhanced form of the equivalent linearisation method using a "single-pole fit function over the transfer function between the first Wiener kernel of the nonlinear force and the first Wiener kernel of the original system".

The capability of the numerical analysis in the time domain of a single-degree-of-freedom nonlinear system, as well as the Wiener theory and Equivalent linearisation in vibro-acoustic models, such as the hybrid FE-SEA method, have been used in the nonlinear analysis carried out in this research.

1.3 Scope of this Work and Thesis Outline

The description of the problem to be addressed in this research has been presented in this introductory chapter, as well as a review of several deterministic and statistical tools available for vibro-acoustic analysis. In the upcoming chapters, these techniques have been explored and improved to develop vibro-acoustic models for the analysis of nonlinear statistical complex systems.

Throughout this investigation, the phenomenon of structure-borne sound generation in a car cabin, has been isolated in a scaled linear statistical system comprised by a flexible structure and a coupled enclosed volume. This vibro-acoustic system is excited through a nonlinear interface by stochastic prescribed displacements, to emulate a nonlinear component of the vibrations transmission path. Key features of the dynamics of the system are explored from experimental measurements and from the developed computational models. This thesis can be briefly outlined as:

- **Chapter 2** - The theoretical background of the Statistical Energy Analysis (SEA) is presented, as well as the description of the vibro-acoustic model of a scaled system representing a structural panel and a car cabin of a vehicle. The SEA estimations are contrasted with experimental data of a randomised experimental rig. As a novel feature, it was experimentally demonstrated that the variance of the coupled structural-acoustic response of a randomised system can be predicted, with a high degree of accuracy, from the statistics of the Gaussian Orthogonal Ensemble (GOE) theory.

- **Chapter 3** - The description of a modified structural-acoustic system that includes a nonlinear device as interface between the excitation and the structure is presented. A simplified model based on an SEA approach is developed to analyse the influence of nonlinear stiffness in the structural response of the statistical system. Data in the time domain was generated from the developed model and contrasted with measurements taken in the experimental rig.

- **Chapter 4** - The Wiener series have been adopted to extract the contribution of the nonlinearity of second order to the response of the system in the frequency domain. The reconstruction of coherence from the contribution of the linear component and second order is described and illustrated from data gathered from simulations in the time domain.

- **Chapter 5** - A generalised form of a hybrid FE-SEA is approach is developed to include known displacements as inputs to a vibro-acoustic model of a complex system. The capability of the approach is explored and contrasted with data gathered from Monte Carlo simulations of a simple statistical-deterministic system.

- **Chapter 6** - A linear equivalent approach is adopted to linearise the determnistic dynamic stiffness matrix of a system, to extend the capability of the generalised hybrid FE-SEA method to include nonlinear deterministic subsystems within the complex structure. The model is validated against experimental measurements of the structural and acoustic responses of the test rig.

- **Chapter 7** - The major outcomes and findings of this research are summarised and presented in the conclusions, as well as suggestions for further work in this field.

Chapter 2

Linear SEA Modelling of a Structural-Acoustic System

2.1 Introduction

Key aspects of the structural and acoustic response of complex systems, as well as the analysis of the vibration transmission path can be explored by modelling isolated coupled substructures that represent global characteristics of a complex built-up system. A complete structure of a vehicle, including the acoustic medium in the car cabin, can be viewed as a complex system in the sense that it is comprised by a large number of deterministic components, such as the relatively rigid structures, as well as flexible panels that can have a statistical nature. Additionally, the rise of sound pressure levels inside the car cabin due to the vibrations of structural components that enclose the acoustic volume, i.e. structure-borne noise, is a consequence of vibrations being transmitted through susbystems, such as the suspension system, which adds more components to the detailed vibro-acoustic model of a vehicle. Nevertheless, several components and their characteristics can be identified as dominant in the noise generation phenomenon, and they can be studied in isolation to extrapolate the findings to the overall structure.

This investigation is firstly focused in developing a framework to analyse the arising of sound pressure levels in an enclosed volume due to vibrations of coupled structural subsystem. In this sense, a structural-acoustic subsystem of the car cabin can be isolated to explore its dynamic characteristics when excited with known inputs, and the dependence of the acoustic response to the structural vibrations can be studied from observations of a scaled experimental setup and a theoretical dynamic model of the system.

In this chapter, a Statistic Energy Analysis (SEA) approach is adopted to model a coupled structural-acoustic system to estimate the dynamic response of the structural component to a known excitation, as well as the acoustic response of the enclosed volume due to the coupling with the vibrating structure. Statistical quantities such as the mean response and variance estimated with the SEA model are validated against experimental data of a randomised scaled system. Besides the estimation of the mean dynamic response, the variance has been predicted from the statistics of the Gaussian Orthogonal Ensemble (GOE), and the experimental validation here presented is the first evidence that the GOE statistics accurately predicts the response variance of coupled random structural-acoustic systems. Results have been published in Andrade et al. (2019).

2.2 Overview and Theoretical Background of the Method

SEA is an energy-based method that requires a significantly lower number of equations, compared to deterministic approaches, since the variables are the averaged energies contained in each subsystem that comprises a built-up system, rather than the vast number of degrees of freedom of each of those subsystems. The total energy is the sum of potential and kinetic energies. As SEA considers that most of the energy in a system is due to resonant modes, potential and kinetic energies are equal in magnitude and therefore, the total SEA energy is twice the kinetic energy (Lyon and DeJong, 1995), which remains constant and invariant on time in the absence of damping[1]. However, it depends on the peak amplitude of vibration, and hence on the frequency. In addition, the predicted energy does not represent the actual energy contained in a system at a particular frequency, but rather the expected averaged value over an ensemble of nominally identical systems.

A built-up structure can be divided into several subsystems in order to determine the energy flow between each other. Such division should consider weak coupling between the subsystems in the sense that the natural frequencies of the coupled subsystem are practically the same as if it was uncoupled (Fahy and Gardonio, 2007). A more practical definition of weak coupling can be that the waves in a vibrating subsystem are weakly transmitted to the coupled subsystem. For example, consider the system comprised by two thin plates coupled by one of the common edges as shown in figure 2.1

In such system, the plate 1 is excited by a vertical force and its vibrational energy is due to the out-of-plane bending waves if no rotation along the edge is considered. If plate 2 is perpendicular to plate 1, the bending waves will transmit in-plane motion to plate 2, which

[1] Lyon and DeJong (1995) consider that the response of systems with a loss factor $\eta < 0.3$ can be regarded to have essentially the same response as if they were free damped.

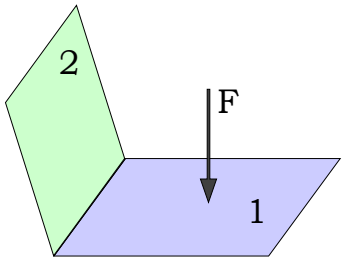

Fig. 2.1 Two thin plates perpendicularly coupled by the edge.

are weaker and therefore, this system can be divided into two weakly coupled subsystems. On the other hand, if both plates are horizontal, bending waves in plate 1 are transmitted to plate 2 in an out-of-plane motion, and the connection can be considered as strong coupling.

SEA is suitable to analyse the response at high frequencies since the response is more sensitive to uncertainties at such frequencies. This occurs when the dimensions of the subsystem are too large compared to the wavelength. On the other hand, if the dimensions of the system are comparable to the wavelength, then the motion is considered to be at low frequency and the system becomes deterministic. Fahy and Gardonio (2007) indicate that information about the transition between low to high frequencies can be obtained from the Frequency Response Function of the system (FRF). The plot shown in figure 2.2 represents the FRF of a flat plate subjected to harmonic excitation, where two zones have been distinguished and separated by the dashed line at about 580 Hz.

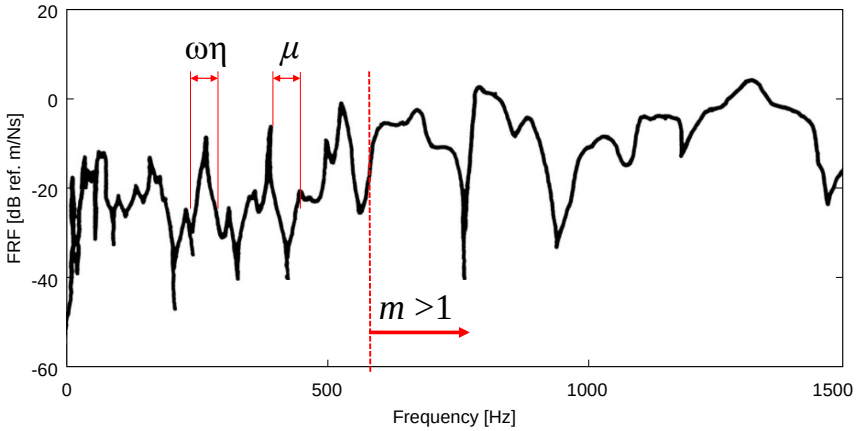

Fig. 2.2 Frequency response function of a thin flat plate [Adapted from Fahy, F. J. and Gardonio, P. (2007). *Sound and structural vibration: radiation, transmission and response*. Academic press.]

The peaks in the FRF plot correspond to the maximum amplitude at the corresponding resonant frequency. In figure 2.2 the zone on the left-hand side of the dashed line presents

sharp and well defined peaks, whereas on the right-hand side such peaks are softer or merged. The parameter that defines such transition is know as the modal overlap factor m, that compares the width of a peak, given by the product of the radial frequency and the loss factor $\omega\eta$, and the spacing of peaks μ. The inverse of the latter is the modal density n, that represents the averaged number of modes that exists in a band of frequency. The modal overlap factor can be defined as

$$m = \frac{\omega\eta}{\mu} = \omega\eta n \tag{2.1}$$

Bocquillet et al. (1999), indicates that it has been traditionally considered that the applicability of SEA requires a high modal overlap, i.e. $m > 1$, as this determines the high frequency range, but further research has shown that this is not a necessary condition. Langley and Cotoni (2004) have worked in the response variance of energy flow in coupled systems, and have found that the applicability of SEA relies in the degree of randomness of the system, characterised by the statistical overlap factor, S_n, introduced by Manohar and Keane (1994), and defined as

$$S_n = \frac{2\sigma_n}{\mu}, \tag{2.2}$$

where σ_n is the standard deviation of the n^{th} natural frequency, i.e. a measure of the randomness in an ensemble, and μ is the mean frequency spacing, as previously defined. The authors indicate that, depending on the type of loading, there is a value that S_n can take that determines the frequency beyond which the response is "stable" and not dominated by individual frequencies. It was shown that for uncoupled systems, smooth mean behaviour occurs at $S_n > 1$.

In general, Norton and Karczub (2003) has summarised the assumptions and criteria that a system or buit-up structure has to meet in order to have reliable results from SEA

1. The response is linear, i.e. constant stiffness and small amplitude of the vibrations.
2. The systems are resonant in the band frequency of analysis.
3. There is equipartition of energy between the resonant modes.
4. The principle of reciprocity applies.
5. The energy flow between coupled subsystems is proportional to the difference between the actual modal energies of each subsystems.

These criteria are adopted in the formulation of the SEA equation, to estimate the averaged energy from a power injection approach.

2.2.1 Formulation of the SEA Equation

A modal approach to derive the SEA equations from the energy exchange between two coupled oscillators can be found in Lyon and DeJong (1995). The oscillators, that represent two coupled subsystems, are considered to be linear, and viscously damped. The authors indicate that the rate of energy interchange between them is proportional to the difference of the vibrating energy contained in each subsystem. Woodhouse (1981) has pointed out that this relationship can be analogous to the thermal energy interchange due to the difference of temperatures between two coupled elements, where the constant of proportionality can be viewed as the thermal conductivity of the coupling element between these two subsystems. Such constant in the dynamical system is known as the power transfer coefficient, which is also dependent on the natural frequencies of the oscillators.

The motion of a subsystem is considered to be uncoupled to the motion of each other in the system. This assumption allows to represent the total energy flow between each coupled oscillator in a system as a sum of the energy interchanged between each pair of coupled oscillators, as long as the subsystems are weakly coupled in order minimise the effect of any correlation of motion between coupled subsystems. The rate of energy flow between two subsystems can be then expressed as

$$P_{jk} = h_{jk}\left[\frac{E_j}{n_j} - \frac{E_k}{n_k}\right], \tag{2.3}$$

where P_{jk} represent the rate of energy interchanged between the j$^{\text{th}}$ and the k$^{\text{th}}$ subsystems, $E_j/n_j - E_k/n_k$ is the difference of the averaged vibrating energies expressed in terms of the modes of uncoupled subsystems, i.e. modal energies; and h_{jk} is the modal-averaged power transfer coefficient. The latter parameter is employed here to stress the fact that the rate of energy flow is dependent on the coupling properties only, but the concept of coupling loss factor η_{jk} is more conventional in the use of SEA (Fahy, 1994), and can be related to h_{jk} as

$$h_{jk} = \omega \eta_{jk} n_j, \tag{2.4}$$

where n_j is the modal density of the j$^{\text{th}}$ subsystem, and ω the radial frequency. Due to the reciprocity, and from comparison of the equations 2.3 and 2.4, it can be concluded that $h_{jk} = h_{kj}$, where $h_{kj} = \omega \eta_{kj} n_k$ represents the coupling parameters of energy exchange from the k$^{\text{th}}$ to the j$^{\text{th}}$ subsystems.

In general, the SEA equation for the j$^{\text{th}}$ subsystem can be obtained from the power balance $P_{\text{in}} = P_{\text{out}}$. Considering that the total input power into a subsystem is both dissipated due to damping and interchanged between the coupled subsystems. The power balance for a built-up system can be then expressed as

$$P_j = \omega \eta_j E_j + \sum_k \omega \eta_{jk} n_j \left(\frac{E_j}{n_j} - \frac{E_k}{n_k} \right), \tag{2.5}$$

where the term $\omega \eta_j E_j$ express the rate at which the energy is dissipated, and the summation accounts for the energy rate interchanged between all the coupled subsystems. At a particular frequency, this rate is proportional to the energy contained in such subsystem, where the constant of proportionality is given by the loss factor η_j. The SEA equation 2.5 can be expressed in matrix form as $\mathbf{C}\hat{\mathbf{E}} = \mathbf{P}$, where the vector $\mathbf{P}$ contains the external power inputs into every subsystem, $\hat{\mathbf{E}}$ represents the modal energies, i.e. E_j/n_j and the entries of the SEA matrix $\mathbf{C}$ are

$$C_{jj} = \omega \left(\eta_j + \sum_{k \neq j} \eta_{jk} \right) n_j \quad \text{and} \tag{2.6}$$

$$C_{jk} = -\omega \eta_{jk} n_j, \quad \text{for } j \neq k. \tag{2.7}$$

The same expression can be derived from a diffuse wave field approach, where the coupling loss factors are computed from wave transmission coefficients. However, Langley (1989) explains that, due to the lack of rigour in the previous derivation, neither the modal nor the wave approach estimates the likely accuracy of SEA when applied to a more general complex system, and indicates that the SEA equation is a particular case of a more general power relation of a wide class of multi-coupled systems, that applies when the system is subjected to the conditions indicated in the previous section, particularly the weak-coupling assumption. In addition, it was explained that the method can also be applied to point-force excited systems, provided that the force is averaged over all the random possible point locations. Though the general model is not directly used in the SEA formulation, the theory developed is helpful to analyse higher degree statistics in random systems.

It is worth emphasising that SEA predicts the ensemble averaged energy of every subsystem that comprises a built-up system, where the loss factors, modal densities and the coupling loss factors are parameters that depend on the properties and geometries of the components, as well as the coupling characteristics. Hence, it is possible to compute the SEA parameters from a modal or wave approach, however, it might be required to perform a numerical analysis or experiments to measure such properties for more complex structures.

2.2.2 SEA Parameters

The SEA parameters are the terms in the SEA equation that depend on the physical properties and coupling characteristics of the subsystems. The physical quantities that are required to obtain such parameter are deterministic, i.e. depend on the precise formulation of the geometry and material properties. However, in SEA, these characteristics are considered to be an average over an ensemble. A more detailed explanation regarding the physical definition of such parameters is attempted in the upcoming subsections.

Loss factors

It is known that the dissipating characteristics in a mechanical oscillator can be described by the viscous damping coefficient b, when it is assumed that the resistive force is proportional to the velocity of the inertial element with mass m. However, in engineering applications that are analysed with the oscillator model, it is more useful to determine how resonant an oscillator is, i.e. how large is the rate of oscillations compared to the rate of energy losses (Smith, 2010). The parameter that measures this ratio is the quality factor Q, which can be defined as the quotient between the resonant frequency ω_n and the specific viscous damping coefficient, i.e.

$$Q = \frac{\omega_n}{b/m} \tag{2.8}$$

In SEA, the interest is rather to characterise how damped a system is, and therefore, the parameter known as loss factor η is employed and defined as the inverse of the quality factor. i.e. $\eta = 1/Q$. From the analysis of the equation of motion of an oscillator, it can be demonstrated that the loss factor is twice the damping ratio, that delimits when a system is underdamped or overdamped, and therefore, an oscillator with $\eta = 2$ can be deemed to be a critically damped oscillator.

As the level of damping in a structural component is dependant on the material properties and varies from mode to mode, Norton and Karczub (2003) point out that it has been considered that the loss factor is the major source of uncertainty in the response, and is a summation of the effects of dissipation through the structural component, dissipation by acoustic radiation and dissipation through the boundaries; where the latter can be neglected for rigidly coupled subsystems.

The loss factor can be determined from experimental data, and several authors have pointed out that the experiments, addressed to measure the dissipated energy, lead to estimate the total loss factor of a structure, i.e. structural and radiation losses. Therefore, in order to quantify the structural component of the loss factor, the experiments should be carried

out in vacuum conditions in an anechoic chamber. For lightweight structures, such as thin walled shells, honeycomb structures, etc., the radiation component is significant and cannot be neglected. However, when the environment is reverberant, the structure of analysis can be considered to be coupled to an acoustic cavity, and therefore, the radiation component becomes a coupling loss factor between a structure and an acoustic cavity (Fahy and Gardonio, 2007). Nevertheless, typical values of the structural component of loss factors of common materials can be found in the literature, whereas the radiating component can be computed from analytical expressions, such as

$$\eta_{\text{rad}} = \frac{\rho_o c_o \overline{\sigma}}{\omega \rho_s h} \tag{2.9}$$

where ρ_o and ρ_s are the fluid density and material density, respectively, h is the plate thickness, c_o is the speed of sound and $\overline{\sigma}$ is the radiation efficiency of the structure.

Modal Densities

The modal density is an important parameter that indicates the number of modes available to store of energy in a system in a frequency band (Lyon and DeJong, 1995), and can can be expressed as the derivative of the mode count with respect to the frequency, i.e.

$$n(\omega) = \frac{dN(\omega)}{d\omega}, \tag{2.10}$$

and therefore, it represents the rate at which the number of modes are expected to increase with the increasing frequency. Analytical expressions are available for simple regular systems, such as a beams, flat rectangular thin plates or cuboids to determine the natural frequencies, and therefore the number of modes in a frequency range. For more complicated systems, the mode count, and hence the modal density, can be obtained from experimental data or from numerical FE models. Alternatively, asymptotic expressions can be found in the literature to estimate the mode count and modal densities for structural systems and acoustic volumes, even though these expressions are limited to specific geometries and boundary conditions, they give and approximation of the modal density of real statistical subsystems.

To illustrate the derivation of modal density, consider a one-dimensional system that can transport axial, torsional and bending waves, and one particular wavelength λ can be associated to each mode. Figure 2.3, for example, represents the first three bending modes of a beam and the associated wave. Lyon and DeJong (1995) indicate that the mode count can

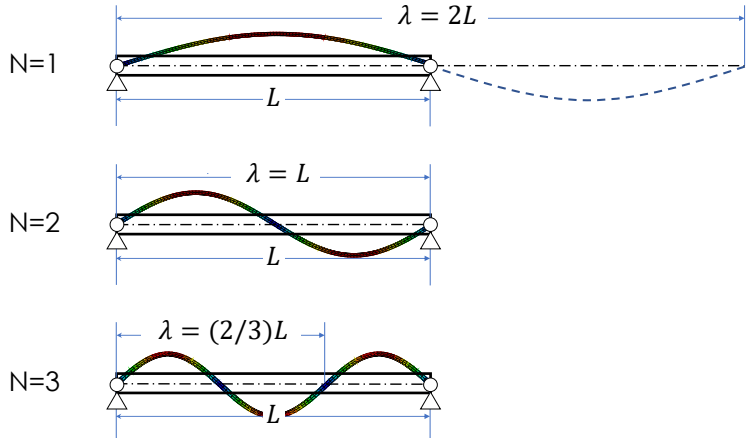

Fig. 2.3 Mode shapes of a beam pinned at both ends.

be directly associated to the wave number, defined as $\mathrm{k} = \frac{2\pi}{\lambda}$, in the form of

$$N(\mathrm{k}) = \frac{\mathrm{k}L}{\pi} \pm \delta_{BC} \tag{2.11}$$

where the constant δ_{BC} normally takes a value between 0 and 1 and takes into account the boundary conditions. In order to determine the modal density for this one-dimensional system, equation 2.11 is derived with respect to the frequency. The derivative of the wave number with respect to the frequency is the inverse of the group velocity c_g, that characterises the speed at which the energy of the wave travels, hence, the modal density of a one-dimensional structure can be expressed as

$$n(\omega) = \frac{L}{\pi c_g} \tag{2.12}$$

A similar approach can be followed in a two-dimensional system, such as membrane or a flat thin plate, that carries in-plane longitudinal and shear waves, as well as out-of-plane bending waves. Considering a rectangular structure, a wave number can be associated to each edge direction, and the mode count can be taken from the possible combinations of wave numbers below the frequency of interest. Lyon and DeJong (1995) demonstrate that the mode count of a two-dimensional structure can be approximated to

$$N(\omega) = \frac{A\mathrm{k}^2}{4\pi} + \Gamma_{BC} P, \tag{2.13}$$

where A is the area of the surface and P the perimeter. The parameter Γ_{BC} accounts for the boundary conditions. It is usually recommended to neglect this parameter for connected

subsystems as it is less significant as the frequency increases. Hence, the modal density can be obtained differentiating the expression 2.13, and can be expressed as

$$n(\omega) = \frac{A\omega}{2\pi c_\phi c_g}, \tag{2.14}$$

where the term c_ϕ represents the wave velocity[2], i.e. ω/k. In general, the group and wave velocities are equivalent, except for bending waves where the group velocity is twice the wave velocity. Expressions to compute the wave and group velocities in isotropic one and two-dimensional systems are given in table 2.1 as function of the Young's modulus E, Shear modulus G, Poisson's ratio ν, density ρ, area of the surface A, cross-section area S, polar moment of area I_p, second moment of area I, torsional moment of rigidity J and radius of gyration κ.

Table 2.1 Group velocities for various types of wave motion in one-dimensional systems.

Type of wave	One-dimensional		Two-dimensional	
	c_ϕ	c_g	c_ϕ	c_g
Axial waves (in-plane axial)	$\left(\frac{E}{\rho}\right)^{\frac{1}{2}}$	c_ϕ	$\left(\frac{E}{\rho(1-\nu^2)}\right)^{\frac{1}{2}}$	c_ϕ
Torsional waves (in-plane shear)	$\left(\frac{GJ}{\rho I_p}\right)^{\frac{1}{2}}$	c_ϕ	$\left(\frac{G}{\rho}\right)^{\frac{1}{2}}$	c_ϕ
Bending waves(out-of-plane bending)	$\omega^{\frac{1}{2}}\left(\frac{EI}{\rho S}\right)^{\frac{1}{4}}$	$2c_\phi$	$(\omega\kappa c_L)^{\frac{1}{2}}$	$2c_\phi$

The equation of the modal density can be applied with good accuracy to flat thin plates or slightly curved shells. For instance, the modal density of out-of-plane bending modes turns out to be independent on the frequency, however, it would not be useful for the analysis of curved structural elements, such as thin cylinders or curved shells. Lyon and DeJong (1995) indicate that approximate approaches can be followed to determine the mode count of curved shell from the equation of resonant frequencies. The authors explain that there is an "accumulation" of modes around a frequency in the curve of mode count against the frequency, that can be viewed in the modal density curve, that shows a peak at the ring

[2]The in-plane wave velocity of a two-dimensional system is usually denoted by c_L and known as longitudinal wave velocity.

frequency,

$$\omega_r = \frac{c_L}{r}, \tag{2.15}$$

where r is the radius of curvature of a simply sported cylinder. For frequencies above the ring frequency, the behaviour of the modal count is similar to the bending modes of a flat thin plate, i.e. the slope of the curve is constant and equals to the modal density of flat thin plates. Langley (1994) has worked on out-of-plane vibration modes of cylindrical and curved plates, and has developed expressions in terms of elliptical integrals for the computation of the mode count and modal densities of such structural elements.

For three-dimensional system such as and acoustic volume, the wave numbers associated to a resonant frequency of a prismatic volume can be expressed by

$$\mathrm{k}_{ijk} = \left[\left(\frac{i\pi}{L_1} \right)^2 + \left(\frac{j\pi}{L_2} \right)^2 + \left(\frac{k\pi}{L_3} \right)^2 \right]^{\frac{1}{2}}, \tag{2.16}$$

where L_1, L_2 and L_3 are the three dimensions that define the volume. Therefore, there are as many wave numbers as combinations of integers i, j and k exist. A modifying parameter should be also included to take into account the boundary conditions. If the longitude L_3 is reduced to zero, the expression can be used for a two-dimensional volume, and if further reducing L_2 to zero it can be employed for a one-dimensional system. The mode count of an acoustic volume can be then expressed as

$$N(\omega) = \frac{V\mathrm{k}^3}{6\pi^2} + \Gamma_1 A\mathrm{k}^2 + \Gamma_2 P\mathrm{k}, \tag{2.17}$$

where, V is the volume, A is the total surface of the volume and P is the perimeter (sum of the lengths of the edges). The criterion that states that for connected systems the parameters Γ_1 and Γ_2 are neglected applies. In general, the modal density of acoustic volumes has the form

$$n(\omega) = \frac{V\omega^2}{2\pi^2 c_o^3} + \frac{A\omega}{8\pi c_o^2} + \frac{P}{16\pi c_o}, \tag{2.18}$$

where, c_o is the speed of the sound in the acoustic medium. Several authors indicate that the second term of the right side of the previous expression is subtractive for open boundaries. In addition, at high frequencies, only the first term is employed as the other two can be neglected, which this is true for large acoustic rooms.

The expressions developed for one, two and three-dimensional structural or acoustical systems estimates the asymptotic or limiting cumulative mode count functions. Blevins

(2006) has found that such expressions give a good approximation at high frequencies, but there are discrepancies at lower frequencies, and has derived of a more general approach to determine the mode count for rectangular volumes, areas and lines. The procedure starts with the mode count of a three-dimensional acoustic volume, derived from the equation that accounts the possible combination of integer numbers that gives the resonant frequencies. The published results shows that the cumulative functions of the mode count of a system oscillates around the asymptotic function at low frequencies, and match the asymptotic mode count as the frequency increases.

Coupling loss factors

The coupling loss factors, η_{jk}, that appear in the SEA equation, are a measure the proportion of the energy that is transmitted between two systems. SEA requires that this parameters are positive quantities and non-dependant on the loss factors. Experimental or numerical procedures can be carried out to determine the coupling loss factors, though analytic expressions have been proposed following the wave transmission and mobility approaches (Totaro et al., 2009). Lyon and DeJong (1995) present the derivation of such expressions from a wave approach for point, line and area coupled systems, as illustrated in figure 2.4.

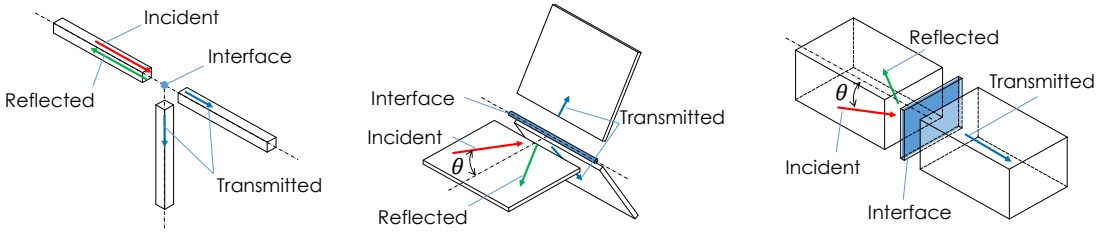

(a) Point coupling (b) Line coupling (c) Surface coupling

Fig. 2.4 Incident, transmitted and reflected waves in coupled systems. [Adapted from Shorter, P. and Cotoni, V. (2016). Statistical energy analysis. In Hambric, S. A., Sung, S. H., and Nefske, D. J., editors, *Engineering Vibroacoustic Analysis: Methods and Applications*, chapter 11, pages 339–383. John Wiley & Sons.]

If it is assumed that no energy is dissipated in the junction, a fraction of the incident power is transmitted to the coupled system, whereas the rest is reflected. The wave transmission coefficient τ_{jk} represents the ratio of the transmitted power to the k^{th} subsystem from the incident power of the j^{th} subsystem. The power transmitted in two and three-dimensional coupling, depends on the angle of incidence, and therefore, in order to compute the average coupling loss factor that accounts for all possible directions, the wave transmission coefficient

must be expressed in integral form for line and surface connections, respectively

$$\left\langle \tau_{jk} \right\rangle_{\text{line}} = \int_{-\pi/2}^{\pi/2} \tau_{jk}(\theta) \cos(\theta) d\theta \quad \text{and} \tag{2.19}$$

$$\left\langle \tau_{jk} \right\rangle_{\text{surface}} = \int_{-\pi/2}^{\pi/2} \tau_{jk}(\theta) \cos(\theta) |\sin(\theta)| d\theta, \tag{2.20}$$

where θ is the angle of incidence and the brackets $\langle\ \rangle$ indicate average over all possible directions of incidence. By balancing the power in the coupled subsystems, Lyon and DeJong (1995) have determined the expressions for the averaged coupling loss factors. Such expressions are presented in table 2.2, and have been derived by Langley (1990) following a wave approach from a more general definition of the SEA equation in terms of Green functions.

Table 2.2 Coupling loss factors as function of the wave transmission coefficient.

Type of coupling	η_{jk}
Point coupling	$\dfrac{c_{g_j}\tau_{jk}}{2\omega L_j}$
Line coupling	$\dfrac{c_{g_j} L \left\langle \tau_{jk} \right\rangle}{\pi\omega A_j}$
Surface coupling	$\dfrac{c_{g_j} A \left\langle \tau_{jk} \right\rangle}{4\omega V_j}$

For point coupled systems, it is known that the wave transmission coefficient can be expressed in terms of the impedances Z in the form of

$$\tau_{jk} = \frac{4\text{Re}\left\{Z_j\right\}\text{Re}\left\{Z_k\right\}}{|Z_j + Z_k|^2}, \tag{2.21}$$

where $\text{Re}\left\{Z_j\right\}$ is the real part of the impedance of the j$^{\text{th}}$ subsystem, likewise for the k$^{\text{th}}$ subsystem. Hence, the expression for the coupling between two point-coupled subsystems can be expressed as

$$\omega\eta_{jk} n_j(\omega) = \left(\frac{2}{\pi}\right) \frac{\text{Re}\left\{Z_j\right\}\text{Re}\left\{Z_k\right\}}{|Z_j + Z_k|^2}. \tag{2.22}$$

Analytical expressions for the impedances can be found in the literature depending on the geometry and type of wave motion (Cremer and Heckl, 2005). A more general derivation of the coupling loss factors has been developed by Shorter and Langley (2005b) from the relationship between the direct field radiation and the diffuse reverberant loading, as part of the framework of an hybrid FE-SEA approach for mid-frequency analysis, which is further explored in chapters 5 and 6 of this thesis.

2.2.3 Response Variance

When analysing the statistics of the energy response, besides the mean or averaged energies, it is of interest to determine the grade at which the system response deviates from the averaged energy. The useful statistical quantity that measures the dispersion of the random energy about its mean is the variance $\mathrm{Var}[E_j]$, which is the squared standard deviation and, according to Soong (2004), it is defined as the second central moment of the random variable as

$$\begin{aligned} \mathrm{Var}[E_j] &= \mathrm{E}\left[\left(E_j - \mathrm{E}\left[E_j\right]\right)^2\right] \\ &= \mathrm{E}\left[E_j^2\right] - \mathrm{E}\left[E_j\right]^2, \end{aligned} \tag{2.23}$$

hence, the variance of the response can be described as the expected value of the squared differences between the energy of the j^{th} subsystem, E_j, and the mean energy $\mathrm{E}[E_j]$, or the difference between the average of the squared energy and the mean energy squared.

As the SEA predicts the mean vibrational energy of a subsystem, it is of much interest to develop a framework to determine higher order statistics of a random system. Lyon and DeJong (1995) indicates four major effects that influence the deviation of the energy from one system of the ensemble to another. In summary, the variance is due to the spatial distribution of the sources of excitation, the variation on the number of resonant modes, fluctuation in the strength of coupling and the randomness of the position at which the response is measured.

Several authors have considered that the natural frequencies of a system conform a Poisson point process and have found that the results describe well the statistics at high frequencies, but for most systems they might be invalid. In two separate but correlated publications Langley and Brown (2004a,b) have employed the random point process theory and the assumption that the frequency spacing statistics have a Rayleigh distribution and conform a Gaussian Orthogonal Ensemble (GOE). Mehta (2004) defines the GOE as a particular type of random matrix that have the following characteristics:

- The matrix is symmetric

- The elements in the matrix are normally distributed (Gaussian) and statistically independent
- The off-diagonal elements have zero mean and same variance
- The diagonal elements have common mean and twice the variance of the off-diagonal elements

For the GOE to apply, Langley and Brown (2004a,b) have found that the system must not have symmetries, such as perfectly parallel edges. However, any imperfection in the shape or material will reduce these symmetries. In addition, the more random the system, the better the natural frequencies conform the GOE, since the statistical overlap can then occur.

Statistics of a single random system

Langley and Brown (2004b) point out that, although simple, the assumption that the frequencies follow a Poisson distribution leads to several inaccuracies, but there are enough numerical and experimental evidence supporting that the natural frequencies of physical systems conform the GOE statistics, and, surprisingly, this is true even though the random matrices that govern their behaviour have no obvious connection to the GOE. Concerning in the statistics of the kinetic energy T, the authors have developed the equation that describes the relative variance r_T^2, defined as the quotient between the variance $\mathrm{Var}[T]$ and the squared average $\mathrm{E}[T]^2$, as follows

$$\begin{aligned} r_T^2 &= \frac{\mathrm{Var}[T]}{\mathrm{E}[T]^2} \\ &= \frac{1}{\pi m}\left\{\alpha - 1 + \frac{1}{2\pi m}\left[1-\exp\left(-2\pi m\right)\right] + E_I\left(\pi m\right)\left[\cosh\left(\pi m\right) - \frac{1}{\pi m}\sinh\left(\pi m\right)\right]\right\}, \end{aligned} \tag{2.24}$$

where m is the modal overlap factor, i.e. $m = \omega\eta n$, E_I is the exponential integral, and the parameter α is a spatial factor that depends on the statistics of the the coefficient of the n^{th} term in the modal expansion of the response, a_n, which in turn depends on the corresponding mode shape and type of loading, i.e. point loading or rain-on-the-roof loading. For N_p incoherent point loads the spatial factor is determined as

$$\alpha = \frac{\mathrm{E}[a_n^2]}{\mathrm{E}[a_n]^2} = \frac{\mathrm{K}-2}{N_p} + 2 \tag{2.25}$$

where K depends on higher order statistics of the mode shapes. For Gaussian mode shapes this value is 3, however, numerical results have found that $\mathrm{K} = 2.75$ fits better for plate

systems (Langley and Brown, 2004b). It can be noted that for a single point load $\alpha = 2.75$, while at the limit $N_p \to \infty$, i.e. rain-on-the-roof load, $\alpha = 2$.

The previous analysis has been performed to determine the relative variance of the energy at a particular frequency. Langley and Brown (2004a) have extended the analysis to determine the statistics of band-averaged energy. They have employed the same GOE statistics determine the relative variance response, considering the kinetic energy averaged over a frequency band $[\omega - \Delta/2, \omega + \Delta/2]$, assuming that the loading is approximately constant over this band and $\Delta \ll \omega$. The authors have expressed the equation for the relative variance as

$$r_T^2(\omega,\Delta) = \frac{\alpha-1}{\pi m}\left(\frac{1}{B^2}\right)\left\{2B\left[\frac{\pi}{2} - \tan^{-1}\left(\frac{1}{B}\right)\right] - \ln\left(1+B^2\right)\right\} + \frac{1}{(\pi m)^2}\left(\frac{1}{B^2}\right)\ln\left(1+B^2\right), \tag{2.26}$$

where B is the bandwidth parameter defined as $B = \Delta/\omega\eta$. As this parameter tends to zero, the relative variance of the kinetic energy are then reduced approximated to

$$r_T^2(\omega) \approx (\alpha-1)/\pi m + 1/(\pi m)^2, \tag{2.27}$$

which is a reduced approximated expression of equation 2.24.

Statistics of a built-up random system

Langley and Cotoni (2004) have extended the analysis of the response variance of a single random system based on the GOE statistics employed in the previous section, in order to develop a straightforward procedure to determine the response variance of energy of each subsystem that comprise a built-up random system. The authors have considered that the energy predicted by SEA equation is the ensemble average of the band averaged total energy, which, for resonant systems, is twice the kinetic energy, i.e. $E_j = \left[2\overline{T}_j\right]$, where the overbar indicates that the quantity is band averaged. In addition, the input power of the SEA equation is considered to be the the ensemble average of the band averaged power input $P_{\text{in},j} = \left[2\overline{P}_j\right]$.

It was found also that there exists a matrix $\mathbf{D}$ that correlates the band averaged modal energy and the band averaged power input in the form of

$$\mathbf{D}\bar{\mathbf{E}} = \bar{\mathbf{P}} \tag{2.28}$$

and the ensemble averaged quantities of $\bar{\mathbf{E}}$ and $\bar{\mathbf{P}}$, i.e. $\mathrm{E}[\bar{\mathbf{E}}]$ and $\mathrm{E}[\bar{\mathbf{P}}]$, correspond to the modal energy and power input quantities of the matrix form of the SEA equation, respectively. For a random system, the matrix $\mathbf{D}$ and the band averaged power input $\bar{\mathbf{E}}$ are comprised by a

mean and a random components.

$$\bar{\mathbf{P}} = \mathbf{P}_{\text{in}} + \mathbf{P}_{\text{ran}} \tag{2.29}$$

$$\mathbf{D} = \mathbf{D}_o + \mathbf{D}_{\text{ran}}, \tag{2.30}$$

where $\mathbf{P}_{\text{in}}$ and $\mathbf{D}_o$ are ensemble averaged quantities, and $\mathbf{P}_{\text{ran}}$ and $\mathbf{D}_{\text{ran}}$ are their respective fluctuations. Further analysis considering that the product of this random fluctuations can be neglected, has led to conclude that the ensemble averaged $\mathbf{D}$ matrix corresponds to the $\mathbf{C}$ matrix of the SEA equation, i.e. $\mathbf{D}_o = \mathbf{C}$. Taking this equality into account, the main result of the analysis carried out by Langley and Cotoni (2004) is that the band averaged energy can be expressed in terms of the mean and fluctuations of the matrices $\bar{\mathbf{P}}$ and $\mathbf{D}$ as follows:

$$\bar{\mathbf{E}} - \hat{\mathbf{E}} = \mathbf{D}_o^{-1}\mathbf{P}_{\text{ran}} - \mathbf{D}_o^{-1}\mathbf{D}_{\text{ran}}\hat{\mathbf{E}}. \tag{2.31}$$

In order to develop an expression for the variance of the energy from equation 2.31, the authors have considered that the entries of the random fluctuations $\mathbf{P}_{\text{ran}}$ and $\mathbf{D}_{\text{ran}}$ are uncorrelated. Although they indicate that there is a certain dependence among the entries of $\mathbf{D}_{\text{ran}}$ in order to ensure that the total power dissipated due to damping is equals to the total input power. The equation for the variance of the band averaged energy is given as

$$\text{Var}\left[\overline{E_j}\right] = \sum_k \left(D_{o,jk}^{-1}\right)^2 \text{Var}\left[P_{\text{ran},k}\right] + \sum_k \sum_{s\neq k} \left[\left(D_{o,jk}^{-1} - D_{o,js}^{-1}\right)\hat{E}_s\right]^2 \text{Var}\left[D_{\text{ran},ks}\right]. \tag{2.32}$$

The quantities $D_{o,jk}^{-1}$ and $\hat{E}_s$ can be obtained from the SEA model and the energy estimation of the system, respectively, whereas the variance of the fluctuations P_{ran} and D_{ran} can be estimated by using the assumptions and results developed by Langley and Brown (2004a,b).

- Variance of input power P_{ran}

When considering the assumption of weak coupling between subsystems, Langley and Cotoni (2004) indicates that the input power is dominated by the "local dynamics" of the subsystem that receives this power. Therefore, the quantity $P_{k,\text{in}}$, that that appears in the SEA equation, is considered to be the mean power injected into the k$^{\text{th}}$ subsystem in isolation. As the equations developed by Langley and Brown (2004a,b) computes the relative variance, the actual variance of the input power can therefore be calculated by multiplying the relative standard deviation times the squared mean power, i.e.

$$\text{Var}\left[P_{\text{ran},k}\right] = P_{\text{in},k}^2 r^2\left(\alpha_k, m_k', B_k'\right), \tag{2.33}$$

where the apostrophe in the quantities that represent the modal overlap m'_k and bandwidth B'_k, indicates that those quantities are computed from the effective loss factor η'_k and, assuming weak coupling, this quantity can be determined from the SEA equation of a "single subsystem" where coupling terms that have a sub-index jk have been dismissed, and therefore only the diagonal entries of the SEA matrix are considered, and then, the effective loss factor has the form

$$\eta'_k = 1/\left(\omega n_k D^{-1}_{o,kk}\right), \tag{2.34}$$

hence, the parameters needed to determine the relative variance $r^2\left(\alpha_k, m'_k, B'_k\right)$ of the band averaged energy are given as

$$m'_k = \omega \eta'_k n' \tag{2.35}$$

$$B'_k = \Delta/\left(\omega \eta'_k\right). \tag{2.36}$$

It can be noted that, for the variance computed at a particular frequency, the band averaged parameter is zero, $B'_k = 0$. In addition, the parameter α_k depends on the type of loading, as described on the previous section.

- Variance of SEA matrix D_{ran}

The off-diagonal terms of the SEA matrix D_{rs}, are related to the energy transferred between the k$^{\text{th}}$ and the s$^{\text{th}}$ coupled subsystems arising from the boundary forces. Langley and Cotoni (2004) conclude that the input power to the k$^{\text{th}}$ subsystem from such boundary forces, has the form of the band-averaged kinetic energy, and therefore the variance of the random part of the SEA matrix is function of the relative variance developed by Langley and Brown (2004a,b) in the form of

$$\text{Var}\left[D^2_{\text{ran},ks}\right] = D^2_{o,ks} r^2(\alpha_{ks}, m'_k, B'_k), \tag{2.37}$$

where the terms m'_k and B'_k have been previously defined and α_{ks} depends of the coupling nature between subsystems, i.e. the force applied s to subsystem k and can be computed from

$$\alpha_{ks} = \frac{2\text{K} - 2}{N_p} + 2, \tag{2.38}$$

where N_p represents the number of coupling points. In the case where the subsystems are line-coupled or area-coupled, this parameters is equal to 2, assuming that the generalised force tends to be complex Gaussian (Langley and Cotoni, 2004).

2.2.4 Energy Density Variance

The extended SEA approach can be used to estimate the variance of the total energy contained in a subsystem, as part of a built-up structure. However, it is not always possible to directly measure the total vibrating energy in a system, as a large number of sensors placed in several locations within the subsystem is required, and therefore average the response over all the measuring points. Due to this limitation, it is of interest to estimate the variance of the energy density at a particular location, rather the total energy. This issue has been addressed by Cotoni et al. (2005), and an expression to calculate the relative variance at a point, r_ε^2, has been derived based on conditional probability in the form of

$$r_\varepsilon^2 = 1 + 2r_E^2, \tag{2.39}$$

where r_E^2 is the relative variance of the total energy. It is indicated that this result is an approximation only and the derivation is not rigorous, and more elaborated expressions can be found in the literature that consider the statistics of the mode shapes and the loading condition. However, the study carried out by Cotoni et al. (2005) suggests that the use of equation (2.39) gives a good approximation between the experiments and the predictions.

2.3 Design of the Experimental Rig

In principle, an SEA model can be developed for linear systems comprised by statistical subsystems, such as slender beams, thin panels, or acoustic volumes. In this study, in order to analyse key aspects of energy transmission, sound radiation and acoustic response; a scaled structural-acoustic model has been proposed to represent a vibrating structural panel of a vehicle and the acoustic car cavity.

The criteria to select the physical geometric characteristics, as well as the material properties of the components of the proposed test rig is based on the modal densities of a full-size car cabin and a large panel, such as the car roof panel, and the frequency range of interest. A rough approximation to establish the frequency below which there are as many acoustic modes in the scaled acoustic volume as there are below 500 Hz in a full-scale car cabin, is to consider the asymptotic formulas for acoustic modal densities in regular volumes. However, more accurate information can be obtained from an FE simulation by extracting the acoustic modes of a CAD model of a car cabin. Figure 2.5 shows the acoustic mode at 80 Hz and the 58^{th} mode found about 500 Hz.

In figure 2.6, there has been plotted the mode count from an FE analysis of both, the car cabin and the scaled acoustic box, whose larger edge is 40% the longitudinal dimension

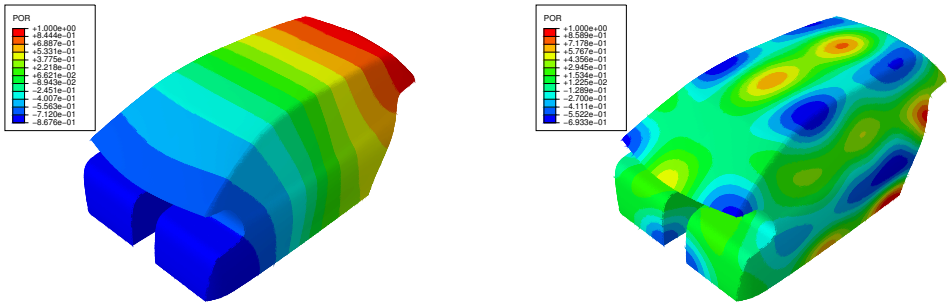

(a) First acoustic mode at 80 Hz. (b) Acoustic mode at 500 Hz.

Fig. 2.5 Acoustic modes of a car cabin from an FE simulation in ABAQUS.

of the car cabin. Additionally, there has been also plotted the asymptotic results of the approximated volumes of the physical systems.

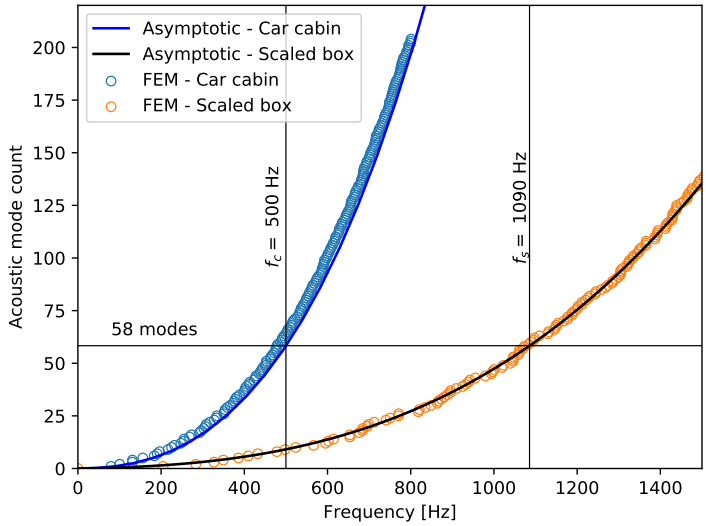

Fig. 2.6 Acoustic mode count of the car cabin and the scaled volume. Discrete blue: FE simulation of a car cabin; continuous blue: asymptotic equivalent of a car cabin; discrete orange: FE simulation of a scaled cavity; continuous black: asymptotic mode count of the scaled box.

It can be noted that the asymptotic estimation of the mode count is slightly underestimated for the full-size car cabin, but the agreement improves for the scaled acoustic box, which is expected as the scaled system has a regular shape.

From figure 2.6, it can be concluded that the proposed scaled model has 58 modes below 1090 Hz, i.e. the same number of modes of the car cabin below 500 Hz, which is the reference frequency to scale the structural component that represents the car roof panel.

An FE analysis has been also performed with a CAD model of a thin car roof panel to extract the number of structural modes below 500 Hz. The first and the 364th mode, found at about 500 Hz, of a roof panel with free edges a boundary conditions are shown in figure 2.7

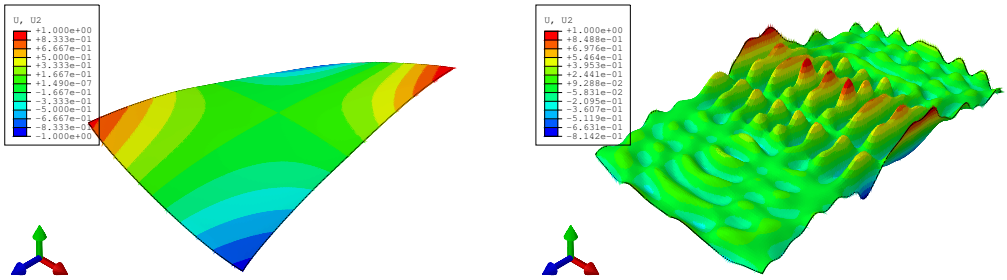

(a) First structural bending mode at 1.6 Hz. (b) Structural bending mode at 500 Hz.

Fig. 2.7 Structural bending modes of a roof panel from an FE simulation in ABAQUS.

The mode count of the full-size roof panel, as well as the asymptotic estimation of an equivalent flat thin plate are plotted on figure 2.8; Additionally, the mode count of an ideal plate that that the same number of modes below the scaled frequency, i.e. 1090 Hz, is represented by the red dashed line.

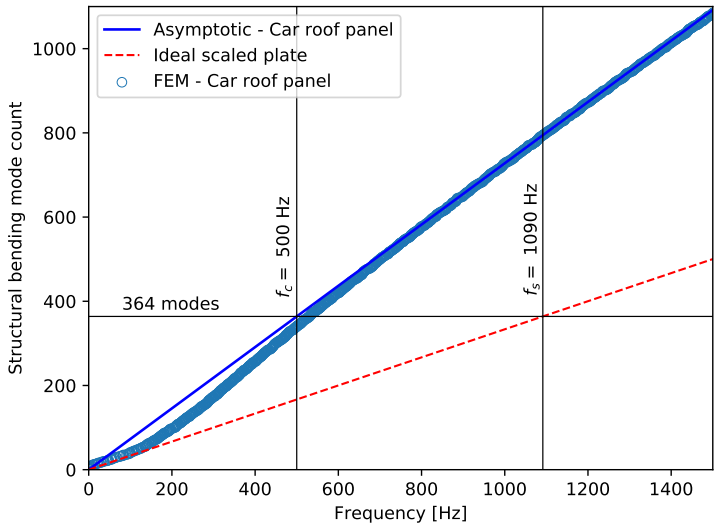

Fig. 2.8 Structural mode count of the roof panel and the scaled plate. Discrete blue: FE simulation of a car roof panel; continuous blue: asymptotic equivalent of a car roof panel; dashed red: ideal mode count of a scaled plate.

It can be noted in figure 2.8 that there is a good agreement between the mode count from the FE analysis and the equivalent asymptotic estimation at frequencies higher than about 600 Hz. The discrepancy at lower frequencies is found to be due to the curvature of the

full-size panel. Nevertheless, the slope of the curve, i.e. the modal density, is coincident to the asymptotic line, indicating that the roof panel can be approximated to a flat thin plate for the SEA analysis, and the modal density n_s of the ideal scaled structural subsystem of the rig can be represented by the slope of the red dashed line of figure 2.8. With this information, and the asymptotic formula given by equation 2.14, the material properties and dimensions can be found by satisfying the condition

$$n_s = \frac{A}{4\pi\kappa c_\phi}, \tag{2.40}$$

where the wave velocity c_ϕ is given in table 2.1, and the radius of gyration of a flat plate is $\kappa = h/\sqrt{12}$.

Finally, the structural subsystem can be randomised by fixing masses at random locations on the surface of the plate. Regarding to the acoustic cavity, rigid baffles can be also placed at random locations within the interior of the scaled acoustic cavity. A schematic representation of the external and internal view of the experimental rig are shown in figures 2.9 and 2.10, respectively. There is also shown the position of the instrumentation, such as accelerometers and a microphone, to measure the structural and acoustic response of the system, respectively, after the excitation by the force exerted by a hammer.

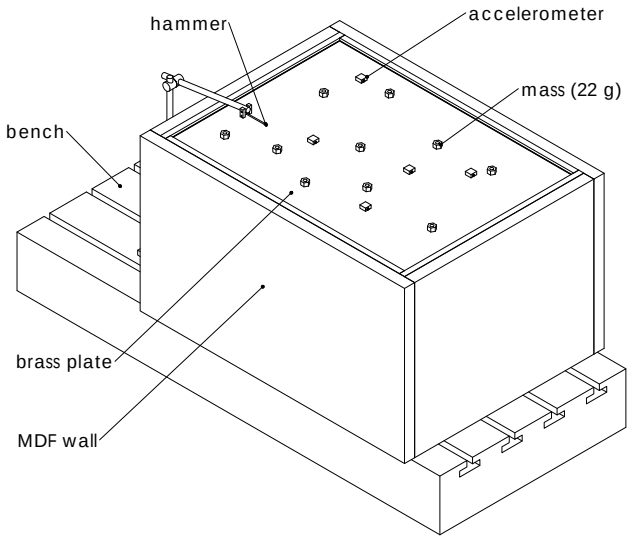

Fig. 2.9 Exterior view of the test rig.

The acoustic properties of the scaled volume, and the material properties and geometry of the plate and the walls that enclose the volume are shown in tables 2.3 and 2.4, respectively.

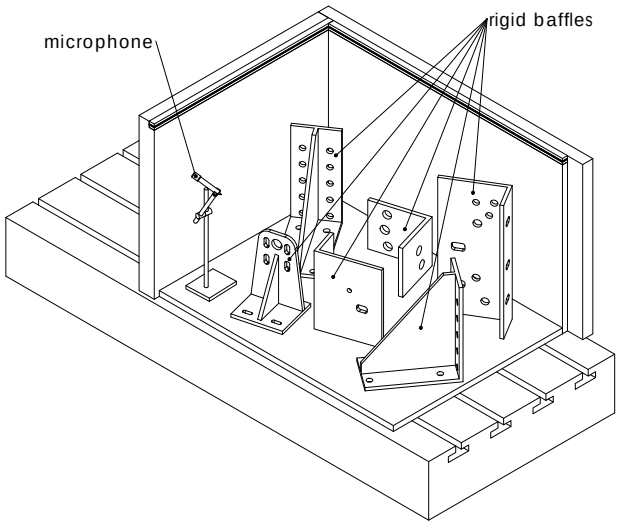

Fig. 2.10 Interior view of the acoustic cavity.

Table 2.3 Acoustic properties.

Medium	c_o [m/s]	ρ_o [kg/m^3]	V [m^3]
Air	343	1.225	0.26

Table 2.4 Structural properties.

Component	E [GPa]	ν	ρ [kg/m^3]	A [m^2]	h [mm]
Brass plate	105	0.346	8470	0.49	0.5
MDF walls	4	0.25	750	0.43 (larger wall) 0.31 (smaller wall)	54

2.4 SEA Modelling of the Structural-Acoustic System

The structural-acoustic system, comprised by the brass plate and the acoustic volume, can be modelled by an SEA approach, where the variables are the energies of such subsystems after the excitation due to a prescribed force. The physical experimental rig, however, is comprised also by four approximately rigid walls and the base, that, even though they can be considered to be deterministic components, their presence in the system might affect the response estimation as energy can be both dissipated and interchanged among these rigid

structures. Therefore, the SEA model here developed considers a system comprised by a flat thin plate, four rigid walls and a regular acoustic volume.[3]

The modal densities of the subsystems have been already estimated using the asymptotic formulas in the design stage of the test rig. Therefore, this section is focussed in the determination of the coupling loss factors, loss factors and power input to the system; from the material properties and the geometric configuration of the experimental setup.

2.4.1 Coupling Loss Factors

As the system is excited through the brass thin plate, the energy can be transferred to both, the rigid walls and to the acoustic cavity, i.e. structural and acoustic coupling, respectively, and the ration of energy transfer is characterised by the coupling loss factors. These parameters are frequency dependent and can be obtained from numerical simulations. In this study, however, analytical expressions are employed as the type of coupling, dimensions and material properties are known.

Line coupling

There are two types of line coupling between two subsystems within this built-up structure: the brass plate connected to an MDF wall at a right angle, and the connection between two vertical MDF walls, also at a right angle. The analytical expression for this type of connection is given in table 2.2, where the diffuse wave transmission coefficient $\langle \tau_{jk} \rangle$ can be found from the equations of motion on the coupling interface, as developed by Langley and Heron (1990).

A plate carrying bending waves can also transmit longitudinal and shear waves to the coupled plate depending on the properties of the connection. Likewise, if a system carries in-plane waves, they can generate out-opf-plane motion in the coupled structure, depending on the properties of the interface. In this analysis, however, it is only considered out-of-plane incident waves, i.e. bending waves on the plate. Figure 2.11 shows the computed wave transmission coefficients due to incident bending waves as function of frequency.

Bending, longitudinal and shear waves in a structural subsystem arise three components of the vibrating energy, i.e. one component for each type of wave, and therefore, each structural system contributes with three variables, i.e. modal energies, that must be computed simultaneously with the SEA equation, increasing the size of the $\mathbf{C}$ matrix. It is worth to mention that the contribution of shear and longitudinal waves to the total vibrating energy of a structural system is smaller than the contribution of bending waves, energy variables due

[3]The base of the system is placed on a rigid bench and, therefore, its dynamic influence is here neglected.

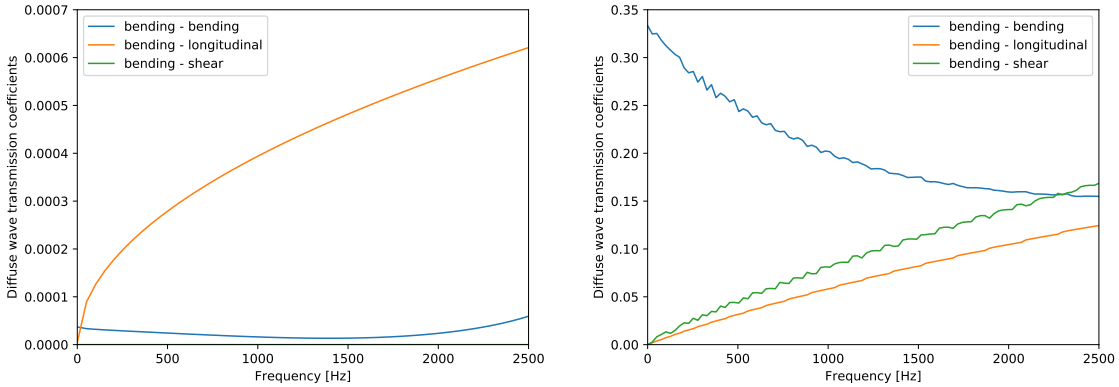

(a) Brass plate to MDF wall.

(b) Between two MDF walls.

Fig. 2.11 Diffuse wave transmission coefficients for right-angle connected plates due to bending waves. Blue: bending to bending; orange: bending to longitudinal; green: bending to shear. The small oscillation are due to the numerical integration procedure over less data points to reduce the computing time, and will not affect the overall SEA results.

in-plane motion are often neglected. In this model, however, the three types of waves were considered as the difference in computing time is not significant.

Acoustic coupling

It was pointed out that the energy in a structural system can be dissipated by structural damping and by acoustic radiation. As the system is coupled to an acoustic cavity, the latter type of loss factor becomes an acoustic coupling loss factor which can be estimated from equation 2.9 as function of the radiation efficiency $\overline{\sigma}$.

It is known that only bending waves can radiate to an acoustic medium, and the efficiency at which the plate radiates can be found from the contributions to radiated power of each mode. However, at higher frequencies, it is not usually feasible to compute the contribution of a vast number of modes of an acoustic cavity. Leppington et al. (1982) indicates that there exist a radiation sound field when the wave number of the acoustic medium k_a exceeds the acoustic number of an infinite plate, given by $(\mathrm{k}_x + \mathrm{k}_y)^{\frac{1}{2}}$ in the two-dimensional space. This condition is known as above coincidence, and the averaged radiation efficiency can be found as

$$\overline{\sigma} = \frac{\mathrm{k}_a}{\left(\mathrm{k}_a^2 - \mathrm{k}_x^2 - \mathrm{k}_y^2\right)^{\frac{1}{2}}}, \tag{2.41}$$

which asymptotically approximates to one. On the other hand, below the coincidence, there is an infinite plate does not radiate and a discontinuity exists at the coincidence condition.

However, the averaged radiation efficiency of a finite plate is a continuous function of the frequency given by

$$\overline{\sigma} = \frac{2}{\pi} \int_{0}^{(\pi/2)} \int_{C_n} G_n(\theta)\, \mathrm{d}\theta \mathrm{d}\phi, \tag{2.42}$$

where the integrands G_n and the limits C_n are functions of the regions of the plate wave numbers in a two-dimensional space defined by the angle θ, and given by equations (2.13) to (2.16) in Leppington et al. (1982). The authors have presented asymptotic equations derived from equation 2.42 for the the conditions below and near coincidence. It is found however that there is a discrepancy between the asymptotic formulas and the analytical solution at lower frequencies (below coincidence), therefore an improved numerical approach has been employed to consider regions that have been neglected in the original formulation of the asymptotic equations, to estimate the averaged radiation efficiency of the structural-acoustic system. Results of $\overline{\sigma}$ for the brass thin plate and the MDF walls are plotted in figure 2.12.

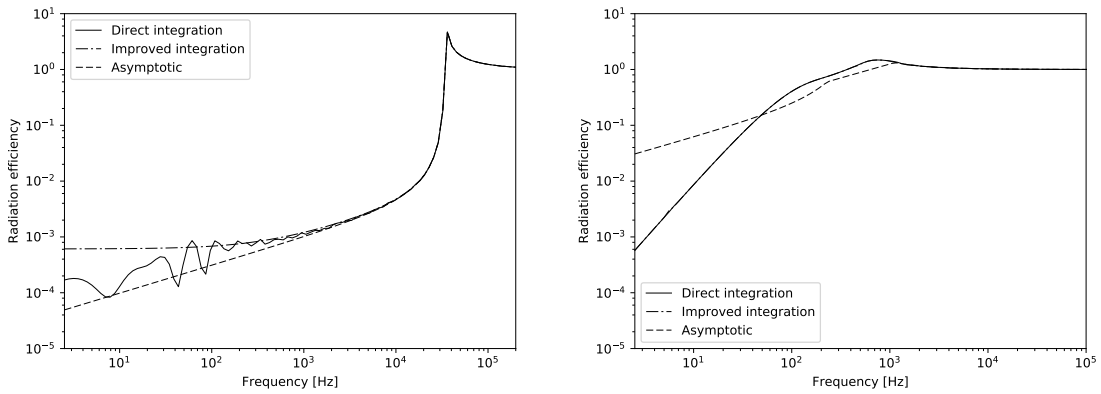

(a) Brass plate to the cavity.

(b) MDF wall to the cavity.

Fig. 2.12 Radiation efficiency to the scaled acoustic volume. Continuous: direct integration of radiation equation; dash-dotted: improved numerical integration; dashed: asymptotic formula. The solution from the improved approach is overlapped with the solution from the direct integration in figure (b).

In a further work, Leppington et al. (1984) have extended the theory to include the effect of constrained edges of the radiating plate, where the authors have pointed out that a correction factor of approximately 2 should be used below the coincidence condition only, as above the coincidence the plate behaves as an infinite structure. In this analysis, however, the initial formulation has been used without any correction due to boundary conditions.

2.4.2 Loss Factors

The vibrating energy that goes to each subsystem within the built-up system, either from the external input or from the coupling to another vibrating subsystem, is ultimately dissipated by the damping characteristics of the material. Nominal values of the loss factor are usually available in the literature. However, as additional masses and rigid baffles are added to the experimental rig, the characteristic of the system are modified and, therefore, the loss factor of each subsystem has been determined from experimental data.

Structural damping

Impact tests were performed on the isolated brass plate and MDF walls separately. The response after the excitation was measured by the accelerometers and the out-of-plane motion was recorded. Due to damping, the response of the system decays in time. A sonogram of a time domain data was created to visualise the decay of the spectrum in time. As the decay is associated with the damping of the structure, the logarithmic decay of the waves at each frequency was analysed to extract the equivalent loss factor. The sonogram of a time domain signal of a single test performed on a randomised plate, as well as the structural loss factor of the structural subsystems are shown in figure 2.13.

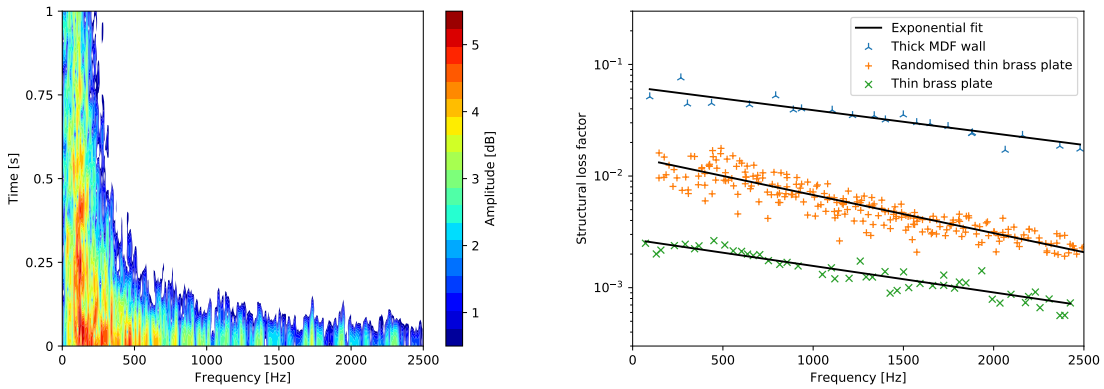

(a) Sonogram. (b) Experimental data.

Fig. 2.13 Structural loss factors obtained by measuring the wave decay in a sonogram after an impact test.

It is visible in figure 2.13a that the waves at higher frequencies decay faster than the waves at lower frequencies. However, as shown in figure 2.13b, the loss factor is lower at higher frequencies. This is expected as higher frequency waves decay from lower amplitudes than low frequency waves. Additionally, it is concluded that the structural loss factor can be

fitted to an exponential law in the frequency domain, and the randomised plate has a higher loss factor due to the attachment interface between the plate and the random masses.

Acoustic damping

The loss factor of the acoustic cavity can be also extracted form the wave decays plotted on a sonogram. In order to isolate the acoustic subsystem, the air volume has been enclosed by rigid walls, i.e. the brass plate of the system has been replaced by a rigid panel. However, the data obtained were not reliable in a broad frequency band, mainly since at higher frequencies the amplitude of the associated waves is masked by background noise. Alternatively, the acoustic cavity was excited by a pure tone signal produced by a small speaker placed inside the cavity. The time domain data were recorded by the microphone inside, from when the acoustic signal stops to when the signal has decayed to the background noise amplitude. An example of a sonogram of a decaying pure tone signal at 209 Hz is shown in figure 2.14a, whereas figure 2.14b shows the extracted loss factors at each frequency tested.

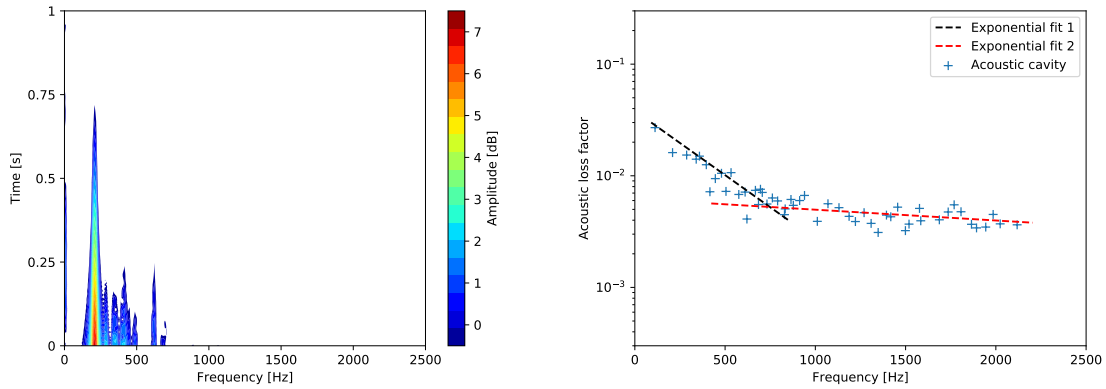

(a) Sonogram

(b) Experimental data.

Fig. 2.14 Acoustic loss factors obtained by measuring the wave decay in a sonogram at resonance frequencies after pure tone excitations.

It can be noted that the acoustic loss factor has two tendencies. At lower frequencies the loss factor is more dependent on the frequency than at higher, as it decays by a factor of ten up to 650 Hz, and a by a factor of two up to 2.5 kHz. A continuous function of the acoustic loss factor, if needed, can be obtained by fitting the data to a polynomial function. In any case, the acoustic loss factor seems to be in the same order of magnitude as the structural loss factor of the randomised brass thin plate.

2.4.3 Power Input

The power input to the system is given by the external force exerted by the hammer on the brass thin plate. Thus, the force is a point-type that excites out-of-plane motion. An expression to express the power input in the frequency domain is given by Norton and Karczub (2003) in the form

$$P_{\text{in}} = \frac{1}{2} |F|^2 \,\text{Re}\left\{Y_{\text{p}}\right\}, \tag{2.43}$$

where $|F|^2$ is the modulus squared of the complex force in the frequency domain and $\text{Re}\left\{Y_{\text{p}}\right\}$ is the real part of the mechanical mobility of the plate. Since bending motion is the main concern in this analysis, Cremer and Heckl (2005) point out that the mechanical mobility of an infinite flat thin plate in out-of-plane motion is real and equals to the inverse point impedance of the plate, i.e. $\text{Re}\left\{Y_{\text{p}}\right\} = 1/Z_p$, which is given by

$$Z_p = \frac{8\rho h^2 c_\phi}{\sqrt{12}}, \tag{2.44}$$

where h is the plate thickness, ρ is the density , and c_ϕ is the previously defined longitudinal wave velocity on the plate.

2.4.4 Dynamic Quantities

An SEA model is intended to estimate the averaged vibrating energy on the subsystem, but it is usually more useful to express this information in terms of dynamic quantities, such as velocity or pressure levels for structural and acoustic subsystems, respectively. In these forms, it can be possible to compare the predicted SEA response to measured data from accelerometers or microphones in the system.

In the frequency domain, the ensemble averaged squared velocity, $\left|v_{\text{SEA},j}\right|^2$, is proportional to the mean energy and expressed as

$$\left|v_{\text{SEA},j}\right|^2 = \frac{2E_j}{M_j}, \tag{2.45}$$

where E_j and M_j are the predicted ensemble averaged energy and the mass of the j^{th} subsystem, respectively. The factor of 2 of the right-hand side of equation 2.45 is omitted if the velocity $v_{\text{SEA},j}$ is expressed as RMS. If the SEA energy is estimated for a unitary input force, the modulus squared of the velocity in equation (2.45) represents the modulus square

mobility transfer function, i.e. modulus squared velocity per unit force.

For acoustic volumes, the SEA energy can be used to estimate the averaged sound pressure levels in terms of the acoustic properties of the cavity. Lyon and DeJong (1995) indicate that the estimated averaged squared sound pressure levels $\left|p_{\text{SEA},k}\right|^2$ of the can be calculated as

$$\left|p_{\text{SEA},k}\right|^2 = \frac{E_k \rho_o c_o^2}{V_k}, \tag{2.46}$$

where ρ_o, c_o, V_k and E_k are the air density, speed of sound, volume and SEA energy, respectively, of the the k$^{\text{th}}$ acoustic subsystem. Likewise to equation (2.45), the modulus squared pressure in equation (2.46) can be viewed as the force-pressure transfer function for a unitary force input.

2.5 Experimental Validation

In order to experimentally validate the SEA model, a large ensemble of nominally identical tests need to be performed on the test rig. Each individual test consists on exciting the system by an instrumented small hammer at a defined point on the plate, with a particular distribution of the small masses and the rigid baffles on the plate and the acoustic cavity, respectively. The out-of-plane response on the brass and the acoustic sound levels were measured by the accelerometers and a microphone, respectively, and recorded during 0.4 s from the instant at which the hammer exerts force on the plate. Due to the linearity of the system, the Fourier transform of the signals are independent on the length of the recording. Therefore, the steady-state SEA approach is justified.

The experimental data has been expressed in terms of velocity rather than acceleration, since the squared velocity is directly proportional to the energy. The complex force-velocity transfer functions can be computed from the acceleration-force cross-spectrum, S_{af}, and force auto-spectrum, S_{ff}. It was found that the mass of the accelerometer affects the measurements of the response of the flexible system due to its impedance. Therefore a correction factor C_z that accounts for the effect of the local impedance is applied. The squared modulus of the force-velocity transfer function of the brass plate is evaluated as

$$\mathrm{E}\left[\left|v_{\text{exp}}\right|^2\right] = C_z \left|\frac{S_{af}}{S_{ff}}\right|^2 \frac{1}{\omega^2}, \quad \text{where} \quad C_z = \left|\frac{Z_p + Z_a}{Z_p}\right|^2, \tag{2.47}$$

Z_p is the point impedance of the plate and Z_a is the impedance of the accelerometer. Neglecting any effect of the attachment of the accelerometer to the plate, the impedance of the accelerometer is $Z_a = i\omega M_a$, where M_a is the mass of the accelerometer, i.e. 22 g.

The time series data recorded by the microphone inside the acoustic volume is processed to express the sound pressure levels in the frequency domain. The force-pressure transfer functions were computed from the pressure-force cross-spectra, and force auto-spectrum, therefore, the modulus squared of the pressure levels to a unit force is

$$\mathrm{E}\left[\left|p_{\mathrm{exp}}\right|^2\right] = \left|\frac{S_{pf}}{S_{ff}}\right|^2. \tag{2.48}$$

2.5.1 Randomised Plate and Deterministic Acoustic Cavity

It is noted from equation (2.32) that the estimation of the variance of energy depends on the statistics of the power input and the random SEA matrix. If one or more of the subsystems has deterministic rather than a statistic behaviour, the entries of the random component of the SEA matrix will be zero for the indexes associated to the deterministic coupled systems, and the source of uncertainty will arise from the random transmitted power only. In order to verify the effect of the power transmitted from a random structural subsystem to a coupled deterministic cavity in the computation of the variance of energy, a set of multiple realisations has been collected for twenty different mass distributions on the plate for a unique configuration of the acoustic volume[4]. The comparison between the experimental mean response and the SEA predictions are plotted in figure 2.15. The experimental and predicted relative variance of energies are shown in figure 2.16.

As it was expected, in figure 2.15a, the experimental mean response of the random subsystem, i.e. the randomised brass plate, agrees fairly well with the SEA estimation. On the other hand, as shown in figure 2.15b, the SEA estimation of the acoustic response seems to be under-predicted in the order of 5 to 10 dB, and the fluctuations around the mean are significantly large, compared to the 'smoother' experimental mean response of the randomised brass plate. This apparent under-prediction of the acoustic response is found to be due to two issues. First, there is a lack of individual samples to average, as it will be further demonstrated when more individual samples were collected for the randomised acoustic cavity. Second, it is assumed that the acoustic field inside the cavity is diffuse, however, acoustic measurements for this set of experiments were taken from a particular location and therefore diffusivity is not ensured. Since the microphone was placed close to

[4]Five nominally identical tests were performed for each random distribution of the masses on the brass plate.

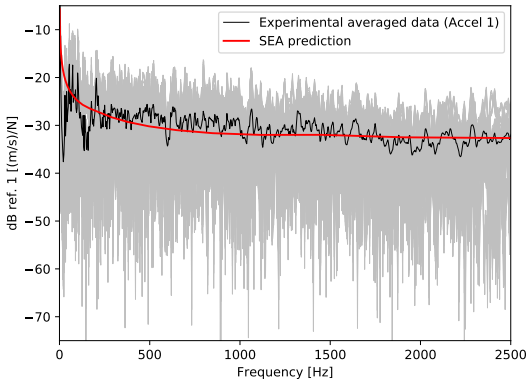

(a) Modulus squared velocity per unit force of the randomised brass plate.

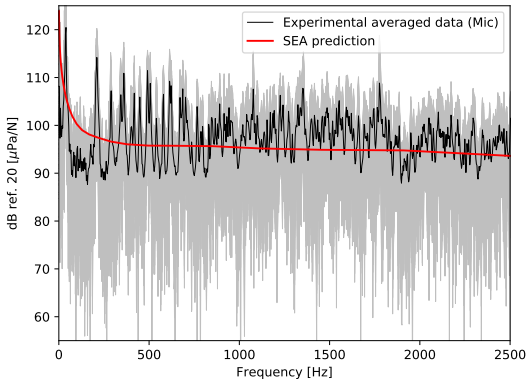

(b) Sound pressure levels per unit force in the deterministic acoustic cavity.

Fig. 2.15 Dynamic response per unit force of the randomised brass plate and the coupled deterministic acoustic cavity due to a point-force excitation on the plate. Grey: responses of each individual realisations; fluctuating black: experimental average; continuous red: SEA estimation.

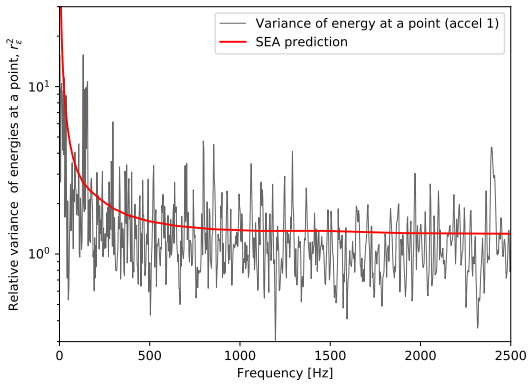

(a) Randomised brass plate.

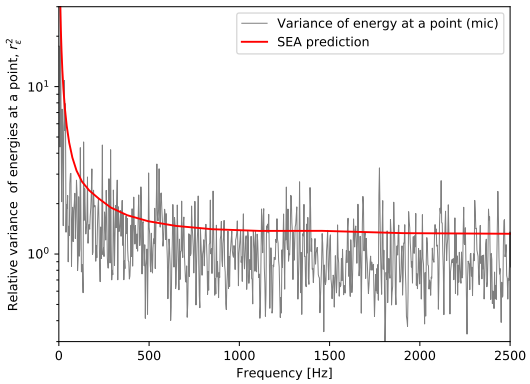

(b) Deterministic acoustic cavity.

Fig. 2.16 Relative variance of energies at a point. Fluctuating black: experimental variance; continuous red: SEA prediction.

the lateral wall and near to one of the edges, it is expected and under-prediction between 3 to 6 dB, as explained by Jacobsen (2011). This issue is addressed in the next subsection where acoustic measurements were taken at several locations within the acoustic volume.

Since the variance of the acoustic energy was computed considering that the term r^2 of the variance of the random matrix is zero, due to the deterministic nature of the cavity, the relative variance of the acoustic energy is expected to be close to the corresponding relative variance of energy of the brass plate. It can be seen that the experimental variance of the randomised brass plate, plotted in Fig 2.16a, is in the same order of magnitude of the

variance of the deterministic acoustic cavity, shown in figure 2.16b; however, although the SEA estimation has the same tendency as the experimental variance, it is over-predicted. Additionally, at several frequencies within the range, the experimental relative variance at a point is lower than one, which is in contradiction with the theory, as described by equation (2.39). It is demonstrated in the following subsection, that the reason for the discrepancy is that the number of samples here considered do not form a sufficiently large ensemble, and the agreement is improved when a larger number of realisations have been performed for different random configurations.

2.5.2 Randomised Plate and Acoustic Cavity

The acoustic cavity was further randomised by placing the rigid baffles at arbitrary positions within the volume. Ten different configurations of the mass distribution on the brass plate were tested for each of the ten random positions of the baffles inside the cavity, making an ensemble of one hundred different random structural-acoustic configurations.[5] The mean response of the randomised brass plate and acoustic cavity are plotted in figure 2.17.

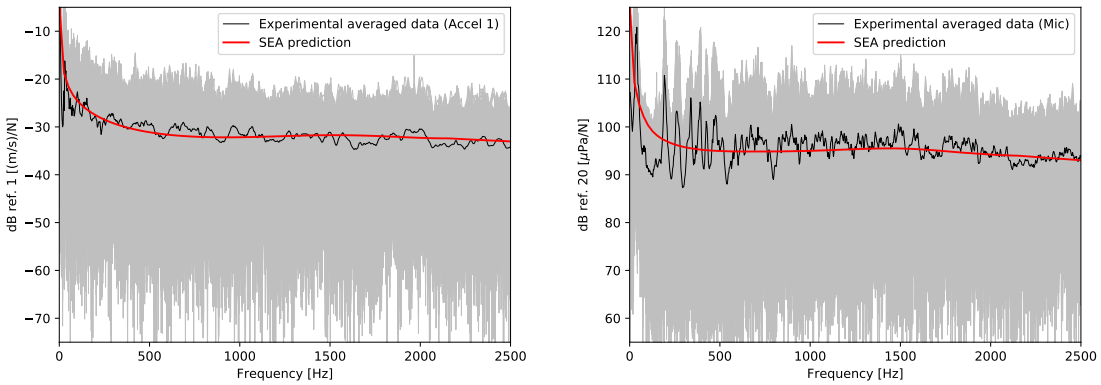

(a) Modulus squared velocity per unit force of the randomised brass plate.

(b) Sound pressure levels per unit force in the randomised acoustic cavity.

Fig. 2.17 Dynamic response per unit force of the random structural-acoustic system due to a point-force excitation on the plate. Grey: responses of each individual realisations; fluctuating black: experimental average; continuous black: SEA estimation.

It can be seen in figure 2.17a that the mean response of the brass plate is well estimated by the SEA model, as the fluctuations of the experimental mean around the predicted are less than 2 dB. The good agreement between the experimental and predicted mean structural response was expected as the brass plate was randomised a total of one hundred times.

[5]Five nominally identical tests were performed for each random structural-acoustic configuration.

Regarding the mean acoustic energy, it can be seen on figure 2.17b that the response is rather deterministic at frequencies below 600 Hz since few acoustic modes are found below that frequency, however, the fluctuation of the experimental mean is significantly lower at higher frequencies and the agreement with the SEA estimation is improved, with a fluctuation of less than 4 dB. Since ten random acoustic configurations were tested, it can be expected that the mean acoustic response of a larger ensemble, i.e. more realisations with further randomisation of the acoustic cavity, will be in better agreement as the tendency of the prediction match well with the observed experimental data.

The experimental variance of energy at a point of the random brass plate, was calculated from the data collected from one of the accelerometers placed on the top of the plate, whereas the variance of the total energy was computed from the data collected from ten accelerometers placed at different positions on the plate. The experimental and SEA variance for the brass plate are shown on figure 2.18.

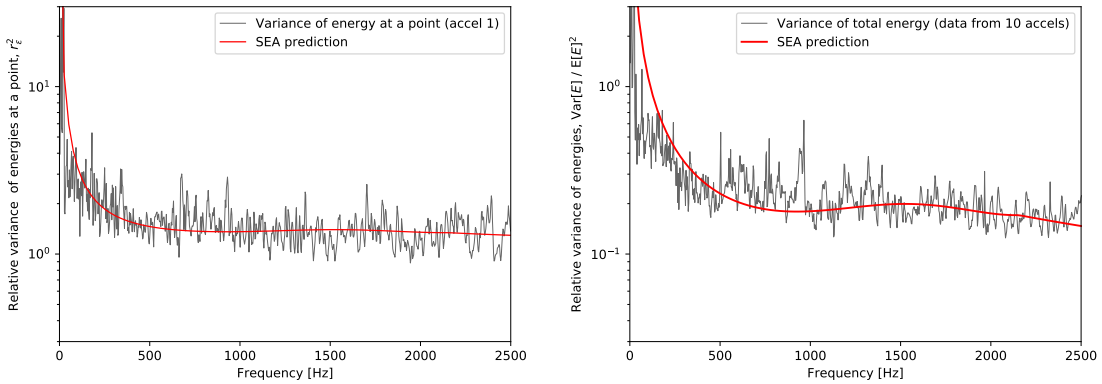

(a) Relative variance of the energy density at a point. Data from one accelerometer placed at a particular location on the plate. SEA estimation with equation 2.39.

(b) Relative variance of the total energy. Data from ten different locations on the plate.

Fig. 2.18 Relative variance of energy of the brass plate. Fluctuating: experimental data; continuous black: SEA prediction.

It is observed that the estimated SEA variance of energies at a point, figure 2.18a, agrees remarkably well with the experimental variance of the response of the brass plate. It is noted that the experimental variance is greater than one at every frequency within the range of interest, which confirms that the discrepancy observed in figure 2.16a was due to an insufficient number of realisations. As shown in figure 2.18b, the agreement is also good between the predicted variance of total energy and the experimental variance computed from the data gathered from the ten accelerometers placed on the plate. This result suggests that the number of measuring points was enough to have a reliable estimation of the experimental

variance of the total energy of the brass plate. With a lower number of accelerometers, the experimental variance was observed to be above the SEA prediction.

The data to compute the relative variance of the acoustic response at a point were collected from a microphone placed in a particular location within the cavity. To calculate the experimental variance of the total acoustic energy of the cavity, further realisations where performed to collect data with the microphone placed at several arbitrary locations within the randomised volume. Two further experimental data sets were collected. The first data set consists of the acoustic response measured in three different locations after fifty realisations, when the acoustic cavity was randomised ten times. The second data set consists of the acoustic response data of twenty-five realisations, and measurements were taken at six different locations in the cavity that was randomised five times[6]. The comparison between the experimental variance and the SEA prediction can be seen on figure 2.19.

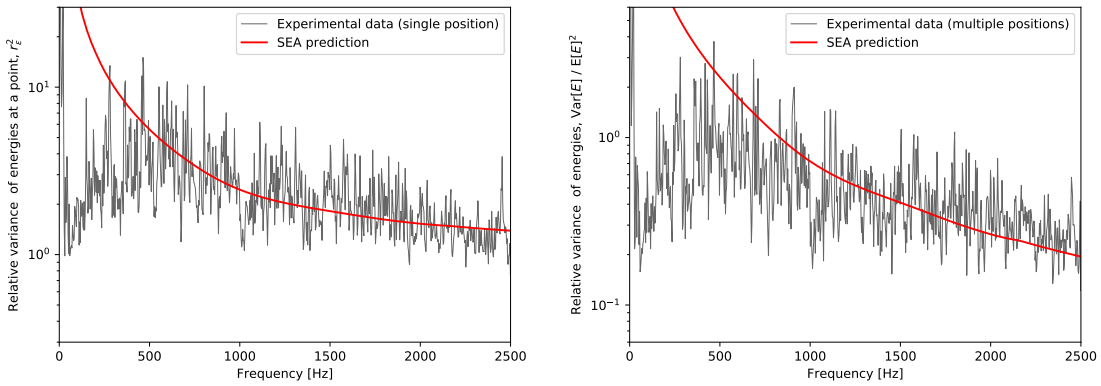

(a) Relative variance of the energy density at a point. Data from the microphone placed at a particular location within the volume. SEA estimation with equation 2.39.

(b) Relative variance of the total energy. Data from the microphone placed in a total of nine arbitrary locations within the volume.

Fig. 2.19 Relative variance of energy of the acoustic cavity . Fluctuating: experimental data; continuous black: SEA prediction.

Due to the deterministic nature of the cavity at lower frequencies, the SEA results are only expected to be reliable at frequencies above 600 Hz. It can be seen on figure 2.19a that the SEA estimation approximates fairly well the experimental relative variance at a point. Additionally, the ten random acoustic configurations, with the corresponding number of randomisations of the brass plate, were sufficient to demonstrate that the experimental relative variance of acoustic energy at a point is above one, as it would have been expected from the Schroeder statistics at higher frequencies Schroeder (1962). The experimental

[6]For both data sets, each acoustic random configuration was tested with five different mass distribution on the brass plate. Three nominally identical test were performed.

variance of the total energy, calculated with data gathered from fifteen different acoustic random configurations and nine measuring points, is found to have the a good agreement with the SEA prediction plotted in figure 2.19b.

2.6 Concluding Remarks

The advantage of an SEA approach to analyse complex systems is that the averaged response and variance can be rapidly estimated form relatively simple expressions, whereas the computation of the averaged structural and acoustic response of physical systems requires a large ensemble of random nominally identical systems, as well as measurements in several locations within the system. A good agreement is found between SEA estimations and experimental mean and variance in the frequency range where there is a high degree of statistical overlap, and therefore poor agreement is found at lower frequencies, when the system is rather deterministic with a statistical overlap less than one.

The prediction of the response variance of complex built-up systems based on the GOE statistics proposed by Langley and Cotoni (2004), has been already validated by Cotoni et al. (2005) for structural systems, and by Jacobsen and Rodríguez Molares (2010) for acoustic systems. However, the results here presented constitute the first experimental evidence that demonstrates the accuracy of the GOE statistics to predict the response variance of coupled structural-acoustic systems.

The experimental setup here presented is further modified to include a nonlinear device between the input and the structural subsystem, i.e. the flat thin plate, and the resulting statistical nonlinear physical system constitute the case study presented in the following chapters of this thesis, to explore key aspects of the nonlinear transmission path and the impact in the structural and acoustic responses of the statistical model.

Chapter 3

Nonlinear Analysis in the Time Domain with an SEA Approach

3.1 Introduction

In the development of a simplified vibro-acoustic model of a vehicle to characterise the influence of possible nonlinearities, or otherwise, in the rise of sound pressure levels due to structural vibrations, i.e. structure-borne noise, it has been considered that the structural-acoustic system, i.e. structural components enclosing a car cabin, has a linear nature, as well as the sound radiation phenomenon. Since the concern of this study is the noise generation due to the vehicle-road interaction, known as road noise, the vibro-acoustic model of a structural panel coupled to an acoustic volume has to be improved to consider the transmission path between the wheel motion to the car structure. A schematic representation of the problem is shown in figure 3.1, where the input to the system is received by the wheels, and the vibrations are transmitted to the structure through the suspension system. The outputs are both the vibrations of the structure and the radiated noise.

The suspension system in a vehicle supports the weight of the structure and is intended to isolate the chassis from the vehicle-road interaction, providing comfort to the driver and occupants. However, it is not possible to provide a high degree of isolation as it will compromise the vehicle handling and performance. Therefore, the excitation from the road-wheels interaction can be transmitted through the components and connections of the suspension system, and they can induce vibrations in the structure, that ultimately radiates sound to the car cabin, i.e. road noise.

It is known that several components in the suspension system have nonlinear characteristics (McGee et al., 2005), and car manufacturers have addressed this issue at frequencies

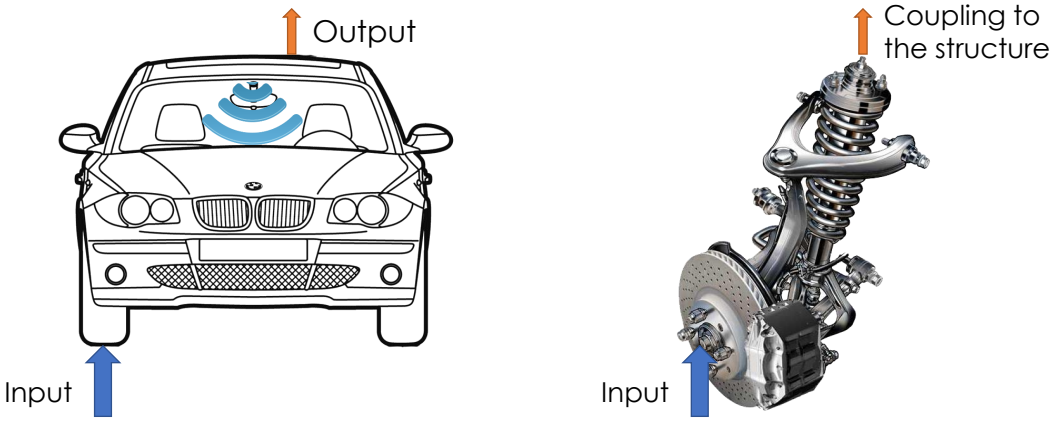

(a) Schematic representation. (b) Suspension system.

Fig. 3.1 Road-wheel interaction and the vibration transmission path.

below the acoustic range to improve vehicle performance, safety and comfort (see for example Demir et al. (2012)), though without regard to the implications, or otherwise, of such nonlinearities in the transmission path in the road noise generation.

As a complete numerical model of the vehicle comprising both, the suspension system and the car structural-acoustic system, results in a prohibitively computationally expensive approach for analysis at the acoustic frequency range of interest, key aspects of the implications of the nonlinearities in the dynamic response of the system can be rather analysed by isolating a structural-acoustic system and a coupled nonlinear component in the transmission path. In this chapter, a simplified model based on the infinite plate theory is developed to characterise the structural response to a prescribed random input through a nonlinear system. Numerical and experimental data in the time domain are in good agreement, and validate the developed simplified approach.

3.2 Physical Nonlinear Structural-Acoustic System

With the aim of characterising the structural-acoustic response of a system to the excitation through a nonlinear path, the experimental rig presented chapter 2 has been modified to include a nonlinear device through which the force, due to a prescribed input, is transmitted to the structural-acoustic system.

3.2.1 Modified Structural-Acoustic Rig

In this analysis, it has been considered a device with nonlinear stiffness that transmits the force in a perpendicular direction to the flat thin plate, generating bending waves that radiate sound to the interior of the acoustic cavity. This characteristic is achieved by a couple of magnets, whose repulsive force is nonlinearly related to the separation between them. One of the magnets is fixed on the plate at the driving point, whereas the other one is fixed at the tip of a rocking beam. The input to the system is given by a shaker that excites the beam to provide random oscillations in the frequency range of interest. A schematic overall representation of the modified experimental rig is presented in figure 3.2, whereas a detailed view of the nonlinear interface is shown in figure 3.3.

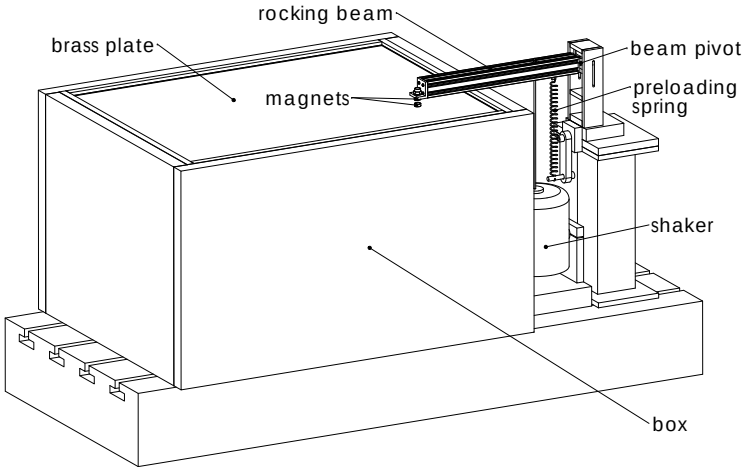

Fig. 3.2 Modified experimental setup. The brass plate placed on the top of the acoustic box is excited by the repulsive force generated due to the oscillations of the rocking beam.

The motion of the magnets is recorded by two accelerometers. The accelerometer fixed at the tip of the beam measures the input to the system, whereas the output is measured by the accelerometer placed underneath the plate at the driving point. Experimental data are recorded in terms of acceleration in the time domain, which can be processed to convert it to displacement by integrating twice the discrete collected data.

The rocking beam is not intended to provide any nonlinear effect to the dynamics of the system, and it has been designed to have any node near the tip of the beam, which appears after the first resonance of a pinned cantilever beam, away from the frequency range of interest. As the analysis is carried out up to 2000 Hz, and the displacement at the tip has to be maximised, the weight and the bending stiffness have to be optimised. An aluminium type V-Slot Linear Rail 40$\times$40 mm of 400 mm length is selected to be implemented as the

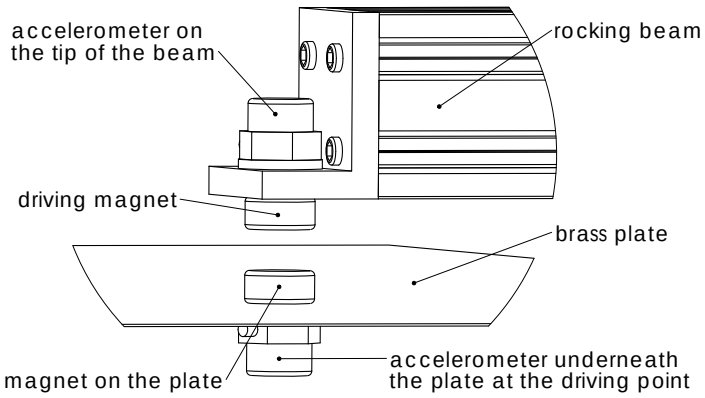

Fig. 3.3 Detail of the tip of the beam and the plate at the diving point. The position of the pair of magnets is shown with the accelerometers that record data of their motion.

rocking mechanism that transmit motion from the shaker to the driving magnet. A section of the beam can be seen in figure 3.4.

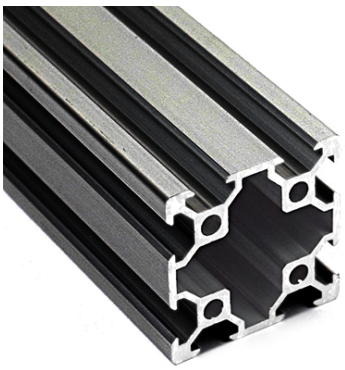

Fig. 3.4 40×40 aluminium rail used as the rocking beam that transmits the the motion from the shaker to the input magnet. (https://ooznest.co.uk)

The beam is pivoted on the frame at one end and connected to the shaker by a piano wire in a section 100 mm away from the pivot. Finally, a linear spring connects the beam to the frame to provide a preload to maintain the system in an equilibrium position at an initial separation between the magnets.

3.2.2 Repulsive Force Between the Couple of Magnets

It is well known that the force between two magnetic poles, as a simple approximation, varies to the inverse squared distance between them, both for forces of attractive or repulsive nature. However, a general expression to analytically compute the magnetic force is not always available, as it depends on the geometry, dimensions and whether the action takes place

in the near or far field. For the case of cylindrical magnets, Vokoun et al. (2009) provides analytical expressions of the magnetic force as a function of the separation, with geometric and magnetic parameters, where, even though they have limits of application, the inverse squared distance between the magnets appears in the equations.

In this study, a simplified version of the expression provided by Vokoun et al. (2009) is adopted to express the repulsive force F as function of the separation r in the form

$$F = -Ar + \frac{B}{(r+C)^2}, \tag{3.1}$$

where the constants A, B and C are found from experimental data of force vs. separation. A couple of neodymium magnets are to be employed in the experimental setup, and data provided by the manufacturer was used to estimate such constants for three different sizes. The corresponding fitting curves to experimental data, as well as the estimated values of the fitting constants of equation 3.1 are presented in figure 3.5 and table 3.1, respectively.

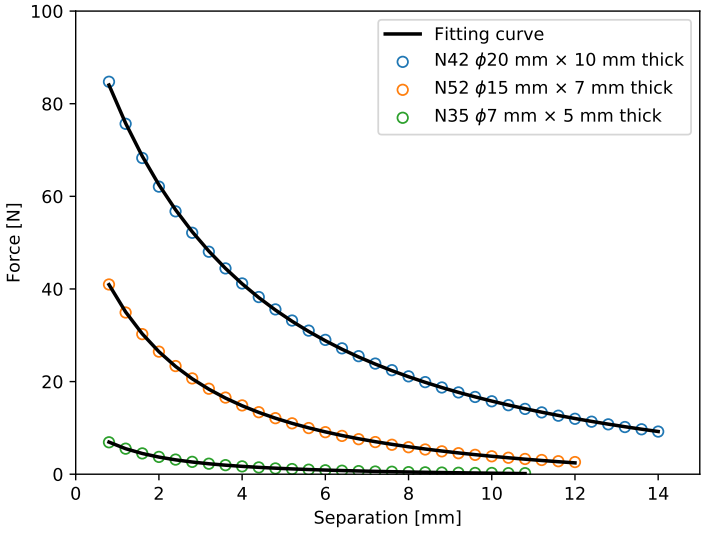

Fig. 3.5 Measured data is provided for three neodymium cylindrical magnets of different size (www.magnetexpert.com).

The total vertical force excerted on the flat thin plate of the structural-acoustic system has two components: a static component F_S due to the repulsive force that one magnet exerts on the other, provided by the linear spring that maintains the beam in a horizontal position in equilibrium, and a dynamic force F_D, that oscillates about the static, due to the relative motion between the magnets. The static and dynamic positions of the magnets are shown in figure 3.6.

Table 3.1 Constants in the magnetic force of equation 3.1

Magnet type	A [N/m]	B $\times 10^{-3}$ [N-m^2]	C $\times 10^{-3}$ [m]
N42 ϕ20 mm $\times$ 10 mm thick	26.86	0.07	2.51
N52 ϕ15 mm $\times$ 7 mm thick	122.30	1.02	4.18
N35 ϕ7 mm $\times$ 5 mm thick	140.23	4.83	6.77

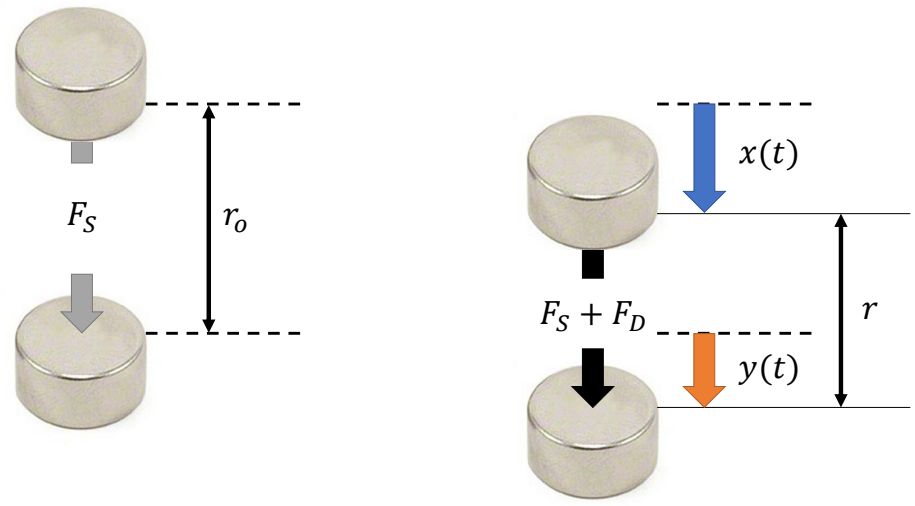

(a) Equilibrium position. (b) Relative motion.

Fig. 3.6 Repulsive magnetic static force in equilibrium and dynamic force due to the relative motion after the input $x(t)$ and output $y(t)$.

Only the dynamic component of the force, which is function of the input $x(t)$ and output $y(t)$, is considered for this analysis, as the concern is the dynamic response of the structural component of the system. From figure 3.6, the separation between the magnets r is equivalent to $r_o - [x(t) - y(t)]$ and, from the magnets law here adopted, i.e. equation 3.1, the dynamic force can be obtained by subtracting the static force from the total, and the resulting F_D can be expressed as

$$F_D = A[x(t) - y(t)] + \frac{B}{(c_1 - [x(t) - y(t)])^2} - c_2, \tag{3.2}$$

where $c_1 = r_o + C$ and $c_2 = B/(r_o + C)^2$. This form guarantees that the dynamic force is zero at the equilibrium position, i.e at $x(t) - y(t) = 0$.

3.3 Simplified Numerical Model

For the analysis of key aspects of the nonlinear transmission path in the dynamic response of the coupled structural-acoustic system, as a first approach, the system comprised by the coupled brass plate and acoustic cavity, and the nonlinear device, can be further simplified assuming that:

- The structural-acoustic rig comprised by the brass thin plate, acoustic cavity and the rigid walls, is a linear system.
- The rigid walls do not radiate sound to the interior.
- The system is excited only by the dynamic magnetic force that exerts the plate at the driving point.
- The brass plate is weakly coupled to the acoustic cavity.

With this considerations, the analysis of the implications of nonlinearities in the transmission path in the response of the system can be carried out by observing the response of the isolated structural system only, i.e. the flat brass thin plate, as this is the system that receives directly the input, and radiates linearly to the acoustic cavity.

Even though the system has been reduced to a structural component and the nonlinear device only, there are three major limitations that need to be addressed in this analysis. Firstly, analytical solutions to nonlinear differential equations are seldom available, and are limited to a particular relationship between the force and displacement, e.g. a cubic nonlinearity of a Duffing oscillator (Kovacic and Brennan, 2011), therefore, numerical approaches are usually adopted to solve the nonlinear equations of motion in the time domain. Secondly, the structural system here presented, i.e. the flat brass thin plate, has a statistical nature in the frequency range of interest, which brings uncertainties to the solution. Finally, a large number of degrees of freedom are needed to model bending waves at high frequencies, increasing the computational cost.

An approach based in the Statistical Energy Analysis, derived from the infinite plate theory, is here adopted to develop a simplified one-degree-of-freedom equivalent system to improve the computing performance of the nonlinear analysis in the time domain.

3.3.1 Infinite Plate and the Equivalent Damper Model

A continuous two-dimension medium can be considered to be an infinite structure if the dimensions, such as length and width, are much larger than the wavelength of the either

in-plane or bending waves. In a more practical definition, a flat thin plate for example, can be considered to be an infinite medium if the motion waves have no interaction with the boundaries, or if such interaction can be neglected (Graff, 2012). To illustrate this definition, consider a flat thin plate that is being excited at a point away from the borders, as presented in figure 3.7. Figure 3.7a shows bending waves travelling away from the driving point of the plate, which is known as direct field. After the waves have reached the boundaries, they can be reflected and travel back to the excitation point, interacting with the ongoing waves, as shown in figure 3.7b. These reflected waves are known as the reverberant field.

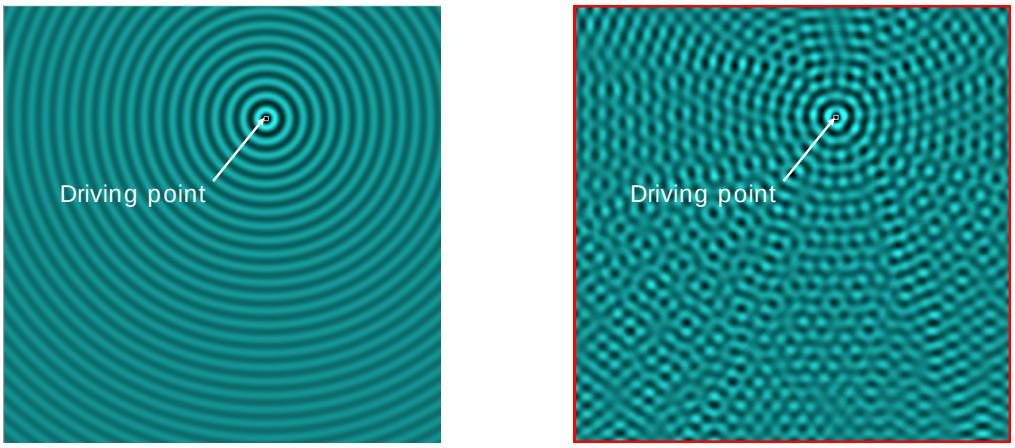

(a) Ongoing waves in the direct field. (b) Direct and reverberant fields.

Fig. 3.7 Bending waves on a flat thin plate excited at a single point. (Simulations performed in www.falstad.com/ripple).

Since in this analysis the plate is considered as an isolated system, with weak interaction with the walls and the acoustic media of the physical system, all of the vibrating energy is dissipated solely within the plate at the rate $\omega E \eta$, as defined by the Statistical energy analysis, therefore, the plate can be considered as a dissipative mechanism, similarly to a damper.

The characteristics of the equivalent damper can be found by further analysing the dissipative nature of the plate. Hambric (2016) points out that, as the structural loss factor of a finite plate increases, the direct field on the plate becomes dominant. This phenomenon can be explained by noting that the plate absorbs energy cyclically, and the waves are eventually attenuated before reaching the boundaries, therefore, the effect of the reflected wave in the direct field becomes negligible.

In figure 3.8, it is shown the magnitude of the mobility frequency response function of a numerical FE model of brass thin plate with two different damping characteristics.

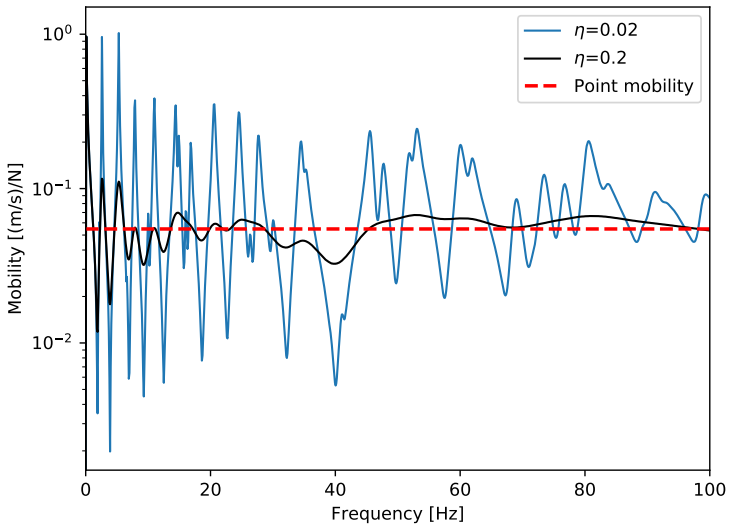

Fig. 3.8 Numerical mobility frequency response function of a brass plate. Blue: lightly damped plate ($\eta = 0.02$); black: heavily damped plate ($\eta = 0.2$); dashed red: point mobility of an infinity flat thin plate ($1/Z_p = 0.058$m-s/N.

It can be noted that as the damping increases, the peaks of the mobility frequency response at the natural frequencies reduce in magnitude. Furthermore, the response of the plate approaches to the mobility of the infinite plate, which is a constant equivalent to the inverse of the point impedance. As the point mobility of an infinite plate can be viewed as the average of the mobility frequency response of a statistical system, the damping characteristic of the equivalent damper of the model corresponds to the point impedance of the plate, i.e. equivalent viscous damping $\lambda = Z_p$, which is a constant found by

$$Z_p = \frac{8\rho h^2 c_\phi}{\sqrt{12}}, \tag{3.3}$$

where ρ, h and c_ϕ are the plate density, thickness and longitudinal wave velocity, respectively. The equivalent single-degree-of-freedom system can be schematically viewed in figure 3.9.

Ideally, the equivalent system would have been comprised by the nonlinear spring and the damper only. However, even though the spring is theoretically a massless device, one of the magnets is fixed to the plate, as well as an accelerometer that measures the motion of the plate. This two components add an inertial characteristic to the plate at the driving point, which has to be taken into account. Therefore, the mass m that appears on the schematic system of figure 3.9b, comprises the mass of the magnet plus the mass of the accelerometer, with a total of 36 g. If the mass is neglected, the model will overestimate any measured response of the physical system.

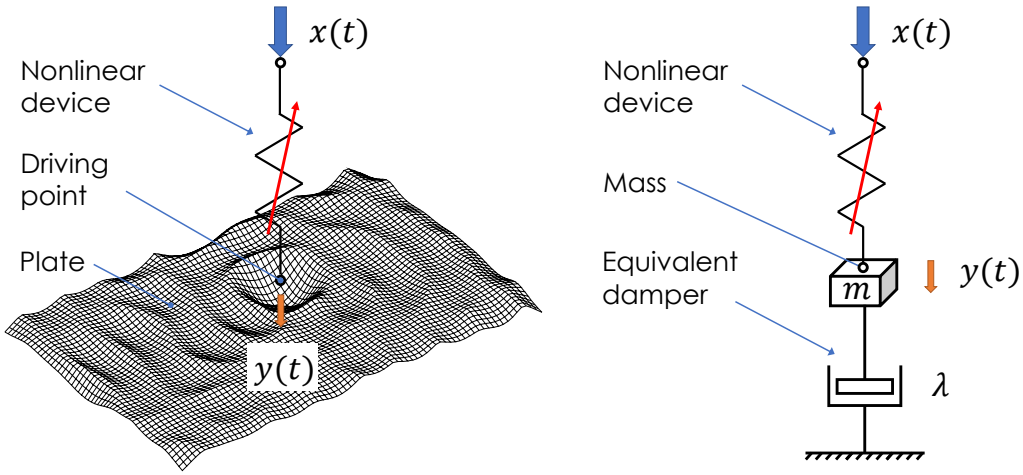

(a) Plate excited through a nonlinear spring. (b) Equivalent damper model.

Fig. 3.9 Equivalent damper model of a flat thin plate.

The equation of motion of the one-degree-of-freedom equivalent damper model can be written as

$$m\ddot{y}(t)+\lambda\dot{y}(t)=A\left[x(t)-y(t)\right]+\frac{B}{\left(c_1-\left[x(t)-y(t)\right]\right)^2}-c_2, \tag{3.4}$$

where the response $y(t)$ is and estimate of the average response of the plate at the driving point due to a random displacement input $x(t)$.

3.3.2 Numerical Simulations to a Brownian Process Input

The equation 3.4, that estimates the averaged response in the time domain of the isolated brass thin plate, has no analytical solution, therefore, a numerical approach is followed to generate data from simulations. The solver ode45 in MATLAB has been employed to numerically compute the response of the system in the time domain for a prescribed random input. As a case study to test the performance of the solver and the capability of the model to capture the effect of the nonlinear device in the response of the system, a Gaussian random input with constant-velocity spectrum throughout the frequency band of 20 to 2000 Hz is adopted. This type of input is known as Brownian process (Gardiner, 1985), whose displacement power spectral density is given by

$$S_{xx}(\omega)=\frac{S_o}{\omega^2}, \tag{3.5}$$

where S_o is the constant power spectral density of the velocity. The displacement spectrum $S_{xx}(\omega)$ has a first order roll-off, i.e. 20 dB per decade, with more energy at lower frequencies than at higher.

The one-degree-of-freedom system described by equation 3.4 with the parameters of the equivalent damper and magnets law has an overdamped nature, and the natural frequency is below the frequency range of interest. Several long simulations were performed with different amplitudes of the input, characterised by the standard deviation σ_x. The numerical results in the time domain, and the corresponding power spectral density of the input and output are plotted in figure 3.10 for the lowest amplitude, and in figure 3.11 for the highest here tested.

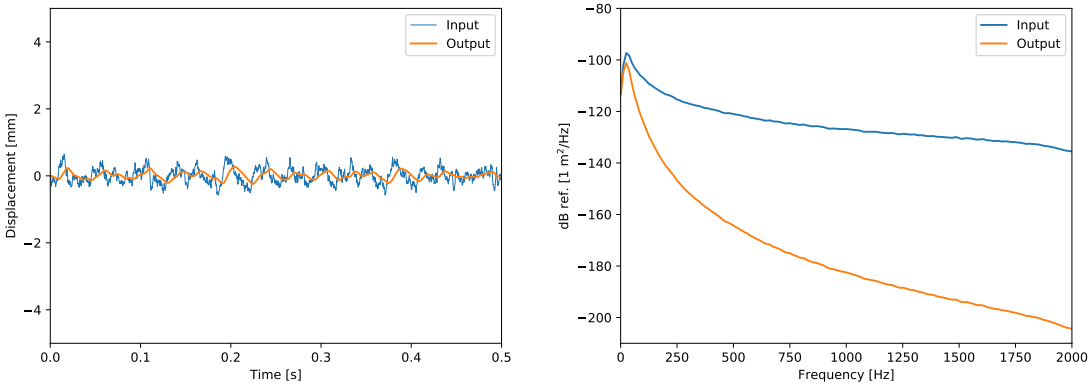

(a) Data in the time domain. (b) Power spectral density.

Fig. 3.10 Numerical results for the equivalent damper model from simulations with low amplitude zero-mean Brownian input ($\sigma = 0.22$ mm).

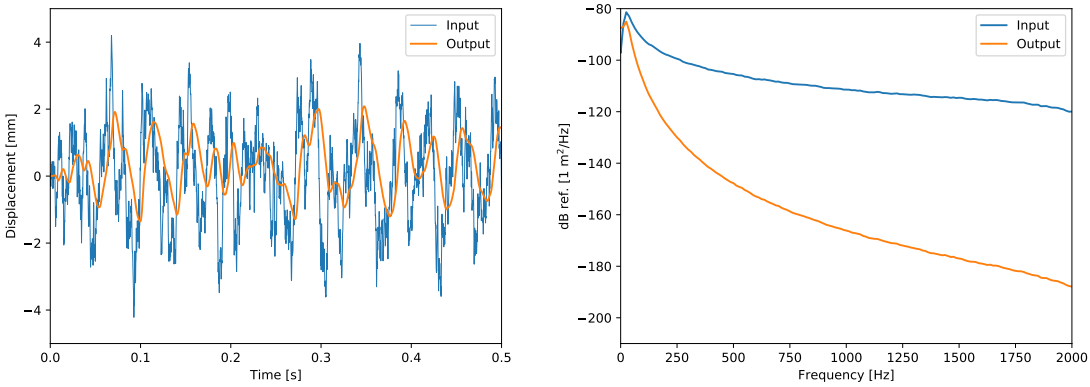

(a) Data in the time domain. (b) Power spectral density.

Fig. 3.11 Numerical results for the equivalent damper model from simulations with higher amplitude zero-mean Brownian input ($\sigma = 1.35$ mm).

The dynamic magnetic force, given by equation 3.5 is plotted versus the net displacement $x(t) - y(t)$ in figure 3.12 for the lower and higher amplitude cases.

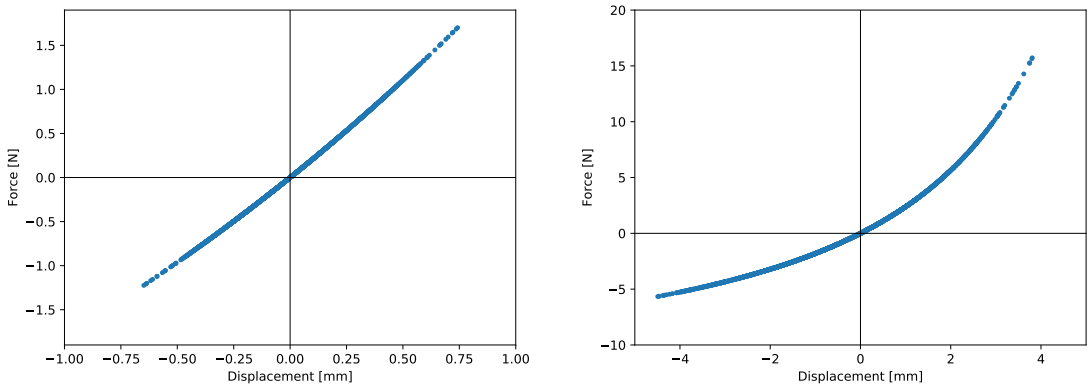

(a) Zero mean Brownian input ($\sigma = 1.35$ mm). (b) Zero mean Brownian input ($\sigma = 0.22$ mm).

Fig. 3.12 Dynamic force vs. net displacement.

It can be seen a nearly linear force-displacement relationship for small displacements (low input). As the amplitude of the input increases, a hardening nonlinear stiffness can be visualised, indicating that the nonlinearity is present in the response of the system. However, due to the overdamped nature of the system, there are no visible harmonics, and nothing can be concluded from the power spectral density plots, as they look similar for the two cases of amplitude, therefore a further analysis is required to understand how the nonlinearity affects the response.

A measure of the degree of how much of the output in the frequency domain is correlated to the input gives an insight of how linear the system is. This measure is known as the coherence function, and a common representation of its form for a single input $x(t)$ and single output $y(t)$ can be written as

$$\gamma^2 = \frac{\left|S_{xy}(\omega)\right|^2}{S_{xx}(\omega)\, S_{yy}(\omega)}, \tag{3.6}$$

where $S_{xx}(\omega)$ and $S_{yy}(\omega)$ are the power spectral densities of the input and output, respectively, and $S_{xy}(\omega)$ is the cross power spectral density between the two signals. It is known that, in absence of any noise, the value of the coherence in the frequency range is equal to one if the system is linear. On the other hand, there can be drops in coherence at the frequencies where the nonlinearity has an effect on the response of the system.

The coherence has been calculated for each of four cases of input amplitude to the equivalent damper model. Results are shown in figure 3.13.

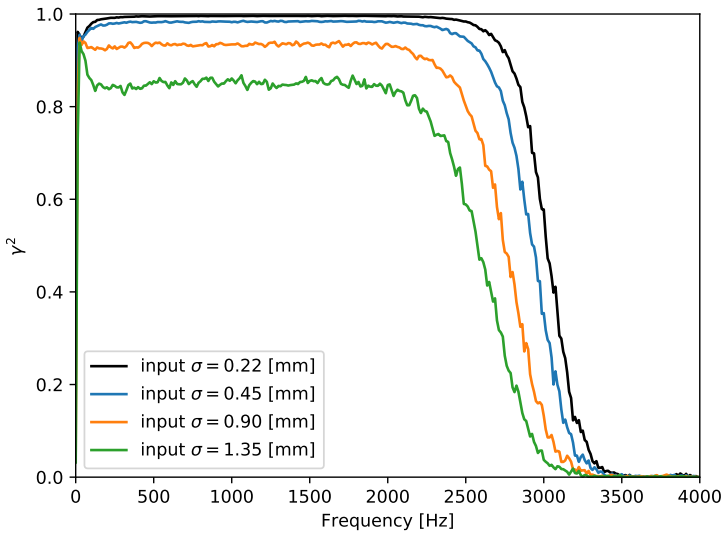

Fig. 3.13 Coherence between input and output of the equivalent damper model. Simulations were performed with different amplitudes of a zero-mean Brownian input $x(t)$.

Results in figure 3.13 indicate that in the frequency band of 20-2000 Hz, the coherence is near to one in the lower amplitude input case, as the system behaves almost linearly. As the amplitude of the input increases, there is a uniform reduction in coherence through the frequency band. As there is no uncorrelated noise in the signals gathered from the simulations, the loss in coherence is solely due to the nonlinear nature of the interface between the input and output.

3.4 Experimental Validation

The equivalent damper model, described by the equation of motion 3.4, can be employed to estimate the mean response of the brass plate for measured inputs in the experimental setup. Two features about the capability of the equivalent single-degree-of-freedom model are to be analysed. Firstly, whether the power spectral density of the time domain data generated from simulations agrees with the corresponding power spectral density of the displacement of the magnet attached to the brass plate, as it represents the response of the plate at the driving point. Secondly, whether the influence of the nonlinearity, and the dependence of the input amplitude observed in the coherence plots between the input and output signals, is similar to the coherence between the results from simulations to the measured input. Two experimental study cases are here analysed: a white noise input to the shaker of the experimental system, and a tailored signal to have a displacement spectrum at the tip of the beam with higher amplitude about a particular frequency.

3.4.1 Response to an Input with Constant Acceleration Power Spectrum

The Brownian process input with constant velocity power spectrum, used in the previous case study, is unlikely to be applied to the experimental setup as a large power input would be required to excite the nonlinear behaviour in the experimental rig at higher frequencies. Therefore, a white noise signal is given to the shaker of the system, to expect the motion of the input magnet to have a nearly constant acceleration power spectrum in the frequency range of interest, i.e. a displacement spectrum $S_{xx}(\omega)$ of second order roll-off with a reduction of 40 dB per decade. Nevertheless, such measured signal is expected to have a larger amplitude at the frequencies where the beam modes are observed. A low and a higher amplitude white noise signals where given to the experimental rig to excite the system in a range of frequencies 20 - 1800 Hz, and data from the two accelerometers that record the motion of the two magnets were gathered in a period of 50 s for each case. The experimental displacement power spectral density of the motion of the input and output magnets, as well as corresponding results from time domain simulations of the equivalent damper model with the experimental input, are shown in figure 3.14.

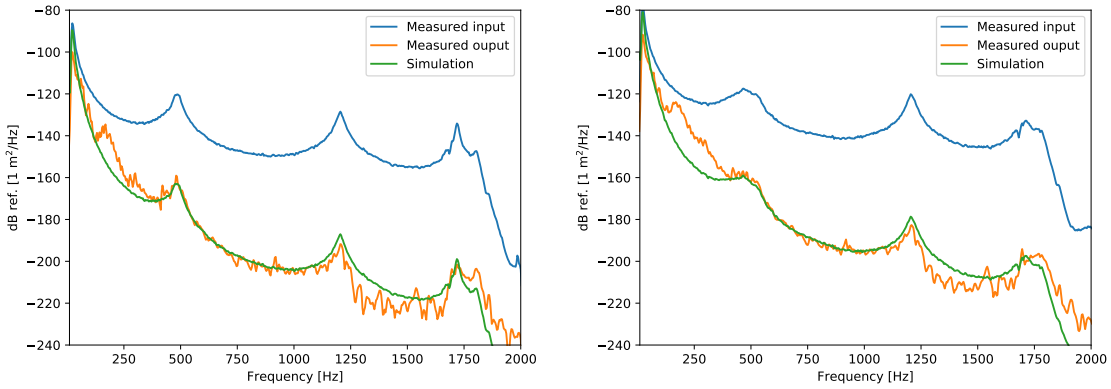

(a) Low input to shaker: 10 V.

(b) Higher input to shaker: 50 V.

Fig. 3.14 Displacement power spectral density from experimental data and simulations. Blue: measured input; orange: measured output; green: estimation from the equivalent damper model.

From the displacement power spectral density plots, for the lower and higher amplitude inputs, it can be concluded that the model estimates with a relatively high degree of accuracy the response of the brass plate at the driving point, i.e. the motion of the output magnet, to a prescribed displacement given to the nonlinear device, i.e. measured motion of the input magnet. However, two main regions of frequency where there is a strong disagreement, about

200 Hz and above 1250 Hz, where found to be due to uncorrelated noise in the environment where the tests were performed.

The effect of the nonlinearity in the transmission path, i.e. the interface between the couple of magnets, can be observed in the coherence plots in figure 3.15, for the lower and higher amplitudes.

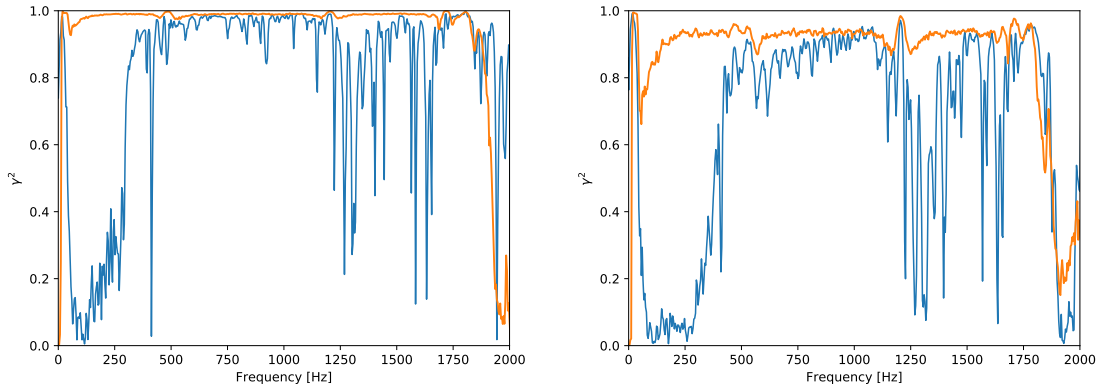

(a) Low input to shaker (10 V).

(b) Higher input to shaker (50 V).

Fig. 3.15 Input to output coherence plots. Blue: from experimental data; orange: estimation from the equivalent damper model.

In general, a good agreement is observed between the coherence of experimental data and from simulations, for the lower and higher input amplitude cases, except in the regions where the disagreement is found to be due to uncorrelated noise. The overall reduction of coherence in the whole frequency band, predicted by the model with a Brownian process input, is also found in this system with an input of second order roll-off, which validates the capability of the model to estimate, both the response and the effect of the nonlinearity in the transmission path.

3.4.2 Response to an Input with Higher Amplitude About a Particular Frequency

With the aim of visualising any effect of the nonlinear transmission path in the power spectral density of the response of the system, such as harmonics, the input signal given to the experimental setup to excite the system needs to be tailored to generate a displacement at the tip of the beam, i.e. the motion of the input magnet, with a power spectral density with higher amplitude about a particular frequency, whereas at other frequencies within the range of interest the power spectral density remains at a lower level.

Re-design of the rocking beam of the experimental rig

The design of the experimental setup has been modified to guarantee that the system has a mode at a frequency of nearly 210 Hz, which is the value of the first resonant frequency of the acoustic cavity, and therefore a large amplitude of motion at the tip of the beam would be expected without the need of an excessive power input provided by the shaker. This is achieved by replacing the rocking beam with another that has a lower flexural rigidity. The selected profile and the corresponding transfer function of the motion measured at the tip of the beam, i.e. where the input magnet is placed, to the input signal to the system are shown in figure 3.16.

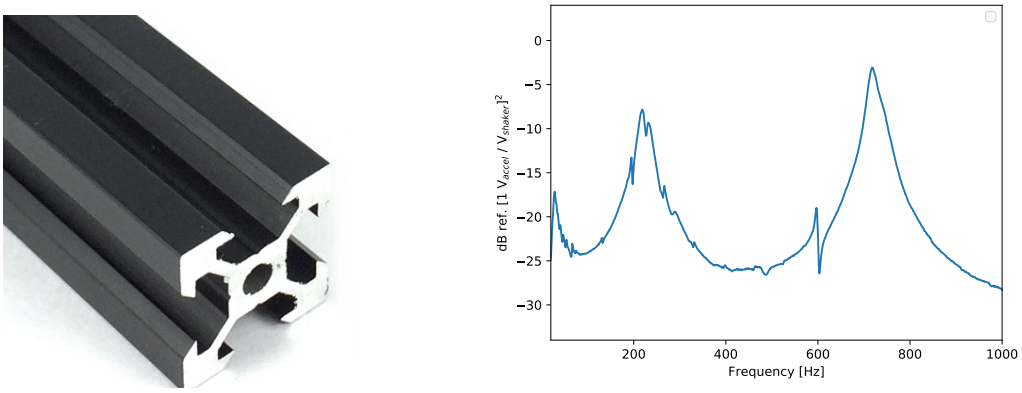

(a) 20×20 aluminium rail.

(b) Modulus squared of the measured transfer function in the system up to 1 kHz.

Fig. 3.16 Profile of the new rocking beam and the measured transfer function of the acceleration at the tip of the beam to the input signal given to the shaker.

Assuming that the subsystem comprised by the shaker, connecting rod, pre-loading spring and rocking beam has a linear nature, the measured transfer function $H(\omega)$ can be used to calculate a random input signal to the system that generates a random response at the tip of the beam with a known power spectral density. If the Fourier transform of the desired signal $x(t)$ at the tip of the beam is known and given by $X(\omega)$, the Fourier transform of the signal that is required as input to the system can be calculated from

$$X_{\text{input}}(\omega) = \frac{X(\omega)}{H(\omega)}, \tag{3.7}$$

and then, the required signal in the time domain can be obtained from the inverse Fourier transform

$$x_{\text{input}}(t) = \int_{-\infty}^{\infty} X(\omega)\, \mathrm{e}^{i\omega t} \mathrm{d}\omega. \tag{3.8}$$

In order to keep dimensional consistency, the transfer function $H(\omega)$ must be expressed in units of displacement per voltage. The computation of the transfer function, and Fourier transforms to obtain a discrete signal $x_{\text{input}}(t)$ is performed using the FFT algorithms provided in MATLAB.

Experimental results: Power spectral density

The power spectral densities of the input signal $x(t)$ and the output $y(t)$ measured in the experimental rig, i.e the motion the input and output magnets, are plotted in figure 3.17, where there has also been plotted the corresponding estimation from the simplified one-degree-of-freedom model after numerical simulations.

As designed, the experimental power spectral density of the input magnet (blue curves in figure 3.17) has a higher amplitude about 210 Hz, with a nearly second order roll-off at other frequencies. This means that the energy remains low and almost constant in most of the range of frequencies, except about the highest amplitude, due to the nearly flat velocity power spectral density that can be obtained when differentiating the displacement signal with respect to time. Additionally, an apparent distortion of the soft spectrum was measured about 600 Hz which corresponds to a discontinuity in the transfer function plotted in figure 3.16b. It was found that this issue is due to a torsional mode of the beam at such frequency, excited due to a small misalignment of the connecting rod between the shaker and the beam. As this torsional mode has a linear effect in the response, there was no need to correct such misalignment as it will not affect the nonlinear analysis.

It is clearly visualised the effect of the nonlinearity in the response as the amplitude of the input increases, as an increment of the amplitude of the response is observed from experimental data at about 420 Hz, corresponding to the second harmonic. This effect is well captured by the equivalent damper model. For the highest input case, a third harmonic can be visualised at from the experimental data at about 630 Hz, and due to the small amplitude, the estimation is almost confused with the effect of the torsional mode about the same frequency. Nevertheless, whether the model estimates the second and third harmonics at a high degree of accuracy can be analysed from coherence plots, for both experimental data and from simulations.

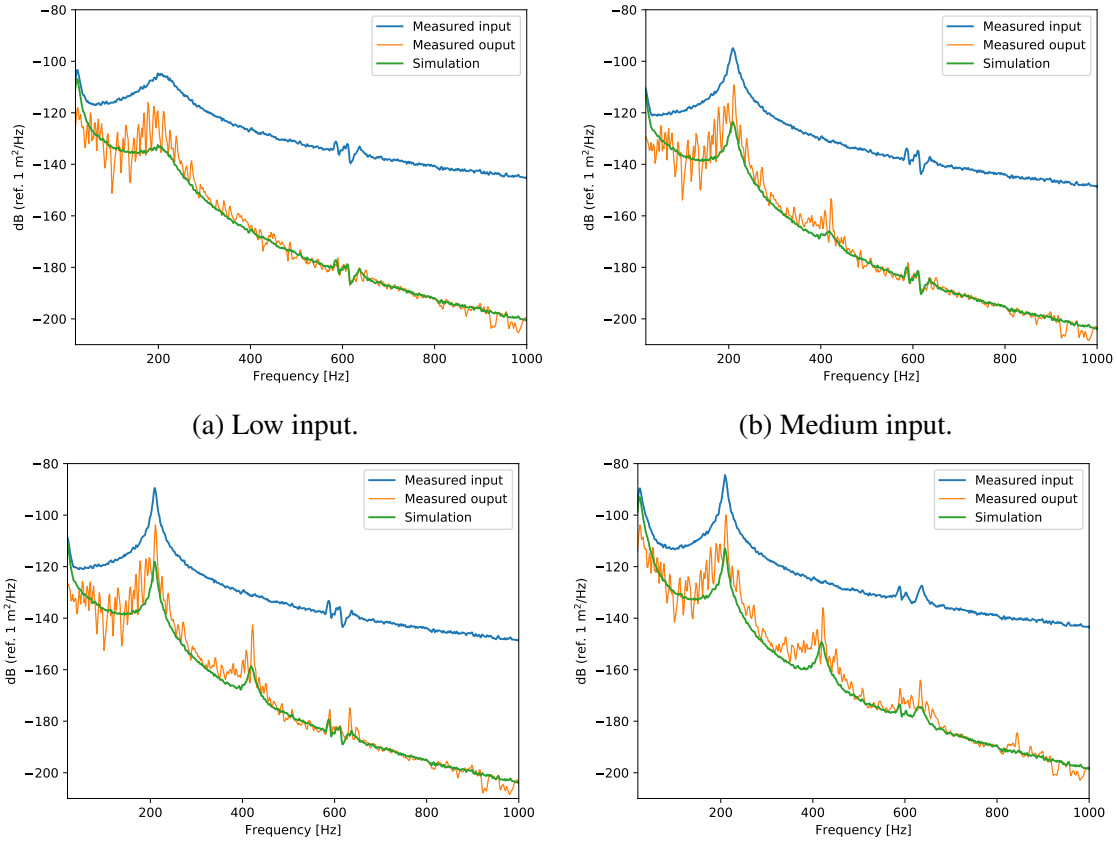

(a) Low input.

(b) Medium input.

(c) Higher input.

(d) Highest input.

Fig. 3.17 Displacement power spectral density from experimental data collected in the modified rig and from simulations. Blue: measured input; orange: measured output; green: estimation from the equivalent damper model.

Experimental results: Coherence

Coherence between the output from both, experimental measurements and data from simulations, and the input are plotted in figure 3.18 for the four amplitudes tested.

It can be seen that the model captures with a high degree of accuracy the drops of coherence at the frequencies where the second and the third harmonics are, i.e. 420 and 630 Hz. At the highest input tested, there can be also visualised a drop at the fourth harmonic at 840 Hz. In the four cases, however, there can be visualised a lack of agreement at low frequencies below 250 Hz, as it was also observed in the previous section where the input had a constant acceleration power spectrum. This low experimental coherence in such range was found to be due to external inputs, and such effect can be observed in multiple coherence plots.

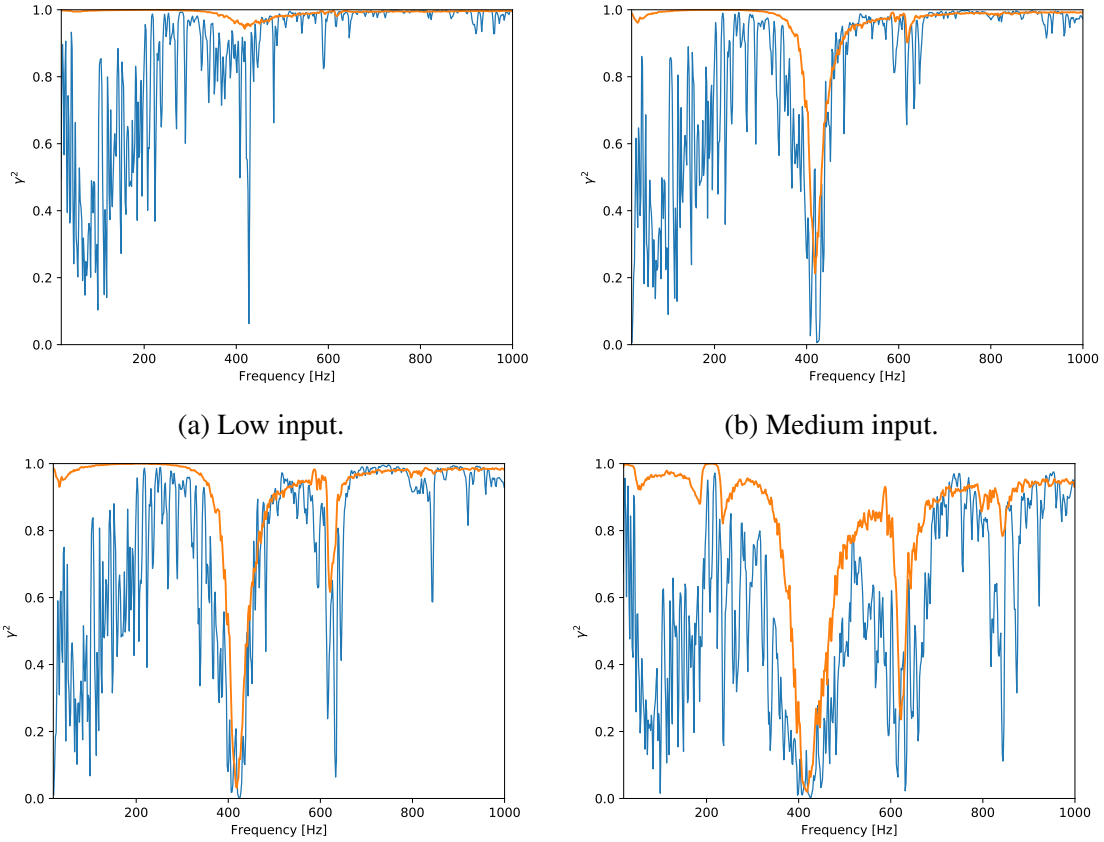

(a) Low input.

(b) Medium input.

(c) Higher input.

(d) Highest input.

Fig. 3.18 Input to output coherence plots from experimental data collected in the modified rig and from simulations. Blue: from experimental data, orange: estimation from the equivalent damper model.

Multiple coherence

The coherence function gives a scalar value that indicates the degree of correlation between the input and output signal. However, this concept is restricted for single- input-single-output systems. In a system that has multiple inputs and multiple outputs there can exist correlations among the input signals, and transmission paths from the input signals to a particular output. According to Potter (1977), a matrix formulation of coherence for multiple-input-multiple-output system helps to better characterise the correlation among multiple signals. If the multiple input and output signals in the frequency domain are given by $\mathbf{X} = (X_1, X_2, \ldots, X_n)^{\mathrm{T}}$ and $\mathbf{Y} = (Y_1, Y_2, \ldots, Y_m)^{\mathrm{T}}$, respectively, the matrix form of the multiple coherence function can be expressed as

$$\Gamma = \mathrm{E}\left[\mathbf{Y}\mathbf{X}^{\mathrm{H}}\right] \mathrm{E}\left[\mathbf{X}\mathbf{X}^{\mathrm{H}}\right]^{-1} \mathrm{E}\left[\mathbf{Y}\mathbf{X}^{\mathrm{H}}\right]^{\mathrm{H}} \mathrm{E}\left[\mathbf{Y}\mathbf{Y}^{\mathrm{H}}\right]^{-1} \tag{3.9}$$

where E[ ] represents the expected value and the superscript "H" is the Hermitian transformation, i.e. transpose conjugate. For the case of multiple-input-single-output systems, equation 3.9 can be simplified to

$$\gamma^2_{\mathbf{x}y} = \frac{\mathbf{S}^{\mathrm{H}}_{\mathbf{x}y}\mathbf{S}^{-1}_{\mathbf{x}\mathbf{x}}\mathbf{S}_{\mathbf{x}y}}{S_{yy}} \tag{3.10}$$

The concept of multiple coherence can be applied to the present study case to characterise the correlation of the measured output $y(t)$ to the measured input $x(t)$ as well as any other external signal that can be considered as input to the system.

An additional measurement was taken while recording the experimental input and output data in the rig, by recording the external noise in the environment where measurements were taken. This additional external signal (acoustic signal), in addition to the recorded data from the input magnet, are considered as multiple inputs, whereas the output remains the measured signal of the output magnet.

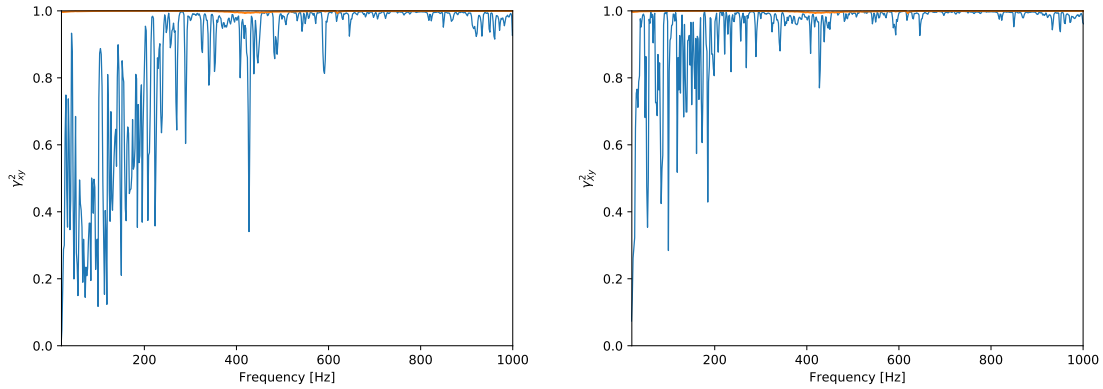

(a) Single-input-single-output. (b) Multiple-inputs-single-output.

Fig. 3.19 Experimental coherence function for a low input case.

In principle, for a low amplitude input to the system, the coherence would have been expected to be close to one as the system behaves nearly linear. However, the coherence below 250 Hz observed in figure 3.19a is significantly low as is the experimental coherence plotted in figure 3.18 for all of the four input cases. As it can be seen in figure 3.19b, the coherence improves when an additional external signal is included as input, i.e. multiple coherence. It can be concluded then that the measured lack of coherence is related to external noise sources in the environment, mostly due to the loud noise recorded by the shaker when it excites the system.

3.5 Discussion

The Statistical Energy Analysis (SEA) approach adopted to analyse a statistical system, as is the case of the flat thin plate of the experimental rig, has been proved to be capable of effectively model the system as an equivalent single-degree-of-freedom system, largely reducing the equations of motion to simplify the analysis in the time domain. The nonlinearity in the transmission path was then easily included in this equivalent system to estimate the response in the time domain from numerical simulations, and the analysis was performed against experimental observations.

Even though the system was not randomised to collect an ensemble of experimental random responses, the power spectral density of the measured displacement for a single realisation does not fluctuate significantly, and therefore, the experimental response agrees with a high degree of accuracy to the estimation from the equivalent damper model, particularly at regions that are not affected by external sources as it was found to be the case below 250 Hz.

The equivalent mass-damper-spring that represents the isolated plate and the magnetic couple has an overdamped nature, and therefore no harmonics are expected in the power spectral density of the response. This issue was demonstrated experimentally and from numerical data gathered from simulations of the equivalent model. In either case, whether harmonics were visible or not in the power spectral density plots, the effect of the nonlinearity in the transmission path was observed experimentally in the coherence plots, and well estimated by the equivalent damper model, as numerical data agrees well with the observations, where a nearly constant reduction of coherence over the frequency band was found for white noise inputs. For the case of the tailored input with a higher amplitude about 210 Hz, the drop in coherence was found only at frequencies where harmonics where prominent.

The advantage of this simplified system relies on the accuracy of the estimation of the mean response of a structural system with statistical nature from simulations in the time domain, which also captures the effect of the nonlinearity in the transmission path in both, the power spectral density of the response as well as in the coherence. Nevertheless, it is limited to model a weakly coupled single structure and therefore, it fails to include the estimation of a coupled subsystem, such as the acoustic cavity in the physical experimental rig.

The analysis here performed to estimate the effects of nonlinearities in the transmission path has been done entirely from data in the time domain. However, in multiple applications of random vibration problems, the time history of a signal is rarely available, but the power spectral density might be known. For the analysis in the frequency domain, if the spectrum of the input is known, the power spectral density of the response can be estimated from the transfer function. As for nonlinear systems there is not such transfer function, chapter 4 focuses in applying the extended Wiener theory in the frequency domain to estimate the

linear and nonlinear components of the power spectral density of the response from Wiener kernels, and analyse the effect of that nonlinearities of second order have in the response of the equivalent damper system here developed.

Chapter 4

Application of the Wiener Series to the Nonlinear Analysis of an SEA Model in the Frequency Domain

4.1 Introduction

A framework based on the SEA approach has been developed in chapter 3, to estimate and quantify the influence of nonlinearities on the dynamic response of a structural system due to nonlinear stiffness in the transmission path. The analysis has been performed from data collected in the time domain, both from experimental measurements and from numerical simulations of the simplified equivalent damper model, where generation of harmonics and the corresponding reduction in coherence have been observed depending on the amplitude of the input. Even though the model is capable to accurately estimate the response and the nonlinear effects, detailed information about the time history of an input signal is not always available. In random vibrations analysis, information about the input signal is given by its power spectral density in the frequency domain, and therefore it is desirable to determine a function that characterises the system to allow to compute the response in the frequency domain. For linear systems, such function is known as the transfer function, and in general terms can be viewed as the ratio between the known output and input. If this concept is applied to a nonlinear system, any output computed with such transfer function, will result in a fraction of the total response of the system, which is given by the coherence. Therefore a further analysis has to be performed to estimate the contribution of the nonlinearities to the total response in the frequency domain, and hence reconstruct the coherence. The Wiener series, initially formulated in the time domain, have been further developed to formulate a

framework to characterise a nonlinear system in the frequency domain from information of the power spectral densities of the input and output (Schetzen, 2006), and hence compute the contribution of the nonlinearities to the total response in the frequency domain.

In this chapter, it is demonstrated that, without loss of generality, Wiener theory can be applied in the frequency domain for inputs that are not necessarily white, but are zero-mean Gaussian processes. Additionally, the power spectral density of each order of the nonlinearity can be derived by autocorrelation. The theory for the first and second order response in the frequency domain has been validated with numerical simulations of a bilinear system, included in the equivalent spring-damper model developed in chapter 3. Additionally, the theory has been applied to reconstruct the total response, and the corresponding coherence, of the structural-acoustic rig that is being the main case study in this research.

4.2 General Concepts on the Wiener Theory

The output $y(t)$ of a time invariant nonlinear system to a stationary input $x(t)$, can be expressed as a summation of the contribution of each order of nonlinearity, i.e.

$$y(t) = y_0(t) + y_1(t) + y_2(t) + y_3(t) + \dots \tag{4.1}$$

where $y_0(t)$ is the mean value, $y_1(t)$ is the linear component, $y_2(t)$ is the response to a quadratic nonlinearity, etc. An early study by Volterra (1887) indicates that each order of the response $y_n(t)$ can be viewed as functionals that depend on the input $x(t)$ and the characteristic of the system of each order of nonlinearity h_n, know as Volterra kernel in the time domain. With this definition, equation 4.1 can be written in a compact form as

$$y(t) = \sum_{n=0}^{\infty} \mathbf{H}_n[h_n, x(t)] \tag{4.2}$$

where $\mathbf{H}_n$ is n^{th} order Volterra functional that has the form

$$y_n(t) = \int_{-\infty}^{\infty} \cdots \int_{-\infty}^{\infty} h_n(\tau_1, \dots, \tau_n)\, x(t-\tau_1) \dots x(t-\tau_n)\, \mathrm{d}\tau_1 \dots \mathrm{d}\tau_n. \tag{4.3}$$

It is know however, that the Volterra theory is not practical to analyse nonlinear systems due to limitations such as convergence and the difficulty to estimate the Volterra kernels. Demetriou (2018), in his doctoral, thesis presents a detailed explanation of the limitations of Volterra series. In order to overcome with such limitations, Wiener (1958) has applied

the Volterra series considering orthogonal functionals. The Wiener representation of the response of each order is then a sumation of orthogonal functionals dependending on the input $x(t)$ and described by kernels k_n that appear in the Volterra series. The total response of the system espressed in terms of Wiener functionals, as presented by Schetzen (2006), can be written as

$$y(t) = \sum_{n=0}^{\infty} \mathbf{G}_n \left[k_n, \sum_{i=0}^{n-1} k_{i(n)}, x(t) \right], \tag{4.4}$$

where the term k_n is known as the n$^{\text{th}}$ order Wiener kernel, whereas $k_{i(n)}$ are the derived kernels of the Wiener G-functional $\mathbf{G}_n$. In general, the derived kernels are functions of k_n, and G-functionals of even orders are dependent of derived kernels with even subindexes only. Likewise, G-functionals of odd orders are dependent of derived kernels with odd subindexes only.

Considering a Gaussian white noise input, Demetriou (2018) has presented a generalised derivation of the Wiener kernels in frequency domain $K_n(\omega_1, \ldots, \omega_n)$ from the definition of kernels in time domain $k_n(\tau_1, \ldots, \tau_n)$, however, little can be found in the literature regarding to the n$^{\text{th}}$ order response of the system in the frequency domain, such as the n$^{\text{th}}$ order power spectral density for non-white Gaussian inputs.

4.2.1 Conventions

When processing signals for the analysis in the frequency domain, quantities such as the Fourier transform or the power spectral density must have consistent units and magnitudes to the signals from where these were derived. Slightly different definitions of the Fourier transform can be found in the literature, such as the sign of the exponential argument or whether a constant $1/2\pi$, $1/\sqrt{2\pi}$ or 1 should be included, among others. Such differences might lead to inconsistencies when comparing the response from estimations and from direct calculations. Hence, a set of conventions are here adopted for application of the Wiener theory in the derivation of the kernels, and the power spectral density of functionals of n$^{\text{th}}$ order

Fourier transform

The convention for Fourier analisis given by Newland (2005) is here adopted, where a factor of $1/2\pi$ is placed on the integral of the time domain signal as it is convenient for random vibration analysis, and the units of the radial frequency ω are rad/s. Therefore, the

double-sided Fourier transform of a signal $x(t)$ is defined as

$$X(\omega) = \frac{1}{2\pi} \int_{-\infty}^{\infty} x(t)\, \mathrm{e}^{-i\omega t} \mathrm{d}t, \tag{4.5}$$

and its inverse, i.e. the original signal in time domain, is given by

$$x(t) = \int_{-\infty}^{\infty} X(\omega)\, \mathrm{e}^{i\omega t} \mathrm{d}\omega. \tag{4.6}$$

Additionally, with this definition of the Fourier transform, the unitary delta function in the frequency domain can be expressed as

$$\delta(\omega) = \frac{1}{2\pi} \int_{-\infty}^{\infty} \mathrm{e}^{-i\omega t} \mathrm{d}t \tag{4.7}$$

Autocorrelation and power spectral density

The autocorrelation function is defined as the expected value of the product between the signal at an arbitrary time and at a delayed time, i.e.

$$R_{xx}(\tau) = \mathrm{E}[x(t)\, x(t+\tau)] = R_{xx}(-\tau) \tag{4.8}$$

In analogue form to the Fourier analysis, the power spectral density of a random signal can be found from its autocorrelation function, and vice versa, from the Wiener-Khinchin theorem (Chatfield, 1996). This two quantities are a Fourier pair and here are defined as

$$S_{xx}(\omega) = \frac{1}{2\pi} \int_{-\infty}^{\infty} R_{xx}(\tau)\, \mathrm{e}^{-i\omega\tau} \mathrm{d}\tau \tag{4.9}$$

$$R_{xx}(\tau) = \int_{-\infty}^{\infty} S_{xx}(\omega)\, \mathrm{e}^{i\omega\tau} \mathrm{d}\omega \tag{4.10}$$

The power spectral density can be conveniently computed from the average of the modulus squared of the signal in time domain. For practical applications, the limits of integration of the Fourier transform of a signal recorded in the time T, i.e. the period, can be placed as from $-T/2$ to $T/2$. With this convention, the double-sided power spectral density

can be expressed in the form

$$S_{xx}(\omega) = \lim_{T\to\infty} \frac{2\pi}{T} \mathrm{E}\left[|X(\omega)|^2\right]. \tag{4.11}$$

4.3 Derivation of the n[th] Order Response in the Frequency Domain

In Hawes (2016) doctoral thesis, a derivation of the first and second order Wiener kernels in the frequency domain can be found. The author has made use of non-white Gaussian inputs and the explicit form of the Wiener functionals in the time domain. A similar approach is followed here to present a generalised form of the n[th] Fourier transform, power spectral density and Wiener kernels.

An n[th] Wiener functional can be explicitly written in the form

$$\begin{aligned} y_n(t) = &\int_{-\infty}^{\infty} \cdots \int_{-\infty}^{\infty} k_n(\tau_1,\ldots,\tau_n)\, x(t-\tau_1)\ldots x(t-\tau_n)\,\mathrm{d}\tau_1\ldots\mathrm{d}\tau_n \\ &+ \sum_{i=1}^{n-1} \int_{-\infty}^{\infty} \cdots \int_{-\infty}^{\infty} k_{i(n)}(\tau_1,\ldots,\tau_i) \prod_{j=1}^{i} x\left(t-\tau_j\right)\mathrm{d}\tau_j \\ &+ k_{0(n)} \end{aligned} \tag{4.12}$$

where, as stated, if the n[th] order is even, kernels with odd subindexes are zero, and vice versa. However, in this analysis, only the first term of the right-hand-side of equation 4.12 is considered, since in the derivation of an expression to measure the Wiener kernels in the frequency domain, the terms with the derived kernels $k_{i(n)}$, which are functions of the Wiener kernel k_n, are cancelled, as demonstrated by Demetriou (2018) for the case of white-noise inputs. Furthermore, it can be proved that for the second order, such terms affect the DC component only, i.e. the mean value of the Fourier transform and Power spectral density.

4.3.1 Fourier Transform of n[th] Order Volterra Functional

Applying the Fourier transform to the first term of the right-hand-side of equation 4.12, and subsequently expressing the inputs $x(t-\tau_n)$ in the form of the inverse Fourier transform, the n[th] order Volterra functional, i.e. the the first term of the Wiener functional, in the frequency

domain can be expressed as

$$\begin{aligned} Y_n(\omega) &= \frac{1}{2\pi}\int_{-\infty}^{\infty}\cdots\int_{-\infty}^{\infty} k_n(\tau_1,\ldots,\tau_n)\,x(t-\tau_1)\ldots x(t-\tau_n)\,\mathrm{e}^{-i\omega t}\mathrm{d}\tau_1\ldots\mathrm{d}\tau_n\mathrm{d}t \\ &= \frac{1}{2\pi}\int_{-\infty}^{\infty}\cdots\int_{-\infty}^{\infty} k_n(\tau_1,\ldots,\tau_n)\,X(\omega_1)\ldots X(\omega_n)\,\mathrm{e}^{-i\omega t}\mathrm{e}^{i\omega_1(t-\tau_1)}\ldots\mathrm{e}^{i\omega_n(t-\tau_n)} \\ &\qquad \mathrm{d}\omega_1\ldots\mathrm{d}\omega_n\mathrm{d}\tau_1\ldots\mathrm{d}\tau_n\mathrm{d}t \\ &= \frac{1}{2\pi}\int_{-\infty}^{\infty}\cdots\int_{-\infty}^{\infty} k_n(\tau_1,\ldots,\tau_n)\,\mathrm{e}^{-i\omega\tau_1}\ldots\mathrm{e}^{-i\omega\tau_n}X(\omega_1)\ldots X(\omega_n)\,\mathrm{e}^{-i(\omega-\omega_1-\ldots-\omega_n)t} \\ &\qquad \mathrm{d}\omega_1\ldots\mathrm{d}\omega_n\mathrm{d}\tau_1\ldots\mathrm{d}\tau_n\mathrm{d}t. \end{aligned} \tag{4.13}$$

The form of the n$^{\text{th}}$ Wiener kernel in the frequency domain can be found by applying n Fourier transforms to $k_n(\tau_1,\ldots,\tau_n)$, i.e.

$$K_n(\omega_1\ldots\omega_n) = \frac{1}{(2\pi)^n}\int_{-\infty}^{\infty}\cdots\int_{-\infty}^{\infty} k_n(\tau_1,\ldots,\tau_n)\,\mathrm{e}^{-i\omega\tau_1}\ldots\mathrm{e}^{-i\omega\tau_n}\mathrm{d}\tau_1\ldots\mathrm{d}\tau_n, \tag{4.14}$$

therefore, equation 4.13 can be expressed in terms of frequency only as

$$\begin{aligned} Y_n(\omega) &= (2\pi)^{n-1}\int_{-\infty}^{\infty}\cdots\int_{-\infty}^{\infty} K_n(\omega_1,\ldots,\omega_n)\,X(\omega_1)\ldots X(\omega_n)\,\mathrm{e}^{-i(\omega-\omega_1-\ldots-\omega_n)t} \\ &\qquad \mathrm{d}\omega_1\ldots\mathrm{d}\omega_n\mathrm{d}t \\ &= (2\pi)^n\int_{-\infty}^{\infty}\cdots\int_{-\infty}^{\infty} K_n(\omega_1,\ldots,\omega_n)\,X(\omega_1)\ldots X(\omega_n)\,\delta(\omega-\omega_1-\ldots-\omega_n) \\ &\qquad \mathrm{d}\omega_1\ldots\mathrm{d}\omega_n. \end{aligned} \tag{4.15}$$

Finally, letting $\omega = \omega_1+\ldots+\omega_n$, the Fourier transform of the n$^{\text{th}}$ order Volterra functional, and the n$^{\text{th}}$ order response in the frequency domain is found to have the form

$$\begin{aligned} Y_n(\omega) = (2\pi)^n\int_{-\infty}^{\infty}\cdots\int_{-\infty}^{\infty} & K_n(\omega_1,\ldots,\omega_{n-1},\omega-\omega_1-\ldots-\omega_{n-1}) \\ & X(\omega_1)\ldots X(\omega_{n-1})\,X(\omega-\omega_1-\ldots-\omega_{n-1})\,\mathrm{d}\omega_1\ldots\mathrm{d}\omega_{n-1}. \end{aligned} \tag{4.16}$$

4.3.2 Power Spectral Density of n[th] Order Volterra Functional

The power spectral density of n[th] order can be found by forming an autocorrelation function of the Volterra functional $y_n(t)$. First, the product of the functional $y_n(t)$ and the delayed functional $y_n(t+\tau)$ can be written explicitly as

$$y_n(t)\,y_n(t+\tau) = \int_{-\infty}^{\infty}\cdots\int_{-\infty}^{\infty} k_n(\tau_1,\ldots,\tau_n)\,k_n(\tau_{n+1},\ldots,\tau_{2n})\,x(t-\tau_1)\ldots x(t-\tau_n)$$
$$x(t+\tau-\tau_{n+1})\ldots x(t+\tau-\tau_{2n})\,\mathrm{d}\tau_1\ldots\mathrm{d}\tau_{2n}. \tag{4.17}$$

Now, taking the averages to both sides of equation 4.17, the left-hand side corresponds to the autocorrelation function of $y_n(t)$, whereas the average of the right-hand side, i.e.

$$\mathrm{E}\left[x(t-\tau_1)\ldots x(t-\tau_n)\,x(t+\tau-\tau_{n+1})\ldots x(t+\tau-\tau_{2n})\right],$$

is the expected value of the product of an even number of zero-mean Gaussian quantities, which, according to Schetzen (2006), can be expressed as a summation of products of the averages of all possible combinations of pairs. To clarify this, if ξ is a Gaussian quantity, the average of the product can be written as

$$\mathrm{E}\left[\xi_1\ldots\xi_{2m}\right] = \sum\prod \mathrm{E}\left[\xi_i\xi_j\right], \quad m = 1,2,3,\ldots, \tag{4.18}$$

where there are $(2m)!/m!2^m$ possible non-repeated combinations. It is found however, that there are only $n!$ possible combinations where all Gaussian variables on the right-hand-side of equation 4.17 are function of τ, hence, assuming symmetry, the average can therefore be expressed as $n!$ times the product of the autocorrelations functions of the input $x(t)$, i.e.

$$n!R_{xx}(\tau_1-\tau_{n+1}+\tau)\ldots R_{xx}(\tau_n-\tau_{2n}+\tau),$$

and the autocorrelation function of the nth Volterra functional, following the same arguments presented in the previous subsection, can be therefore expressed as

$$\begin{aligned}
R_{y_n y_n}(\tau) &= n! \int_{-\infty}^{\infty} \cdots \int_{-\infty}^{\infty} k_n(\tau_1,\ldots,\tau_n)\, k_n(\tau_{n+1},\ldots,\tau_{2n}) \\
&\qquad R_{xx}(\tau_1-\tau_{n+1}+\tau)\ldots R_{xx}(\tau_n-\tau_{2n}+\tau)\,\mathrm{d}\tau_1\ldots\mathrm{d}\tau_{2n} \\
&= n! \int_{-\infty}^{\infty} \cdots \int_{-\infty}^{\infty} k_n(\tau_1,\ldots,\tau_n)\, k_n(\tau_{n+1},\ldots,\tau_{2n})\, S_{xx}(\omega_1)\ldots S_{xx}(\omega_n) \\
&\qquad \mathrm{e}^{i\omega_1(\tau_1-\tau_{n+1}+\tau)}\ldots\mathrm{e}^{i\omega_n(\tau_n-\tau_{2n}+\tau)}\mathrm{d}\tau_1\ldots\mathrm{d}\tau_{2n}\mathrm{d}\omega_1\ldots\mathrm{d}\omega_n \\
&= n! \int_{-\infty}^{\infty} \cdots \int_{-\infty}^{\infty} k_n(\tau_1,\ldots,\tau_n)\,\mathrm{e}^{i\omega_1\tau_1}\ldots\mathrm{e}^{i\omega_n\tau_n} k_n(\tau_{n+1},\ldots,\tau_{2n})\,\mathrm{e}^{-i\omega_1\tau_{n+1}}\ldots\mathrm{e}^{-i\omega_n\tau_{2n}} \\
&\qquad S_{xx}(\omega_1)\ldots S_{xx}(\omega_n)\mathrm{e}^{i(\omega_1+\ldots+\omega_n)\tau}\mathrm{d}\tau_1\ldots\mathrm{d}\tau_{2n}\mathrm{d}\omega_1\ldots\mathrm{d}\omega_n \\
&= n!\,(2\pi)^{2n} \int_{-\infty}^{\infty} \cdots \int_{-\infty}^{\infty} K_n(-\omega_1,\ldots,-\omega_n)\, K_n(\omega_1,\ldots,\omega_n)\, S_{xx}(\omega_1)\ldots S_{xx}(\omega_n) \\
&\qquad \mathrm{e}^{i(\omega_1+\ldots+\omega_n)\tau}\mathrm{d}\omega_1\ldots\mathrm{d}\omega_n. \qquad (4.19)
\end{aligned}$$

Finally, letting $\omega = \omega_1 + \ldots + \omega_n$, and from the definition of the Wiener-Khinchin theorem, given by equation 4.10, the power spectral density of the nth order of the response is found to have the form

$$\begin{aligned}
S_{y_n y_n}(\omega) = n!\,(2\pi)^{2n} \int_{-\infty}^{\infty} \cdots \int_{-\infty}^{\infty} &|K_n(\omega_1,\ldots,\omega_{n-1},\omega-\omega_1-\ldots-\omega_{n-1})|^2 \\
&S_{xx}(\omega_1)\ldots S_{xx}(\omega-\omega_1-\ldots-\omega_{n-1})\,\mathrm{d}\omega_1\ldots\mathrm{d}\omega_{n-1}. \qquad (4.20)
\end{aligned}$$

It is worth stressing that the power spectral density of the nth order of the nonlinearity given by equation 4.20, is valid for the first and second orders, neglecting the DC component. For higher orders, however, all of the terms of the Wiener functional expressed by equation 4.12 must be considered in the derivation.

4.3.3 Measurement of the Wiener Kernel of nth Order

In order to determine the Wiener kernels in the frequency domain, an expression of the nth order cross-correlation must be established. Firstly, the product of the nth Volterra functional

times the n delayed inputs can be expressed as

$$y_n(t)\,x(t-\gamma_1)\ldots x(t-\gamma_n) = \int_{-\infty}^{\infty}\cdots\int_{-\infty}^{\infty} k_n(\tau_1,\ldots,\tau_n)\,x(t-\tau_1)\ldots x(t-\tau_n)$$
$$x(t-\gamma_1)\ldots x(t-\gamma_n)\,\mathrm{d}\tau_1\ldots\mathrm{d}\tau_n. \tag{4.21}$$

By averaging both sides of equation 4.21, the left-hand side represents the n[th] cross-correlation function, and, with the same argument used in the previous subsection, the averaged term of the right-hand-side can be written as $n!$ times the product of n autocorrelation functions of the input $x(t)$, i.e.

$$R_{x^n y_n}(\gamma_1,\ldots,\gamma_n) = n!\int_{-\infty}^{\infty}\ldots\int_{-\infty}^{\infty} k_n(\tau_1,\ldots,\tau_n)\,R_{xx}(\tau_1-\gamma_1)\ldots R_{xx}(\tau_n-\gamma_n)\,\mathrm{d}\tau_1\ldots\mathrm{d}\tau_n \tag{4.22}$$

where γ_n is the time delay. Applying the Wiener-Khinchin theorem to equation 4.22, the n[th] cross-spectrum is found to be

$$\begin{aligned} S_{x^n y_n}(\kappa_1,\ldots,\kappa_n) &= \frac{n!}{(2\pi)^n}\int_{-\infty}^{\infty}\cdots\int_{-\infty}^{\infty} k_n(\tau_1,\ldots,\tau_n)\,R_{xx}(\tau_1-\gamma_1)\ldots R_{xx}(\tau_n-\gamma_n) \\ &\qquad \mathrm{e}^{-i\kappa_1\gamma_1}\ldots\mathrm{e}^{-i\kappa_n\gamma_n}\mathrm{d}\tau_1\ldots\mathrm{d}\tau_n\mathrm{d}\gamma_1\ldots\mathrm{d}\gamma_n, \\ &= \frac{n!}{(2\pi)^n}\int_{-\infty}^{\infty}\cdots\int_{-\infty}^{\infty} K_n(\omega_1,\ldots,\omega_n)\,R_{xx}(\tau_1-\gamma_1)\ldots R_{xx}(\tau_n-\gamma_n) \\ &\qquad \mathrm{e}^{-i\kappa_1\gamma_1}\ldots\mathrm{e}^{-i\kappa_n\gamma_n}\mathrm{e}^{i\omega_1\tau_1}\ldots\mathrm{e}^{i\omega_n\tau_n} \\ &\qquad \mathrm{d}\tau_1\ldots\mathrm{d}\tau_n\mathrm{d}\gamma_1\ldots\mathrm{d}\gamma_n\mathrm{d}\omega_1\ldots\mathrm{d}\omega_n. \end{aligned} \tag{4.23}$$

By letting $\tau_n = \zeta_n + \gamma_n$, and further arrangements, the n$^{\text{th}}$ cross-spectrum can be written in the frequency domain as

$$\begin{aligned} S_{x^n y_n}(\kappa_1,\ldots,\kappa_n) = \frac{n!}{(2\pi)^n} \int_{-\infty}^{\infty}\cdots\int_{-\infty}^{\infty} K_n(\omega_1,\ldots,\omega_n) R_{xx}(\zeta_1)\ldots R_{xx}(\zeta_n) \\ \mathrm{e}^{-i(\kappa_1-\omega_1)\gamma_1}\ldots\mathrm{e}^{-i(\kappa_n-\omega_n)\gamma_n}\mathrm{e}^{i\omega_1\zeta_1}\ldots\mathrm{e}^{i\omega_n\zeta_n} \\ \mathrm{d}\zeta_1\ldots\mathrm{d}\zeta_n\mathrm{d}\gamma_1\ldots\mathrm{d}\gamma_n\mathrm{d}\omega_1\ldots\mathrm{d}\omega_n \\ = n!\int_{-\infty}^{\infty}\cdots\int_{-\infty}^{\infty} K_n(\omega_1,\ldots,\omega_n) S_{xx}(\omega_1)\ldots S_{xx}(\omega_n) \\ \mathrm{e}^{-i(\kappa_1-\omega_1)\gamma_1}\ldots\mathrm{e}^{-i(\kappa_n-\omega_n)\gamma_n}\mathrm{d}\gamma_1\ldots\mathrm{d}\gamma_n\mathrm{d}\omega_1\ldots\mathrm{d}\omega_n \\ = n!(2\pi)^n\int_{-\infty}^{\infty}\cdots\int_{-\infty}^{\infty} K_n(\omega_1,\ldots,\omega_n) S_{xx}(\omega_1)\ldots S_{xx}(\omega_n) \\ \delta(\kappa_1-\omega_1)\ldots\delta(\kappa_n-\omega_n)\mathrm{d}\omega_1\ldots\mathrm{d}\omega_n. \end{aligned} \tag{4.24}$$

Finally, letting the frequency $\kappa_n \to \omega_n$, an expression of the n$^{\text{th}}$ cross-spectrum can found in terms of the n$^{\text{th}}$ order Wiener kernel and the power spectral density of the input of n combinations, which can be expressed as

$$S_{x^n y_n}(\omega_1,\ldots,\omega_n) = n!(2\pi)^n K_n(\omega_1,\ldots,\omega_n) S_{xx}(\omega_1)\ldots S_{xx}(\omega_n). \tag{4.25}$$

It is now required to find an explicit expression of $S_{x^n y_n}$ in terms of the output in the frequency domain, i.e. $Y(\omega)$. Using the definition of the inverse Fourier transform, and

considering that the process is stationary, the n[th] cross-correlation can be written as

$$\begin{aligned}
R_{x^n y_n}(\gamma_1,\ldots,\gamma_n) &= \mathrm{E}\left[\int_{-\infty}^{\infty} Y(\omega)\,\mathrm{e}^{i\omega t}\mathrm{d}\omega \int_{-\infty}^{\infty} X(\omega_1)\,\mathrm{e}^{i\omega_1(t-\gamma_1)}\mathrm{d}\omega_1 \ldots \int_{-\infty}^{\infty} X(\omega_n)\,\mathrm{e}^{i\omega_n(t-\gamma_n)}\mathrm{d}\omega_n\right] \\
&= \mathrm{E}\left[\int_{-\infty}^{\infty}\cdots\int_{-\infty}^{\infty} Y(\omega)X(\omega_1)\ldots X(\omega_n)\,\mathrm{e}^{i\omega t}\mathrm{e}^{i\omega_1 t}\ldots\mathrm{e}^{i\omega_n t}\right. \\
&\qquad \left.\mathrm{e}^{-i\omega_1\gamma_1}\ldots\mathrm{e}^{-i\omega_n\gamma_n}\mathrm{d}\omega\mathrm{d}\omega_1\ldots\mathrm{d}\omega_n\right] \\
&= \frac{1}{T}\int_{-\infty}^{\infty}\mathrm{E}\left[\int_{-\infty}^{\infty}\cdots\int_{-\infty}^{\infty} Y(\omega)X(\omega_1)\ldots X(\omega_n)\,\mathrm{e}^{i\omega t}\mathrm{e}^{i\omega_1 t}\ldots\mathrm{e}^{i\omega_n t}\right. \\
&\qquad \left.\mathrm{e}^{-i\omega_1\gamma_1}\ldots\mathrm{e}^{-i\omega_n\gamma_n}\mathrm{d}\omega\mathrm{d}\omega_1\ldots\mathrm{d}\omega_n\right]\mathrm{d}t
\end{aligned} \tag{4.26}$$

The integrals over the frequency ω and time t can be simplified from equation 4.26 by letting $\omega = \omega_1 + \ldots + \omega_n$ noting that

$$\int_{-\infty}^{\infty}\int_{-\infty}^{\infty} Y(\omega)\,\mathrm{e}^{i\omega t}\mathrm{e}^{i\omega_1 t}\ldots\mathrm{e}^{i\omega_n t}\mathrm{d}\omega\mathrm{d}t = 2\pi Y(-\omega)\,. \tag{4.27}$$

Hence, the n[th] cross-correlation in terms of frequency only can be expressed as

$$\begin{aligned}
R_{x^n y_n}(\gamma_1,\ldots,\gamma_n) &= \frac{2\pi}{T}\mathrm{E}\left[\int_{-\infty}^{\infty}\cdots\int_{-\infty}^{\infty} Y(-\omega)X(\omega_1)\ldots X(\omega_n)\,\mathrm{e}^{-i\omega_1\gamma_1}\ldots\mathrm{e}^{-i\omega_n\gamma_n}\mathrm{d}\omega_1\ldots\mathrm{d}\omega_n\right] \\
&= \int_{-\infty}^{\infty}\cdots\int_{-\infty}^{\infty} S_{x^n y_n}(\kappa_1,\ldots,\kappa_n)\,\mathrm{e}^{-i\omega_1\gamma_1}\ldots\mathrm{e}^{-i\omega_n\gamma_n}\mathrm{d}\omega_1\ldots\mathrm{d}\omega_n,
\end{aligned} \tag{4.28}$$

and, letting $\kappa_n \to \omega_n$, applying the Wiener-Khinchin theorem to equation 4.28 an expression for the n[th] cross-spectrum can be extracted in terms of the output in the frequency domain as

$$S_{x^n y_n}(\omega_1,\ldots,\omega_n) = \frac{2\pi}{n!T}\mathrm{E}\left[Y(-\omega)X(\kappa_1)\ldots X(\kappa_n)\right] \tag{4.29}$$

Finally, the n[th] order Wiener kernel in the frequency domain is found by equating equations 4.25 and 4.29 as

$$K_n(\omega_1,\ldots,\omega_n) = \frac{1}{n!\,(2\pi)^{n-1}\,T}\,\frac{\mathrm{E}[Y^*(\omega)\,X(\omega_1)\ldots X(\omega_n)]}{S_{xx}(\omega_1)\ldots S_{xx}(\omega_n)} \tag{4.30}$$

4.4 Case Study: Bilinear System

In order to test the capability of the Wiener theory to determine the contribution of a higher order of nonlinearity to the response of a nonlinear system, a simple mass-damper-spring is considered, where the spring has a bilinear hardening stiffness in the sense that its magnitude is higher for positive net displacements than for negative displacements about the equilibrium position. An schematic representation of the proposed system is shown in figure 4.1.

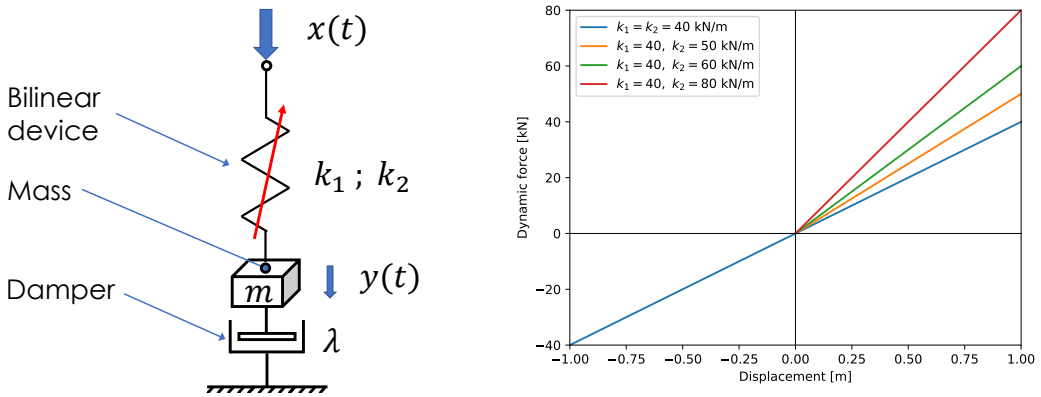

(a) Bilinear system.

(b) Dynamic force vs. displacement.

Fig. 4.1 Description of the characteristic of the bilinear system of the case study.

The equation of motion of the system with bilinear stiffness can be written as

$$m\ddot{y}(t) + \lambda\dot{y}(t) + [\epsilon_a + \epsilon_b \mathrm{sgn}(y(t))]\,y(t) = x(t), \tag{4.31}$$

where ϵ_a and ϵ_b are constants, whose difference gives the lower stiffness k_1 and its sum gives the higher stiffness k_2, depending on whether the displacement $y(t)$ is negative or positive, respectively, accounted by the sign function "sgn( )". The parameters used in equation 4.31 have been chosen to characterise the system as underdamped, in order to clearly visualise the evolution of the harmonics as the nonlinearity is more noticeable. Four cases have been considered, starting with the linear case. The parameters are shown in table 4.1, where there has been also included the averaged natural frequency ω_n.

Table 4.1 Parameters of the nonlinear differential equation of motion of the system.

m [kg]	λ [N-s/m]	Bilinear case $\times 10^3$	$k_1 = \epsilon_a - \epsilon_b$ [kN/m]	$k_2 = \epsilon_a + \epsilon_b$ [kN/m]	ω_n [rad/s]
1	16.4	$\epsilon_a = 40$; $\epsilon_b = 0$	40	40	200.0
		$\epsilon_a = 45$; $\epsilon_b = 5$	40	50	211.8
		$\epsilon_a = 50$; $\epsilon_b = 10$	40	60	222.5
		$\epsilon_a = 60$; $\epsilon_b = 20$	40	80	241.4

4.4.1 Numerical Simulations in the Time Domain

A Gaussian white noise has been considered as force input $x(t)$ to the bilinear system. A random Gaussian process with zero mean and variance equals to one has been generated in MATLAB, and the solver ode45 has been employed to compute a numerical solution of equation 4.31 in the time domain for each of the bilinear cases. The simulations were sampled at 500 Hz, and a total of 20 000 individual realisations were performed with a time length of $T = 5$ s each, comprising the input and output ensembles from where the averages in the frequency domain were taken after a Fourier analysis.

Two frames of 200 s of the response of the system $y(t)$ are plotted in figure 4.2 for the linear case, i.e. $k_1 = k_2 = 40$ N/m, and for the bilinear case where k_2 is twice the lower stiffness k_1. For the linear case, it can be seen that the response is symmetric about zero, i.e the equilibrium position. Furthermore, as the system is linear, it was expected that the distribution of the response is also Gaussian. As the system becomes bilinear, the magnitude of the stiffness for positive displacements is higher, therefore, smaller positive displacements are expected. This can be visualised in figure 4.2c, where the response is not symmetric about zero any more, and the distribution clearly does not fit a Gaussian probability density function.

4.4.2 First and Second Order Wiener Kernels

The application of the Wiener theory for the derivation of the expressions for the n^{th} order response in the frequency domain can, in principle, allows one to reconstruct the total response by adding the contribution of all n orders of the nonlinear response. In practice, a large ensemble is needed for the average $\mathrm{E}[Y^*(\omega_1)X(\omega_1)\ldots X(\omega_n)]$, that appears in the computation of the Wiener kernels, to converge, making it impractical to reconstruct the total response from higher orders of nonlinearity. The aim in this case study, however, is to evaluate whether the response of the system can be reconstructed by adding the contribution

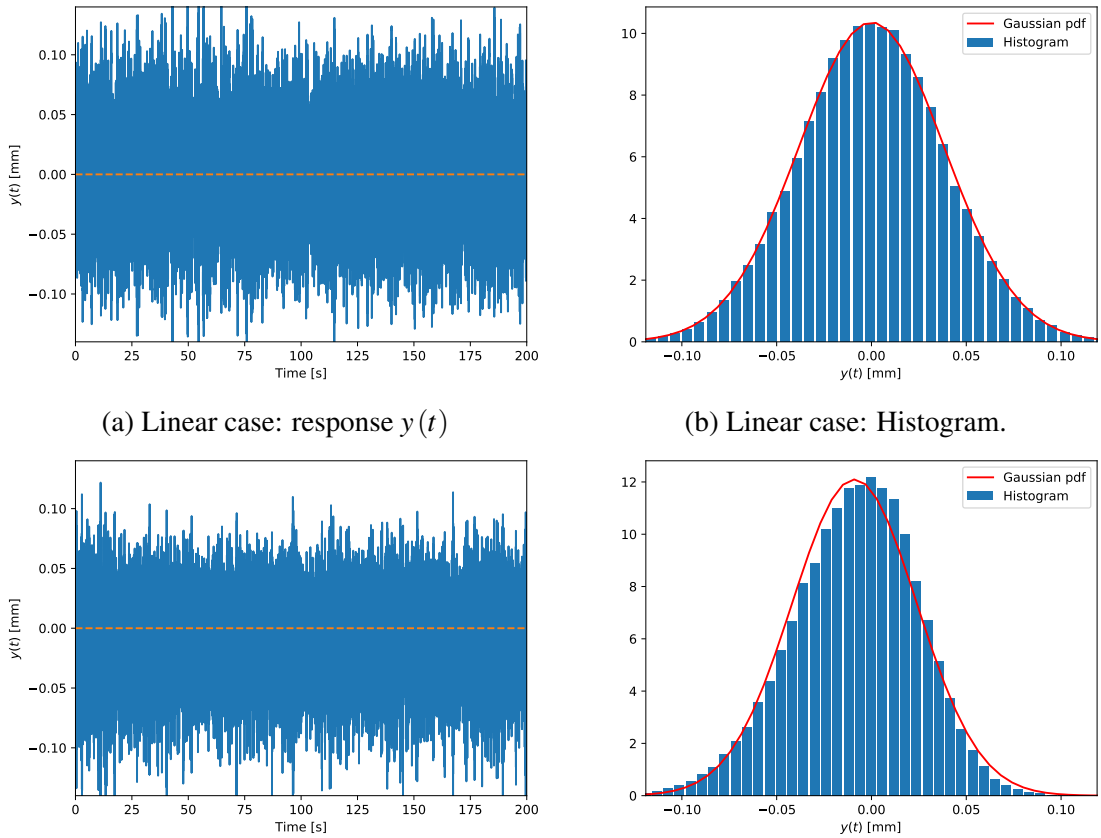

(a) Linear case: response $y(t)$

(b) Linear case: Histogram.

(c) Bilinear case: response $y(t)$

(d) Bilinear case: Histogram.

Fig. 4.2 Response in the time domain to a Gaussian white noise force input $x(t)$.

of the second order to the response of first order, i.e. linear component, when the nonlinearty of the system is weak.

The first order Wiener kernel evaluated from equation 4.30 for the case $n = 1$ and $\omega = \omega_1$, can be written as

$$K_1(\omega) = \frac{1}{T} \frac{\mathrm{E}[Y^*(\omega) X(\omega)]}{S_{xx}(\omega)}, \tag{4.32}$$

which is equivalent to the transfer function of the linear system. Figure 4.3 shows a plot of the single-sided modulus squared first order Wiener kernel $|K(\omega)|^2$, in dB scale, of each of the four cases of bilinearity here considered.

It can be seen that as the nonlinearity is more prominent, i.e. the difference between the stiffnesses k_1 and k_2 increases, the natural frequency increases. This is due to the hardening nature of the stiffness of the system. Additionally, the amplitude of the first order Wiener kernel below the resonance is lower for bilinear cases than for the linear one. This behaviour

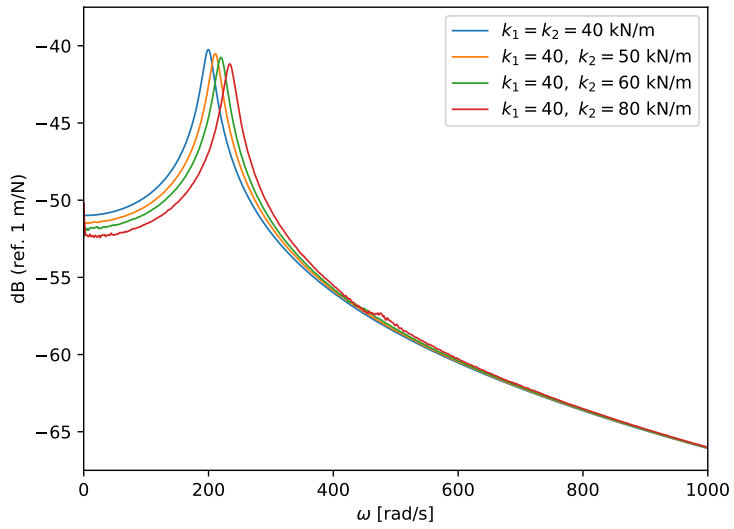

Fig. 4.3 Single-sided squared modulus of the first order Wiener kernels, for each combination of the constants ϵ_a , ϵ_b.

is due to responses of lower amplitude when the stiffness k_2 is higher, making the system to look more stiff.

The use of equation 4.30 for the case $n = 2$ will give an expression of the second order Wiener kernel in terms ω_1 and ω_2. In the notation adopted to derive the expressions of the n$^{\text{th}}$ Fourier transform and the power spectral density, however, the Wiener kernel is expressed in terms of $\omega_1, \ldots \omega_{n-1}, \omega - \omega_1 - \ldots - \omega_{n-1}$. Letting $\omega = \omega_1 + \omega_2$, the second order Wiener kernel can be expressed in terms of ω_1 and $\omega - \omega_1$ in the form

$$K_2(\omega_1, \omega - \omega_1) = \frac{1}{4\pi T} \frac{\mathrm{E}[Y^*(\omega) X(\omega_1) X(\omega - \omega_1)]}{S_{xx}(\omega_1) S_{xx}(\omega - \omega_1)}, \tag{4.33}$$

maintaining the adopted notation to compute the the power spectral density of the second order of the response. The double-sided modulus square of the second order Wiener kernel, plotted in terms of ω and ω_1, is shown in figure 4.4 for each of the four bilinear cases.

As expected, the second order Wiener kernel of the linear case, shown in figure 4.4a looks like very low amplitude noise bouncing around the resonance, and as the ensemble becomes larger, the kernel takes even more negligible values that tend to zero. On the other hand, as it can be seen in figures 4.4b, 4.4c and 4.4d; the second order Wiener kernel takes higher values about the resonance and at the second harmonic, suggesting that the power spectral density of second order could be more significant at these frequencies.

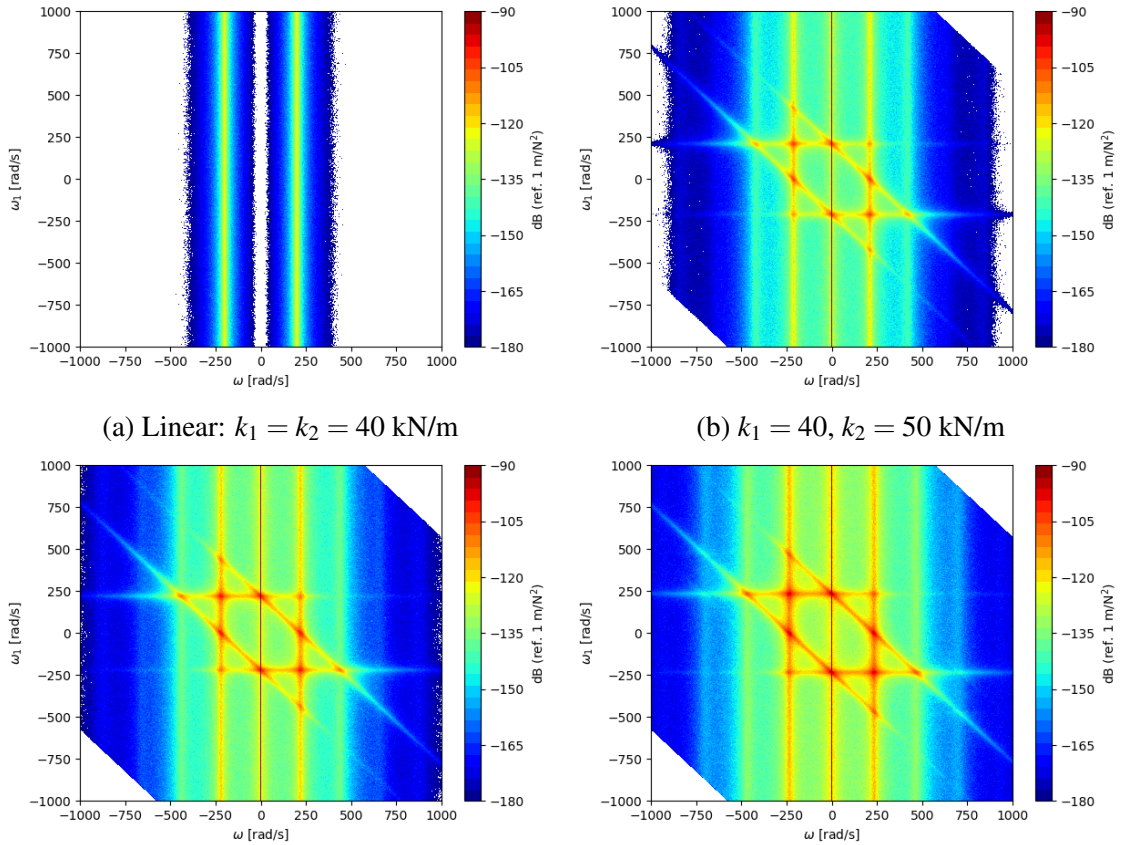

(a) Linear: $k_1 = k_2 = 40$ kN/m

(b) $k_1 = 40$, $k_2 = 50$ kN/m

(c) $k_1 = 40$, $k_2 = 60$ kN/m

(d) $k_1 = 40$, $k_2 = 80$ kN/m

Fig. 4.4 Double-sided squared modulus of the second order Wiener kernel, in dB scale. Values below 180 dB have been deliberately removed (white regions)

4.4.3 Power Spectral Density of First and Second Orders

The response of first order, for the case $n = 1$, can be estimated from equation 4.20 where $\omega = \omega_1$. In this case, there are no integrals and the power spectral density has the form given by the linear theory, i.e.

$$S_{y_1 y_1}(\omega) = (2\pi)^2 |K_1(\omega)|^2 S_{xx}(\omega). \tag{4.34}$$

For the case where $n = 2$, the response of second order has an integral form in the domain ω_1, and, from equation 4.20, the form of the power spectral density of second order is given by

$$S_{y_2 y_2}(\omega) = 2(2\pi)^4 \int_{-\infty}^{\infty} |K_2(\omega_1, \omega - \omega_1)|^2 S_{xx}(\omega_1) S_{xx}(\omega - \omega_1) \, \mathrm{d}\omega_1. \tag{4.35}$$

Results of the single-sided power spectral density are plotted in figure figure 4.5.

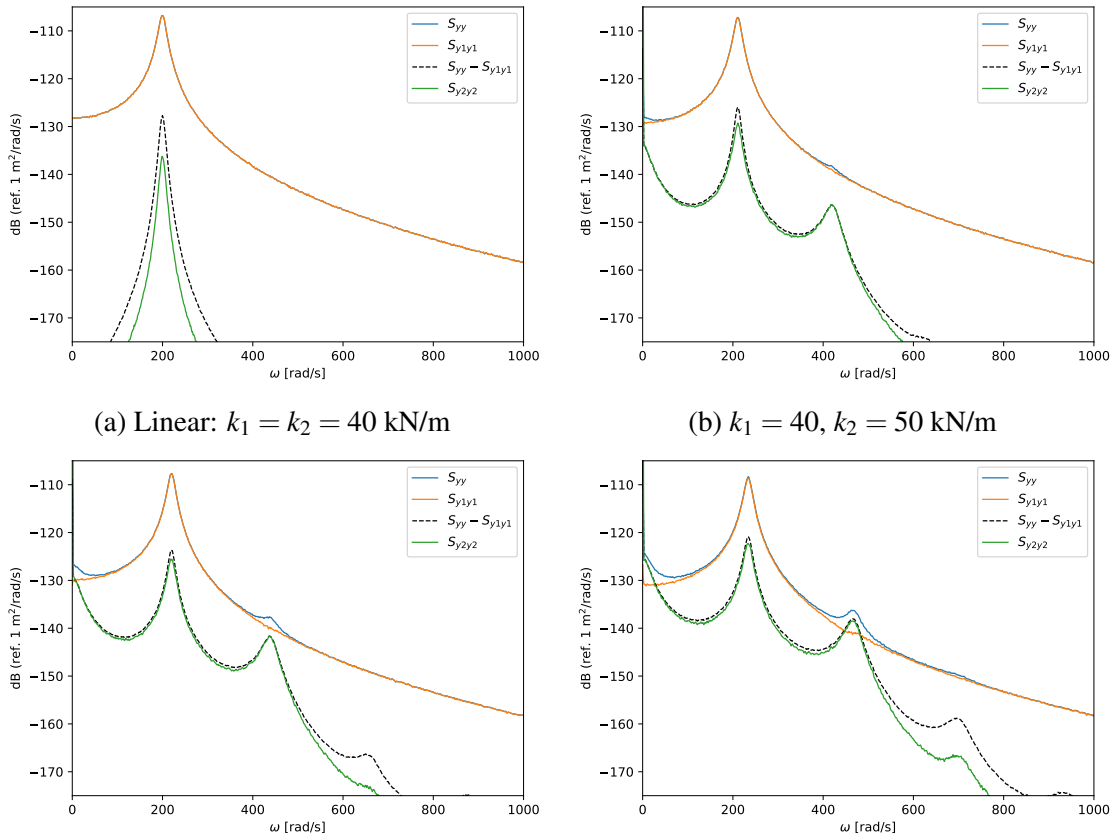

(a) Linear: $k_1 = k_2 = 40$ kN/m

(b) $k_1 = 40$, $k_2 = 50$ kN/m

(c) $k_1 = 40$, $k_2 = 60$ kN/m

(d) $k_1 = 40$, $k_2 = 80$ kN/m

Fig. 4.5 Single-sided power spectral density in dB scale. Blue: power spectral density of the total response; orange: first order response; dashed black: difference between the total and the first order response; green: second order response.

For the linear case, figure 4.5a, the total power spectral density of the response (blue) is coincident with the response first order (orange), as this two curves are overlapped, and the difference between the two is negligible. As the bilinearity is more prominent, it can be seen in figures 4.5b and 4.5c, that there is a discrepancy between the total response and the contribution of first order, that is more noticeable about zero and about the frequency of the second harmonic. This discrepancy, shown by the dashed black curve, is almost coincident with the contribution of the second order in the frequency range up to 500 rad/s. For the case where the stiffness k_2 is twice the magnitude of k_1, shown in figure 4.5d, a slight difference is noticeable at about 720 rad/s, which indicates that the third harmonic is becoming to be significant, and the response of a higher order is needed to overcome such difference.

4.4.4 Coherence Plots

Due to the scale used to plot the power spectral density, it might be difficult to visualise in detail at what degree the contribution of the second order is sufficient to reconstruct the total response of the system. The nth order power spectral density can be normalised with respect to the total response, i.e.

$$\sum_{i}^{n} \frac{S_{y_i y_i}}{S_{yy}} = 1, \tag{4.36}$$

where the ratio of the first order, i.e $S_{y_1 y_1}/S_{yy}$, corresponds to the coherence of the system, and, as it can be viewed as a measure of how linear a system is, it is possible to visualise at which ranges of frequency the nonlinearity of the system has an effect on the response, and the degree at which the fractions of further orders of the response overcome with the loss of coherence. The fraction of first order and second order, as well as the summation, are plotted in figure 4.6

Since the system where $k_1 = k_2$ is linear, it is expected that the coherence is equal to one in the whole frequency range, i.e. the fraction of first order; and the fraction of the second, and further orders, to be zero. This result can be effectively visualised in figure 4.6a, where both, the coherence (blue) and the summation of first and second order (green) are one, except for a small drop at the natural frequency, which was found to be due to leakage and not due to a nonlinear effect. As the bilinearity is more prominent but weak, it can be seen in figures 4.6b and 4.6c that there is loss of coherence at the frequencies near zero and at the second harmonic mostly, and the second order contribution overcomes this loss as the summation is close to one.

For the highest degree of bilinearity in this case study, it was pointed out that a third harmonic can be visualised in the total response of the system. In figure 4.6d, this effect can be seen in the loss of coherence at about 720 rad/s, that is no overcome entirely with the computation of the response of second order, and higher orders of the response are needed for stronger bilinearities.

4.5 Application to the Experimental Rig

The forms of the Wiener kernels in the frequency domain have been employed to calculate the degree of contribution to the response of the flat thin plate of the experimental structural-acoustic rig. The known input to the system, given by the motion of the input magnet, has a higher content of energy about 210 Hz to excite a harmonic at 420 Hz due to the quadratic

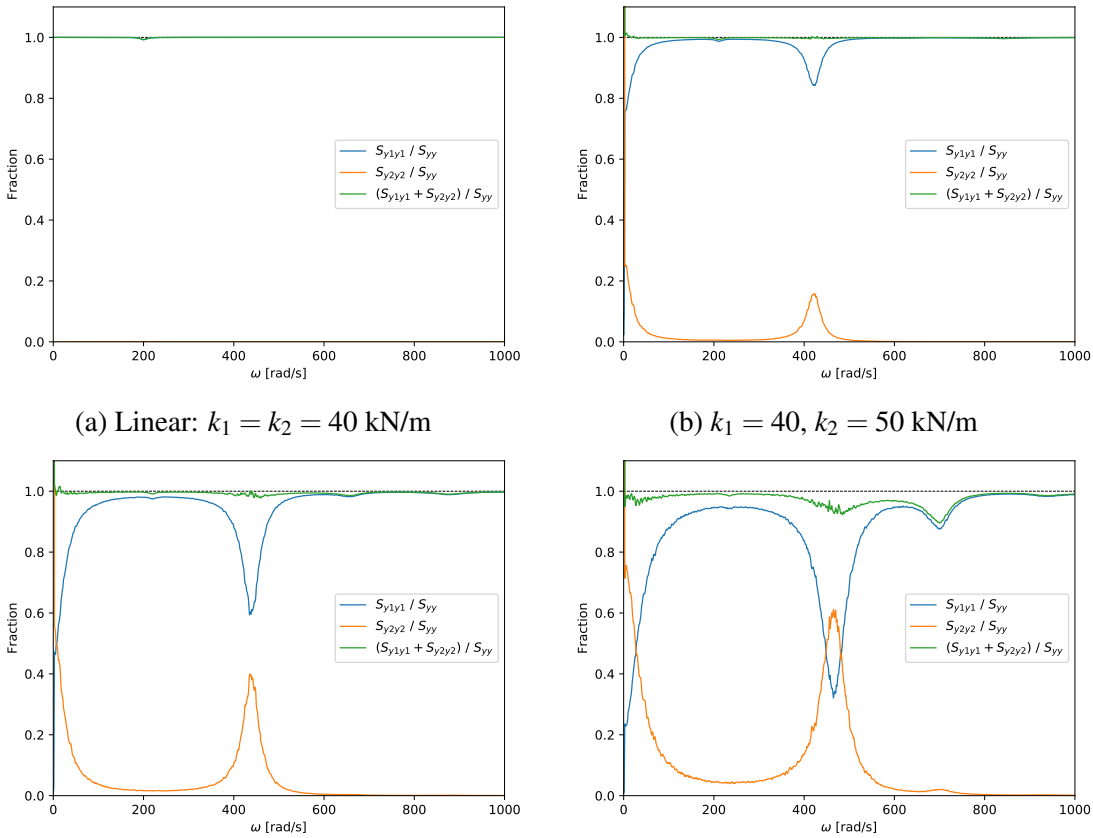

(a) Linear: $k_1 = k_2 = 40$ kN/m

(b) $k_1 = 40$, $k_2 = 50$ kN/m

(c) $k_1 = 40$, $k_2 = 60$ kN/m

(d) $k_1 = 40$, $k_2 = 80$ kN/m

Fig. 4.6 Normalised contribution to the total response of the system. Blue: contribution of first order; orange: contribution of second order; green: first and second order contribution.

component of the nonlinearity, as it was observed in the experimental results presented in chapter 3. Experimental data collected from a long test during 500 s and sampled at 5 Hz were split in a total of 400 individual frames. An ensemble of the Fourier transform of each frame for both the input and output data was created to estimate the Wiener kernels of first and second order, which are plotted in figure 4.7.

The dynamic response of the system, as well as the estimated response contribution of first and second order calculated with equations 4.34 and 4.35, respectively, are shown in figure 4.8.

As expected, the linear component of the transmission path has a high content of amplitude at about 210 Hz, as the input has most of the energy about such frequency, whereas no information is given with respect to the second harmonic. On the other hand, the response of the second order estimates at a relatively high accuracy most of the remaining difference of the response, given by the dashed line in figure 4.8, including the response at the second

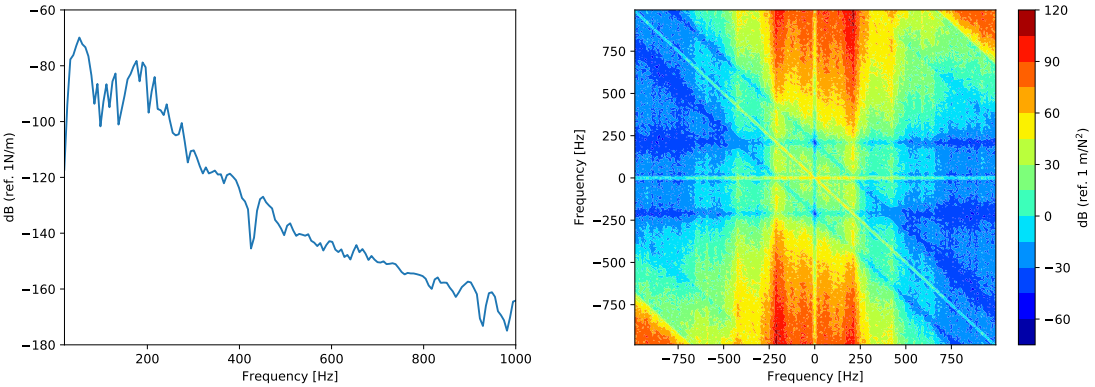

(a) $|K_1|^2$ (b) $|K_2|^2$

Fig. 4.7 Modulus squared of the first and second order Wiener kernels.

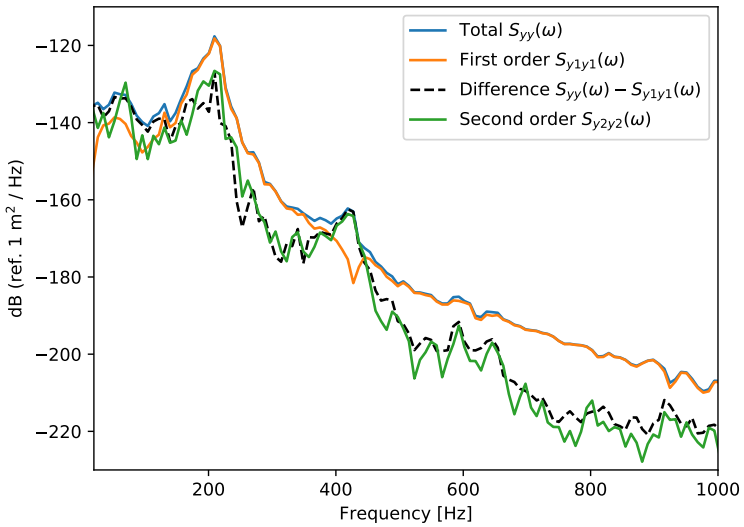

Fig. 4.8 Displacement power spectral density of the brass thin plate at the point of excitation. Blue: total response of the system; orange: contribution of first order, dashed black: difference between the total response and the first order contribution; green: contribution of second order.

harmonic. Even though the level of the power spectral density of the response of second order is about the expected, it is actually slightly above the difference given by the black dashed line. The reason for this is that the average of the product of three Gaussian quantities, given by the second order Wiener Kernel, converges from above, and a large number of individual frames would be required to get the average converged to a more acceptable value. This issue is better visualised in the coherence plots that represent the ratio between each

contribution to the total, shown in figure 4.9, and therefore it is expected that the sum of both ratios, presented in figure 4.10, take values between 0 and 1.

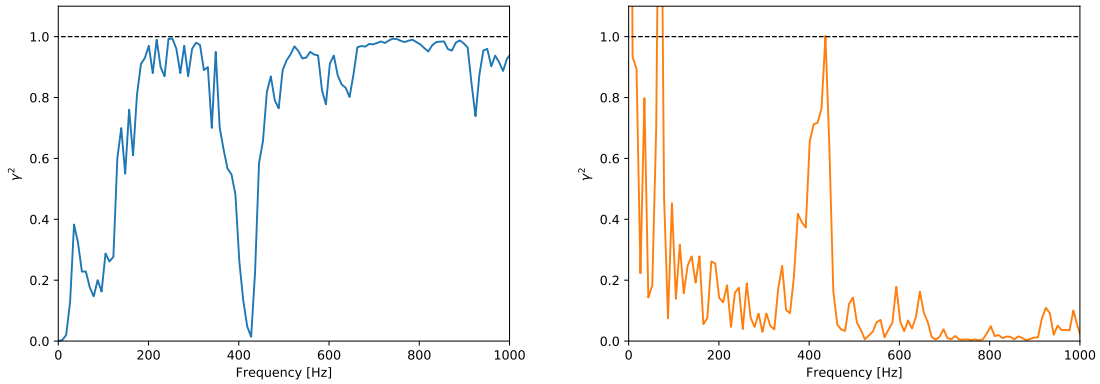

(a) First order to the total response.

(b) Second order to the total response.

Fig. 4.9 Ratio between the contribution of first and second orders to the total response of the nonlinear system.

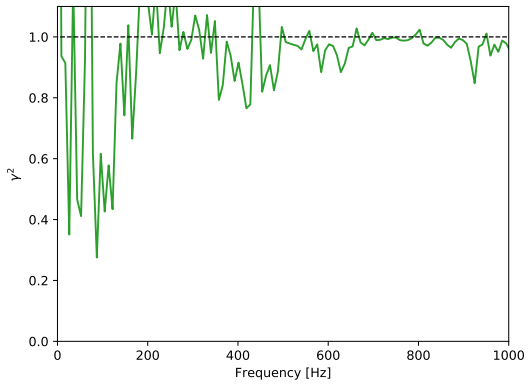

Fig. 4.10 Ratio between the sum of the contribution of first and second orders to the total response of the nonlinear system.

Even though the reconstructed coherence takes values larger than one at several frequencies, as can be observed in figure 4.10, it can be concluded that the approach estimates at a relatively good degree the contribution of second order, plotted in figure 4.9b, except below 250 Hz since, as discussed on chapter 3, the lack of coherence at this low frequency range is due to external sources of noise in the environment. A better agreement with a total coherence between 0 and 1 at each frequency in the range of interest, can be achieved by recording experimental data from a test running for longer time.

4.6 Discussion

Any continuous nonlinear function can be expressed as a sum of multiple components of n orders, as from a Taylor expansion. The Wiener series uses this concept to express the response of a linear system a sum of n orders, where the zeroth and first orders are the mean and the linear components, and their application to compute the components of the response of the system of higher orders have been proved successful from data gathered from simulations of the equivalent damper model.

The use of a theoretical bilinear spring as interface between the input and the structural system (flat thin plate) allows one to visualise the generation of harmonics of second, third and further orders as the difference between the stiffness at negative and positive net displacements increases. For the cases here analysed, its can be seen that the second order nonlinearity is dominant, where the third order is visible when the nonlinear stiffness at positive displacements is as much as twice the stiffness at negative ones. Therefore, the contribution of the nonlinearity estimated from the Wiener kernels is sufficient to reconstruct the coherence between the input and output, i.e. the ratio of the first and second order responses to the total. This dominant contribution of second order of nonlinearity was also validated from experimental data collected in the test rig, where a drop in coherence at the second harmonic at 420 Hz was observed due to the input with high content of energy at 210 Hz, as presented in one of the experimental tests chapter 3. In addition, the reconstructed coherence is low at frequencies below 250 Hz, where it was demonstrated that this is due to the background noise in the environment from several sources, including the sound produced by the shaker when it is in action, as it was confirmed by the multiple coherence analysis that included the external acoustic signal recorded by a microphone located next to the shaker.

The main drawback of the formulation of the components of the response to higher orders of nonlinearity in terms of Wiener kernels, is that many individual frames are required to have the average of Gaussian quantities converged to value at each frequency. This, in addition to the need of computation of all possible combinations of $\omega_1 + \omega_2 + \ldots + \omega_n$ at ω makes the current formulation unreliable for applications such as active noise control, where the total output needs to be readily estimated from the characteristic set of functions of the nonlinear system. This issue is a matter of further investigation to improve the formulation in order to reduce the number of frames needed to compute the required averages in the frequency domain, by considering the response of nonlinear orders as uncorrelated signals in a multiple input single output system.

Chapter 5

Hybrid FE-SEA Method: Derivation for Prescribed Forces and Displacements

5.1 Introduction

It has been stated that the vibroacoustic-analysis of complex built-up systems can be performed by adopting standard methods such as the Finite Element approach (FE), or Boundary Element methods (BE), however these techniques are limited to a low-frequency range due to the large number of degrees of freedom that would be needed to model short wavelengths of higher frequencies. Furthermore, the dynamic response of a system can be sensitive to imperfections making the response to have a statistical behaviour rather than deterministic. The latter case, i.e. high frequency analysis, can be performed by a Statistical Energy Analysis (SEA), as presented in chapter 2, to estimate the mean response and variance, in terms of vibrational energy. The capability of both, the FE and SEA approaches, can be combined to analyse the mid-frequency range (Cicirello et al., 2012) in what is known as the hybrid FE-SEA method.

Hybrid FE-SEA techniques have been developed and improved over the past two decades, and have been addressed to model vibro-acoustic systems comprised by deterministic structures, such as stiff frames, and statistical components like flat thin plates. The resulting number of degrees of freedom of the equations of motion are largely reduced, as only the deterministic systems need to be discretised, and each of the statistical subsystems contributes with one variable only, i.e. the statistical mean energy. Shorter and Langley (2005a) have initially derived the equations of a hybrid method where the compatibility between a displacement-based and a energy-based models have been made possible from the diffuse

field reciprocity relationship for structural-acoustic systems, previously developed by Shorter and Langley (2005b)

The built-up system comprised by a structural-acoustic subsystems excited through a nonlinear device, which is the reference model in this study, can be viewed as a deterministic-statistical system, where, as already described, the flat thin plate and the acoustic cavity are statistical components, and the nonlinear interface can be considered to be a deterministic subsystem. Therefore, a hybrid FE-SEA model can be in principle adopted to analyse the structural and acoustic response and the influence, or otherwise, of the nonlinearities in the vibrations transmission path. However, the current state of art of this approach has two major drawbacks that need to be addressed. Firstly, the equations of motion are derived for prescribed forces exciting one or more degrees of freedom of the system, but the input in this case study is given as prescribed displacements rather than forces. Secondly the dynamic stiffness matrix of the deterministic subsystems considers only constant spring stiffness, therefore, the method must be improved to analyse systems with nonlinear relations between force and displacement of the deterministic components of the built-up system.

This chapter is concerned in deriving a generalised set of equations of a hybrid FE-SEA approach to estimate the mean response of a complex deterministic-statistical system, where the inputs are given in terms of prescribed forces and/or displacements to the deterministic degrees of freedom. It was found that the equations are not necessarily reversible, meaning that if a set of displacements displacements estimated from the hybrid approach with prescribed forces are used as input to the same randomised system, the response will be altered due to the statistical nature of the system. The generalised form of the hybrid FE-SEA equations are validated with numerical results from Monte Carlo FE simulations performed in a complex statistical-deterministic system.

5.2 General Concepts of the Hybrid FE-SEA Approach

One of the key concepts that allows to couple a displacement-based approach with a energy-based approach is the diffuse field reciprocity, initially presented by Shorter and Langley (2005b), and further extended by Langley (2007), which, in general terms, indicates that the diffuse field excitation is proportional to the radiation impedance at the point where the force is applied in a statistical system. Considering a system that has both deterministic and random boundaries, the deterministic boundaries are any of the regions that are connected to other systems or excited by an external force, allowing energy transfer; whereas random boundaries are those that are not known precisely. In absence of random boundaries, the response of the system can be referred to as the "direct field" of the deterministic boundary,

and the deterministic degrees of freedom, $\mathbf{q}_{\mathrm{d}}$ due to an excitation force $\mathbf{f}_{\mathrm{d}}$ can be directly correlated by the direct field dynamic stiffness matrix $\mathbf{D}_{\mathrm{dir}}$ (Shorter and Langley, 2005b).

To account the effects of the scattering of the direct field in the response of the system, it is assumed that the influence of the random boundary can be represented by a "blocked force" $\mathbf{f}_{\mathrm{rev}}$ acting on the deterministic boundary. Hence, the forces and degrees of freedom of a system can be related as

$$\mathbf{D}_{\mathrm{dir}}\mathbf{q}_{\mathrm{d}} = \mathbf{f}_{\mathrm{d}} + \mathbf{f}_{\mathrm{rev}} \tag{5.1}$$

The reverberant field can be related to the direct field, considering that after a wave is reflected in a random boundary it can be incident to the deterministic boundary, and then scattered into a single outgoing direct field component. With this argument, Shorter and Langley (2005b) explain that the statistics of the "blocked reverberant force" can be estimated if the statistics of the reverberant field components are known, and as the amplitudes of the direct and reverberant fields are can be correlated by means of a scattering matrix. In order to have an ensemble with the maximum uncertainty (minimum information about random boundaries), the mean of such scattering matrix over an ensemble must be equal zero, and therefore the statistics of $\mathbf{f}_{\mathrm{rev}}$ can be expressed as

$$\mathrm{E}\left[\mathbf{f}_{\mathrm{rev}}\right] = 0 \tag{5.2}$$

$$\mathrm{E}\left[\mathbf{f}_{\mathrm{rev}}\mathbf{f}_{\mathrm{rev}}^{H}\right] = \alpha \mathrm{Im}\left\{\mathbf{D}_{\mathrm{dir}}\right\} \tag{5.3}$$

Shorter and Langley (2005b) indicate that equation 5.3 represents the diffuse-field reciprocity and can be interpreted as: "the magnitude of a reverberant force on a connection to a diffuse field is proportional to the resistive radiation impedance". In other words, the statistics of the reverberant force can be determined from the resistive part of the direct field dynamic stiffness matrix. The proportionality factor α describes the amplitude of the reverberant field, and is found to be a function of the total energy of the statistical subsystem in the form

$$\alpha = \frac{4E}{\pi\omega n} \tag{5.4}$$

where E is the total energy contained in the system, and n is the asymptotic modal density. Shorter and Langley (2005a) have employed the reciprocity to generalise the calculation of coupling loss factors and to develop a hybrid FE-SEA approach to analyse the vibro-acoustics in the mid-frequency range.

It is worth mentioning that further developments on the reciprocity has been carried out by Langley (2007), where the author has adopted a modal approach to derive a generalised

expression of the reciprocity relationship for non-fully diffuse fields. This extended result is expressed as

$$\mathrm{E}\left[\mathbf{f}_{\mathrm{rev}}\mathbf{f}_{\mathrm{rev}}^{H}\right] = \frac{4E}{\pi\omega n}\mathrm{Im}\left\{\mathbf{D}_{\mathrm{dir}}\right\} + \frac{2}{\pi m}\left(2\mathrm{Re}\left\{\mathbf{S}_{\mathrm{ff}}\right\} + q(m)\mathbf{S}_{\mathrm{ff}}\right) \tag{5.5}$$

where $\mathbf{S}_{\mathrm{ff}}$ is the cross spectral matrix of the applied force, and $q(m)$ is a function that depends on the statistics of the random point process. This generalised expression helps to overcome with some difficulties arising when computing energy variance. However, Langley (2010) indicates that the first term on the right side of the previous expression is dominant in the majority of cases of interest, as is the case of systems with large number of degrees of freedom on the boundaries with random uncorrelated forcing.

5.3 General Derivation of the Hybrid FE-SEA Equations

The equations of motion of individual statistical systems with a number of deterministic degrees of freedom at the boundaries, expressed by the matrix equation 5.1, can be included in the the governing equations of motion of a complex deterministic-statistic system in the form

$$\mathbf{D}_{\mathrm{tot}}\mathbf{q} = \mathbf{f}_{\mathrm{ext}} + \sum_{j}\mathbf{f}_{\mathrm{rev}}^{(j)}, \tag{5.6}$$

where $\mathbf{q}$ is the vector of displacements of the degrees of freedom of the system, $\mathbf{f}_{\mathrm{ext}}$ is the set of external forces applied to the system, $\mathbf{f}_{\mathrm{rev}}^{(j)}$ is the force arising from the reverberant field of the j^{th} statistical subsystem, and the $\mathbf{D}_{\mathrm{tot}}$ is the sum of the deterministic matrix of the system $\mathbf{D}_{\mathrm{d}}$, that can be obtained from an FE model, and the corresponding direct field matrices of each j^{th} statistical system $\mathbf{D}_{\mathrm{dir}}^{(j)}$, i.e.

$$\mathbf{D}_{\mathrm{tot}} = \mathbf{D}_{\mathrm{d}} + \sum_{j}\mathbf{D}_{\mathrm{dir}}^{(j)} \tag{5.7}$$

With the purpose of expressing the set of equations of motion as function of prescribed displacements and forces, equation 5.6 can be written as

$$\begin{pmatrix}\mathbf{D}_{\mathrm{pp}} & \mathbf{D}_{\mathrm{pf}}\\ \mathbf{D}_{\mathrm{fp}} & \mathbf{D}_{\mathrm{ff}}\end{pmatrix}_{\mathrm{tot}}\begin{pmatrix}\mathbf{q}_{\mathrm{p}}\\ \mathbf{q}_{\mathrm{f}}\end{pmatrix} = \begin{pmatrix}0\\ \mathbf{f}_{\mathrm{ext}}\end{pmatrix} + \sum_{j}\begin{pmatrix}0\\ \mathbf{f}_{\mathrm{rev}}^{(j)}\end{pmatrix}, \tag{5.8}$$

where the subindexes "$_{\mathrm{p}}$" and "$_{\mathrm{f}}$" denote "prescribed" and "free/forced", respectively. The total dynamic stiffness matrix has been also rearranged as a set sub-matrices. It is assumed

that there are no external forces applied to the degrees of freedom whose displacements have been already prescribed. With this notation, the averaged the cross-spectral matrix of displacements can also be written as a set of sub-matrices in the form

$$\mathbf{S}_{\mathrm{qq}} = \begin{pmatrix} \mathrm{E}\left[\mathbf{q}_{\mathrm{p}}\mathbf{q}_{\mathrm{p}}^{\mathrm{H}}\right] & \mathrm{E}\left[\mathbf{q}_{\mathrm{p}}\mathbf{q}_{\mathrm{f}}^{\mathrm{H}}\right] \\ \\ \mathrm{E}\left[\mathbf{q}_{\mathrm{f}}\mathbf{q}_{\mathrm{p}}^{\mathrm{H}}\right] & \mathrm{E}\left[\mathbf{q}_{\mathrm{f}}\mathbf{q}_{\mathrm{f}}^{\mathrm{H}}\right] \end{pmatrix} \tag{5.9}$$

where $\mathrm{E}[\,]$ is the operator of expectation or average over an ensemble and the superindex "$^{\mathrm{H}}$" denotes "Hermitian", i.e. the conjugate transpose operation. Note that the motion of the degrees of freedom where the displacements are prescribed, $\mathbf{q}_{\mathrm{p}}$, is deterministic, and therefore the average is only taken on the displacements of the degrees of freedom that may or may not be forced, $\mathbf{q}_{\mathrm{f}}$, which are unknown. Performing the matrix product of the second row of equation 5.8, the latter set of displacement, can be written as

$$\mathbf{q}_{\mathrm{f}} = \mathbf{D}_{\mathrm{ff}}^{-1}\left(\mathbf{f}_{\mathrm{ext}} + \sum_{j}\mathbf{f}_{\mathrm{rev}}^{(j)} - \mathbf{D}_{\mathrm{pf}}\mathbf{q}_{\mathrm{p}}\right) \tag{5.10}$$

$$\mathbf{q}_{\mathrm{f}}^{\mathrm{H}} = \left(\mathbf{f}_{\mathrm{ext}}^{\mathrm{H}} + \sum_{k}\mathbf{f}_{\mathrm{rev}}^{\mathrm{H}(k)} - \mathbf{q}_{\mathrm{p}}^{\mathrm{H}}\mathbf{D}_{\mathrm{pf}}^{\mathrm{H}}\right)\mathbf{D}_{\mathrm{ff}}^{-\mathrm{H}}, \tag{5.11}$$

Assuming that the ensemble has the maximum uncertainty, according to the diffuse field reciprocity, the average of the reverberant forces and the product tend to the following limits:

$$\mathrm{E}\left[\mathbf{f}_{\mathrm{rev}}^{(j)}\right] = 0 \tag{5.12}$$

$$\sum_{j,k}\mathrm{E}\left[\mathbf{f}_{\mathrm{rev}}^{(j)}\mathbf{f}_{\mathrm{rev}}^{(k)}\right] = \sum_{j}\frac{4E_j}{\pi\omega n_j}\mathrm{Im}\left\{\mathbf{D}_{\mathrm{dir}}^{(j)}\right\}, \tag{5.13}$$

respectively, where E_j and n_j are the energy and the modal density of the j^{th} statistical subsystem. Hence, the entries of the matrix of equation 5.9 can be explicitly expressed as

$$\mathrm{E}\left[\mathbf{q}_{\mathrm{p}}\mathbf{q}_{\mathrm{p}}^{\mathrm{H}}\right] = \mathbf{S}_{\mathbf{q}_{\mathrm{p}}\mathbf{q}_{\mathrm{p}}} \tag{5.14}$$

$$\mathrm{E}\left[\mathbf{q}_{\mathrm{p}}\mathbf{q}_{\mathrm{f}}^{\mathrm{H}}\right] = \left(\mathbf{q}_{\mathrm{p}}\mathbf{f}_{\mathrm{ext}}^{\mathrm{H}} - \mathbf{S}_{\mathbf{q}_{\mathrm{p}}\mathbf{q}_{\mathrm{p}}}\mathbf{D}_{\mathrm{fp}}^{\mathrm{H}}\right)\mathbf{D}_{\mathrm{ff}}^{-\mathrm{H}} \tag{5.15}$$

$$\mathrm{E}\left[\mathbf{q}_{\mathrm{f}}\mathbf{q}_{\mathrm{p}}^{\mathrm{H}}\right] = \mathrm{E}\left[\mathbf{q}_{\mathrm{p}}\mathbf{q}_{\mathrm{f}}^{\mathrm{H}}\right]^{\mathrm{H}} \tag{5.16}$$

$$\mathrm{E}\left[\mathbf{q}_{\mathrm{f}}\mathbf{q}_{\mathrm{f}}^{\mathrm{H}}\right] = \mathbf{D}_{\mathrm{ff}}^{-1}\left(\mathbf{S}_{\mathrm{FF}} + \sum_{j}\frac{4E_j}{\pi\omega n_j}\mathrm{Im}\left\{\mathbf{D}_{\mathrm{dir,\,ff}}^{(j)}\right\}\right)\mathbf{D}_{\mathrm{ff}}^{-\mathrm{H}}, \tag{5.17}$$

where $\mathbf{S}_{\mathbf{q}_\mathrm{p}\mathbf{q}_\mathrm{p}}$ is the cross-spectral matrix of the prescribed displacements, and $\mathbf{S}_{\mathrm{FF}}$ can be viewed as the total deterministic external input applied to the system given by

$$\mathbf{S}_{\mathrm{FF}} = \mathbf{S}_{\mathbf{f}\mathbf{f}_{\mathrm{ext}}} - \mathbf{f}_{\mathrm{ext}}\mathbf{q}_\mathrm{p}^\mathrm{H}\mathbf{D}_{\mathrm{fp}}^\mathrm{H} - \mathbf{D}_{\mathrm{fp}}\mathbf{q}_\mathrm{p}\mathbf{f}_{\mathrm{ext}}^\mathrm{H} + \mathbf{D}_{\mathrm{fp}}\mathbf{S}_{\mathbf{q}_\mathrm{p}\mathbf{q}_\mathrm{p}}\mathbf{D}_{\mathrm{fp}}^\mathrm{H}, \tag{5.18}$$

where $\mathbf{S}_{\mathbf{f}\mathbf{f}_{\mathrm{ext}}}$ is the cross-spectral matrix of the external applied force.

5.3.1 Hybrid FE-SEA Equations

The power into the j$^{\mathrm{th}}$ statistical subsystem can be expressed in terms of the displacements of the degrees of freedom, $\mathbf{q}$, and the direct and reverberant components of the dynamic stiffness matrix of the subsystem, $\mathbf{D}_{\mathrm{dir}}^{(j)}$ and $\mathbf{D}_{\mathrm{rev}}^{(j)}$, respectively, in the form

$$P_{\mathrm{in}}^{(j)} = \frac{\omega}{2}\mathbf{q}^\mathrm{H}\left[\mathbf{D}_{\mathrm{dir}}^{(j)} + \mathbf{D}_{\mathrm{rev}}^{(j)}\right]\mathbf{q}. \tag{5.19}$$

Noting that the product $\mathbf{D}_{\mathrm{rev}}^{(j)}\mathbf{q}$ is the negative reverberant force, equation 5.19 can be rewritten for a set of prescribed and free/forced degrees of freedom as

$$P_{\mathrm{in}}^{(j)} = \frac{\omega}{2}\begin{pmatrix}\mathbf{q}_\mathrm{p}^\mathrm{H} & \mathbf{q}_\mathrm{f}^\mathrm{H}\end{pmatrix}\begin{pmatrix}\mathbf{D}_{\mathrm{dir,\,pp}}^{(j)} & \mathbf{D}_{\mathrm{dir,\,pf}}^{(j)} \\ \mathbf{D}_{\mathrm{dir,\,fp}}^{(j)} & \mathbf{D}_{\mathrm{dir,\,ff}}^{(j)}\end{pmatrix}\begin{pmatrix}\mathbf{q}_\mathrm{p} \\ \mathbf{q}_\mathrm{f}\end{pmatrix} + \frac{\omega}{2}\begin{pmatrix}\mathbf{q}_\mathrm{p}^\mathrm{H} & \mathbf{q}_\mathrm{f}^\mathrm{H}\end{pmatrix}\begin{pmatrix}0 \\ -\mathbf{f}_{\mathrm{rev}}\end{pmatrix}. \tag{5.20}$$

Inserting equations 5.10 and 5.11 in equation 5.20, the power into the j$^{\mathrm{th}}$ statistical subsystem can be expressed explicitly by the deterministic and random terms, due to the reverberant forces, in the form

$$P_{\mathrm{in}}^{(j)} = \frac{\omega}{2}\left[\mathbf{q}_\mathrm{p}^\mathrm{H}\mathbf{D}_{\mathrm{dir,\,pp}}^{(j)}\mathbf{q}_\mathrm{p} + \mathbf{q}_\mathrm{p}^\mathrm{H}\mathbf{D}_{\mathrm{dir,\,pf}}^{(j)}\mathbf{q}_\mathrm{f} + \mathbf{q}_\mathrm{f}^\mathrm{H}\mathbf{D}_{\mathrm{dir,\,fp}}^{(j)}\mathbf{q}_\mathrm{p} + \left(\mathbf{f}_{\mathrm{ext}}^\mathrm{H} - \mathbf{q}_\mathrm{p}^\mathrm{H}\mathbf{D}_{\mathrm{fp}}^\mathrm{H}\right)\mathbf{D}_{\mathrm{ff}}^{-\mathrm{H}}\mathbf{D}_{\mathrm{dir,\,ff}}^{(j)}\mathbf{D}_{\mathrm{ff}}^{-1}\left(\mathbf{f}_{\mathrm{ext}} - \mathbf{D}_{\mathrm{fp}}\mathbf{q}_\mathrm{p}\right)\right] \tag{5.21a}$$

$$+\frac{\omega}{2}\left[\sum_k \mathbf{f}_{\mathrm{rev}}^{\mathrm{H}(k)}\mathbf{D}_{\mathrm{ff}}^{-\mathrm{H}}\mathbf{D}_{\mathrm{dir,\,ff}}^{(j)}\mathbf{D}_{\mathrm{ff}}^{-1}\mathbf{f}_{\mathrm{rev}}^{(j)}\right] \tag{5.21b}$$

$$-\frac{\omega}{2}\left[\sum_k \mathbf{f}_{\mathrm{rev}}^{\mathrm{H}(k)}\mathbf{D}_{\mathrm{ff}}^{-\mathrm{H}}\mathbf{f}_{\mathrm{rev}}^{(j)}\right]. \tag{5.21c}$$

The deterministic part given by the term 5.21a is known as the external power into the j$^{\mathrm{th}}$ subsystem due to prescribed forces and/or displacements, $P_o^{(j)}$. Inserting the components of the cross-spectral matrix of displacements given by equations 5.14 to 5.17, as well as the total deterministic external force given by equation 5.18,and considering that the power due

to the displacement depends on the imaginary part of the direct field matrix only, the external power input can be explicitly expressed as

$$\begin{aligned} P_o^{(j)} = & \frac{\omega}{2}\sum_{r,s}\mathrm{Im}\left\{D^{(j)}_{\text{dir pp, }rs}\right\}\left[S_{\mathbf{q}_\mathrm{p}\mathbf{q}_\mathrm{p}}\right]_{r,s} \\ & + \frac{\omega}{2}\sum_{r,s}\mathrm{Im}\left\{D^{(j)}_{\text{dir pf, }rs}\right\}\left[\left(\mathbf{q}_\mathrm{p}\mathbf{f}^{\mathrm{H}}_{\text{ext}} - \mathbf{S}_{\mathbf{q}_\mathrm{p}\mathbf{q}_\mathrm{p}}\mathbf{D}^{\mathrm{H}}_{\text{fp}}\right)\mathbf{D}^{-\mathrm{H}}_{\text{ff}}\right]_{r,s} \\ & + \frac{\omega}{2}\sum_{r,s}\mathrm{Im}\left\{D^{(j)}_{\text{dir fp, }rs}\right\}\left[\mathbf{D}^{-1}_{\text{ff}}\left(\mathbf{f}_{\text{ext}}\mathbf{q}^{\mathrm{H}}_\mathrm{p} - \mathbf{D}_{\text{fp}}\mathbf{S}_{\mathbf{q}_\mathrm{p}\mathbf{q}_\mathrm{p}}\right)\right]_{r,s} \\ & + \frac{\omega}{2}\sum_{r,s}\mathrm{Im}\left\{D^{(j)}_{\text{dir ff, }rs}\right\}\left[\mathbf{D}^{-1}_{\text{ff}}\mathbf{S}_{\text{FF}}\mathbf{D}^{-\mathrm{H}}_{\text{ff}}\right]_{r,s} \end{aligned} \tag{5.22}$$

The first random term of the power into the j$^{\text{th}}$ statistical subsystem given by the term 5.21b can be further analysed for the case where the the indexes $j \neq k$. By applying the reciprocity, given by equation 5.13, the term 5.21b can be expressed as

$$\frac{\omega}{2}\left[\sum_k \mathbf{f}^{\mathrm{H}(k)}_{\text{rev}}\mathbf{D}^{-\mathrm{H}}_{\text{ff}}\mathbf{D}^{(j)}_{\text{dir, ff}}\mathbf{D}^{-1}_{\text{ff}}\mathbf{f}^{(j)}_{\text{rev}}\right] = \sum_k \omega\eta_{kj}n_k\frac{E_k}{n_k}, \quad \text{for } j \neq k, \tag{5.23}$$

where

$$\omega\eta_{kj}n_k = \frac{2}{\pi}\sum_{r,s}\mathrm{Im}\left\{D^{(j)}_{\text{dir ff, }rs}\right\}\left[\mathbf{D}^{-1}_{\text{ff}}\mathrm{Im}\left\{\mathbf{D}^{(k)}_{\text{dir ff}}\right\}\mathbf{D}^{-\mathrm{H}}_{\text{ff}}\right]_{r,s}, \quad \text{for } j \neq k. \tag{5.24}$$

By isolating the direct field matrix of the j$^{\text{th}}$ subsystem from the total dynamic matrix (equation 5.7), i.e.

$$\mathbf{D}^{(j)}_{\text{dir, ff}} = \mathbf{D}_{\text{ff}} - \mathbf{D}_{\text{d ff}} - \sum_{k\neq j}\mathbf{D}^{(k)}_{\text{dir}}\ , \tag{5.25}$$

the term 5.21b can be rewritten for the case where the indexes $j = k$, in the form

$$\frac{\omega}{2}\left[\sum_k \mathbf{f}^{\mathrm{H}(k)}_{\text{rev}}\mathbf{D}^{-\mathrm{H}}_{\text{ff}}\mathbf{D}^{(j)}_{\text{dir, ff}}\mathbf{D}^{-1}_{\text{ff}}\mathbf{f}^{(j)}_{\text{rev}}\right] = \frac{\omega}{2}\left[\sum_k \mathbf{f}^{\mathrm{H}(k)}_{\text{rev}}\mathbf{D}^{-\mathrm{H}}_{\text{ff}}\mathbf{D}_{\text{ff}}\mathbf{D}^{-1}_{\text{ff}}\mathbf{f}^{(j)}_{\text{rev}}\right] \tag{5.26a}$$

$$- \frac{\omega}{2}\left[\sum_k \mathbf{f}^{\mathrm{H}(k)}_{\text{rev}}\mathbf{D}^{-\mathrm{H}}_{\text{ff}}\mathbf{D}^{(j)}_{\text{d, ff}}\mathbf{D}^{-1}_{\text{ff}}\mathbf{f}^{(j)}_{\text{rev}}\right] \tag{5.26b}$$

$$- \frac{\omega}{2}\left[\sum_k \mathbf{f}^{\mathrm{H}(k)}_{\text{rev}}\mathbf{D}^{-\mathrm{H}}_{\text{ff}}\sum_{k\neq j}\mathbf{D}^{(k)}_{\text{dir, ff}}\mathbf{D}^{-1}_{\text{ff}}\mathbf{f}^{(j)}_{\text{rev}}\right] \tag{5.26c}$$

The term 5.26a cancels out with the second random term of the power into the subsystem given by 5.21c. The terms 5.26b and 5.26c can be rewritten as

$$\frac{\omega}{2}\left[\sum_{k\neq j}\mathbf{f}_{\text{rev}}^{\text{H}(k)}\mathbf{D}_{\text{ff}}^{\text{-H}}\mathbf{D}_{\text{d, ff}}^{(j)}\mathbf{D}_{\text{ff}}^{\text{-1}}\mathbf{f}_{\text{rev}}^{(j)}\right]=\omega\eta_{d,j}n_j \quad \text{and} \tag{5.27}$$

$$\frac{\omega}{2}\left[\sum_{k}\mathbf{f}_{\text{rev}}^{\text{H}(k)}\mathbf{D}_{\text{ff}}^{\text{-H}}\sum_{k\neq j}\mathbf{D}_{\text{dir, ff}}^{(k)}\mathbf{D}_{\text{ff}}^{\text{-1}}\mathbf{f}_{\text{rev}}^{(j)}\right]=\sum_{k}\omega\eta_{jk}n_j\frac{E_j}{n_j}\ , \tag{5.28}$$

respectively, where

$$\omega\eta_{d,j}n_j=\frac{2}{\pi}\sum_{r,s}\text{Im}\left\{D_{\text{d ff, }rs}\right\}\left[\mathbf{D}_{\text{ff}}^{-1}\text{Im}\left\{\mathbf{D}_{\text{dir ff}}^{(j)}\right\}\mathbf{D}_{\text{ff}}^{-\text{H}}\right]_{r,s} \quad \text{and} \tag{5.29}$$

$$\omega\eta_{jk}n_j=\frac{2}{\pi}\sum_{r,s}\text{Im}\left\{D_{\text{dir ff, }rs}^{(k)}\right\}\left[\mathbf{D}_{\text{ff}}^{-1}\text{Im}\left\{\mathbf{D}_{\text{dir ff}}^{(j)}\right\}\mathbf{D}_{\text{ff}}^{-\text{H}}\right]_{r,s} \tag{5.30}$$

5.3.2 Assembly by Balance of Power

The total power into the j$^{\text{th}}$ system is dissipated at a rate of $\omega\eta_j E_j$, where η_j is the loss factor. By balancing the deterministic external power given by equation 5.22, and the random components expressed by equations 5.23, 5.27 5.28; and noting that $\eta_{jk}n_j=\eta_{kj}n_k$, the balance of power can be written in the form

$$\omega\left(\eta_j+\eta_{d,j}\right)n_j\frac{E_j}{n_j}+\sum_{k}\omega\eta_{jk}n_j\left(\frac{E_j}{n_j}-\frac{E_k}{n_k}\right)=P_0^{(j)} \tag{5.31}$$

Equation 5.31 is coincident with the general FE-SEA expression given by Cotoni et al. (2007) for prescribed forces as inputs, which in turn is identical to the form of the SEA equation when the term $\eta_{d,j}=0$, as is the case of undamped deterministic systems.

5.3.3 Summary of the Equations of the Generalised FE-SEA Method

The entries of the displacements cross-spectral matrix $\mathbf{S}_{\text{qq}}$, that represent the response of the degrees of freedom of the system to prescribed forces $\mathbf{f}_{\text{ext}}$ and or displacements $\mathbf{q}_{\text{p}}$ are given

by

$$\mathrm{E}\left[\mathbf{q}_\mathrm{p}\mathbf{q}_\mathrm{p}^\mathrm{H}\right] = \mathbf{S}_{\mathbf{q}_\mathrm{p}\mathbf{q}_\mathrm{p}} \tag{5.32}$$

$$\mathrm{E}\left[\mathbf{q}_\mathrm{p}\mathbf{q}_\mathrm{f}^\mathrm{H}\right] = \left(\mathbf{q}_\mathrm{p}\mathbf{f}_\mathrm{ext}^\mathrm{H} - \mathbf{S}_{\mathbf{q}_\mathrm{p}\mathbf{q}_\mathrm{p}}\mathbf{D}_\mathrm{fp}^\mathrm{H}\right)\mathbf{D}_\mathrm{ff}^{-\mathrm{H}} \tag{5.33}$$

$$\mathrm{E}\left[\mathbf{q}_\mathrm{f}\mathbf{q}_\mathrm{p}^\mathrm{H}\right] = \mathrm{E}\left[\mathbf{q}_\mathrm{p}\mathbf{q}_\mathrm{f}^\mathrm{H}\right]^\mathrm{H} \tag{5.34}$$

$$\mathrm{E}\left[\mathbf{q}_\mathrm{f}\mathbf{q}_\mathrm{f}^\mathrm{H}\right] = \mathbf{D}_\mathrm{ff}^{-1}\left(\mathbf{S}_\mathrm{FF} + \sum_j \frac{4E_j}{\pi\omega n_j}\mathrm{Im}\left\{\mathbf{D}_{\mathrm{dir,\,ff}}^{(j)}\right\}\right)\mathbf{D}_\mathrm{ff}^{-\mathrm{H}}, \tag{5.35}$$

where the total set of deterministic external loads in equation 5.35 is expressed as

$$\mathbf{S}_\mathrm{FF} = \mathbf{S}_{\mathbf{f}\mathbf{f}_\mathrm{ext}} - \mathbf{f}_\mathrm{ext}\mathbf{q}_\mathrm{p}^\mathrm{H}\mathbf{D}_\mathrm{fp}^\mathrm{H} - \mathbf{D}_\mathrm{fp}\mathbf{q}_\mathrm{p}\mathbf{f}_\mathrm{ext}^\mathrm{H} + \mathbf{D}_\mathrm{fp}\mathbf{S}_{\mathbf{q}_\mathrm{p}\mathbf{q}_\mathrm{p}}\mathbf{D}_\mathrm{fp}^\mathrm{H}. \tag{5.36}$$

The SEA energies of the statistical systems in equation 5.35 are found by solving the SEA equation

$$\omega\left(\eta_j + \eta_{d,j}\right)n_j\frac{E_j}{n_j} + \sum_k \omega\eta_{jk}n_j\left(\frac{E_j}{n_j} - \frac{E_k}{n_k}\right) = P_0^{(j)}, \tag{5.37}$$

where the deterministic losses of the deterministic subsystems, and the coupling loss factors are found from

$$\omega\eta_{d,j}n_j = \frac{2}{\pi}\sum_{r,s}\mathrm{Im}\left\{D_{\mathrm{d\,ff},\,rs}\right\}\left[\mathbf{D}_\mathrm{ff}^{-1}\mathrm{Im}\left\{\mathbf{D}_{\mathrm{dir\,ff}}^{(j)}\right\}\mathbf{D}_\mathrm{ff}^{-\mathrm{H}}\right]_{r,s} \quad \text{and} \tag{5.38}$$

$$\omega\eta_{jk}n_j = \frac{2}{\pi}\sum_{r,s}\mathrm{Im}\left\{D_{\mathrm{dir\,ff},\,rs}^{(k)}\right\}\left[\mathbf{D}_\mathrm{ff}^{-1}\mathrm{Im}\left\{\mathbf{D}_{\mathrm{dir\,ff}}^{(j)}\right\}\mathbf{D}_\mathrm{ff}^{-\mathrm{H}}\right]_{r,s}, \tag{5.39}$$

respectively, and the averaged external power input is given by

$$\begin{aligned}
P_o^{(j)} = {} & \frac{\omega}{2}\sum_{r,s}\mathrm{Im}\left\{D_{\mathrm{dir\,pp},\,rs}^{(j)}\right\}\left[S_{\mathbf{q}_\mathrm{p}\mathbf{q}_\mathrm{p}}\right]_{r,s} \\
& + \frac{\omega}{2}\sum_{r,s}\mathrm{Im}\left\{D_{\mathrm{dir\,pf},\,rs}^{(j)}\right\}\left[\left(\mathbf{q}_\mathrm{p}\mathbf{f}_\mathrm{ext}^\mathrm{H} - \mathbf{S}_{\mathbf{q}_\mathrm{p}\mathbf{q}_\mathrm{p}}\mathbf{D}_\mathrm{fp}^\mathrm{H}\right)\mathbf{D}_\mathrm{ff}^{-\mathrm{H}}\right]_{r,s} \\
& + \frac{\omega}{2}\sum_{r,s}\mathrm{Im}\left\{D_{\mathrm{dir\,fp},\,rs}^{(j)}\right\}\left[\mathbf{D}_\mathrm{ff}^{-1}\left(\mathbf{f}_\mathrm{ext}\mathbf{q}_\mathrm{p}^\mathrm{H} - \mathbf{D}_\mathrm{fp}\mathbf{S}_{\mathbf{q}_\mathrm{p}\mathbf{q}_\mathrm{p}}\right)\right]_{r,s} \\
& + \frac{\omega}{2}\sum_{r,s}\mathrm{Im}\left\{D_{\mathrm{dir\,ff},\,rs}^{(j)}\right\}\left[\mathbf{D}_\mathrm{ff}^{-1}\mathbf{S}_\mathrm{FF}\mathbf{D}_\mathrm{ff}^{-\mathrm{H}}\right]_{r,s}.
\end{aligned} \tag{5.40}$$

For a structure with N statistical subsystems, the matrix form of the SEA equation 5.37 can be written as

$$\omega \begin{pmatrix} \left(\eta_1 + \eta_{d,1} + \sum_{k\neq 1}^{N} \eta_{1k}\right) n_1 & \cdots & -\eta_{1N} n_1 \\ \vdots & \ddots & \vdots \\ -\eta_{N1} n_N & \cdots & \left(\eta_N + \eta_{d,N} + \sum_{k\neq N}^{N} \eta_{Nk}\right) n_N \end{pmatrix} \begin{pmatrix} \frac{E_1}{n_1} \\ \vdots \\ \frac{E_N}{n_m} \end{pmatrix} = \begin{pmatrix} P_o^{(1)} \\ \vdots \\ P_o^{(N)} \end{pmatrix} \tag{5.41}$$

where the entries of the FE-SEA matrix are given by the expressions for $\omega\eta_{d,j}n_j$ and $\omega\eta_{jk}n_j$, in equations 5.29 and 5.30, respectively. It is worth noting that the generalised set of the FE-SEA equations is mostly dependent on the components of the dynamic stiffness matrix associated to free/forced degrees of freedom "$_{\mathrm{ff}}$", whereas the degrees of freedom with prescribed displacements "$_{\mathrm{pp}}$" are found in the expression of the external power input.

As no forces, neither external loads nor reverberant, are considered to be present at the degrees of freedom where the displacements are prescribed, the hybrid FE-SEA equations are not expected to be reversible, in other words, if part of the set of displacements estimated from a prescribed input force are used as input to the same random system, the new estimated response would not be necessary coincident with the initial estimation for prescribed forces. In fact, this apparent mismatch is physically consistent, as the displacements that are estimated with the original formulation for prescribed forces are statistical, and, when part of them are used as new prescribed inputs, they adopt a deterministic nature. This issue is investigated with a numerical model of a randomised statistical-deterministic complex system.

5.4 Numerical Validation

The capability of a hybrid FE-SEA approach to estimate the mean response has been numerically and experimentally validated in systems with known input forces (see for example Cotoni et al. (2007)). In this section, the generalised set of FE-SEA equations are to be employed to estimate the mean response of a system where the the displacements are prescribed, and validated against numerical data from FE simulations.

Two major issues are addressed in this section. Firstly, it is of interest to analyse the accuracy of the generalised FE-SEA approach to estimate the ensemble averaged response of a system, where the input is given in terms of prescribed displacements. Secondly, it was theorised that the ensemble averaged response of a statistical-deterministic system whose

force input is known, is not necessarily the same as the case where the input is the averaged displacement at the coordinates where the force was applied. Therefore, as this discrepancy can be observed in the generalised FE-SEA equations, it is also of interest to observe such difference from numerical data.

In order to verify both issues regarding to the validation of the generalised approach, the procedure to follow is:

1. A unit force f_0 is prescribed and given as input to an ensemble of randomised system modelled by a FE approach, as well as to the corresponding FE-SEA model.

2. The ensemble averaged response of the system is calculated from the set of FE simulations at the coordinates $q_0, q_1, \ldots, q_n$. In parallel, the corresponding mean response from the FE-SEA model is estimated at the same set of coordinates.

3. The now know averaged displacement at the coordinate where the force was applied, q_0, is given as prescribed input to a new ensemble of the same randomised system. Likewise, the corresponding estimated mean response at such coordinate is given as input in the generalised set of FE-SEA equations.

4. The new set of mean displacements $q_1, q_2, \ldots, q_n$, both from the FE simulations and the generalised FE-SEA model, are analysed to determine whether there is a discrepancy between the results of the system where the input is the force f_0, and where the corresponding displacement q_0 is prescribed; as well as the accuracy of the estimation.

A flow diagram is presented in figure 5.1 to illustrate the procedure to validate the generalised FE-SEA equations.

5.4.1 Description of the Numerical FE Model

In order to study key aspects of the generalised hybrid FE-SEA approach and the accuracy of the response estimation of a statistical-deterministic system, a simple system comprised by two flat thin plates (statistical subsystems) interconnected by an axial spring (deterministic subsystem) is proposed as a case study. The statistical components are randomised by placing ten small masses at random locations on the surface of each plate, adding a 15% of the total mass of each structure. A Monte Carlo approach is adopted to generate an ensemble of numerical responses of the system for different random distributions of the masses on the statistical systems, and therefore compare the obtained mean response with the FE-SEA estimations. The numerical model generated by an FE software is presented in figure 5.2[1].

[1] A PYTHON script used to automatise the computation of the randomised ensemble response in the FE package ABAQUS is given in appendix A.

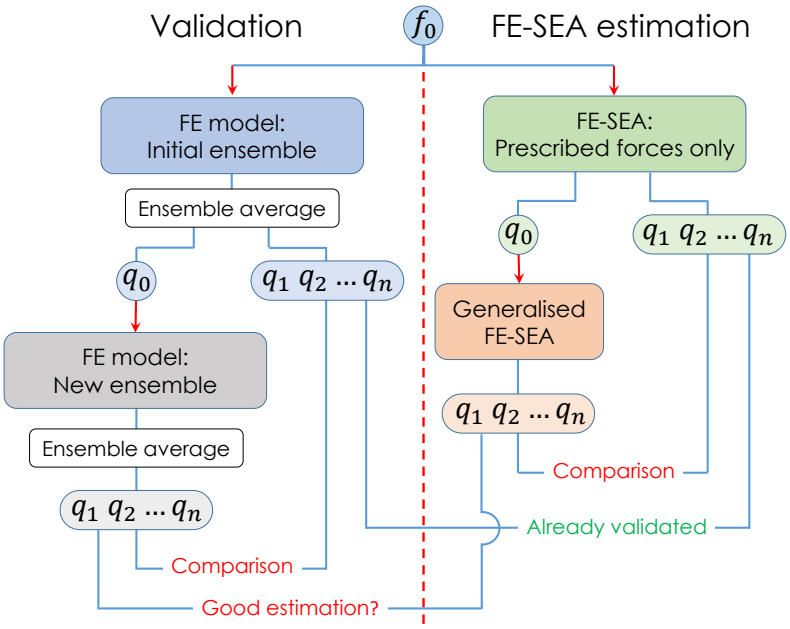

Fig. 5.1 Flow diagram of the validation procedure from FE Monte Carlo simulations (left-hand side), and the FE-SEA estimation (right-hand side).

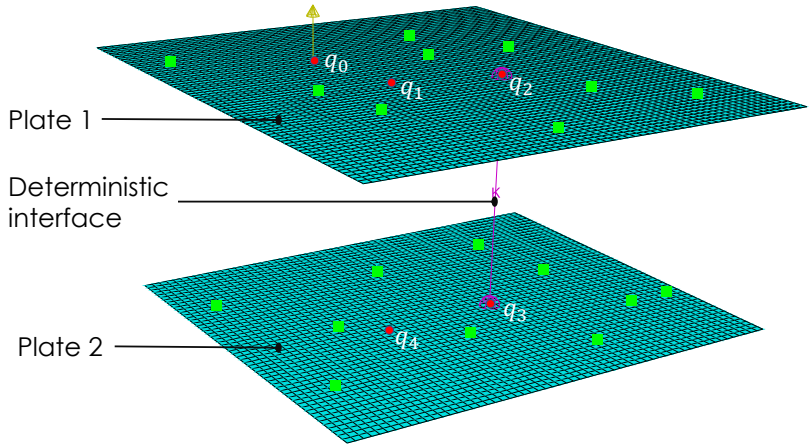

Fig. 5.2 FE model of a random structural system generated in ABAQUS.

The generalised set of coordinates here considered have one degree of freedom each, corresponding to the out-of-plane motion. They are described as follows:

- q_0 Point where the input is prescribed.
- q_1 Isolated point on the subsystem that receives the input (plate 1).
- q_2 Plate 1 - spring interface.
- q_3 Spring - plate 2 interface.

- q_4 Isolated point on the interconnected subsystem (plate 2).

The statistical subsystems, i.e. each of the two flat thin plates, have the same parameters as one of the models analysed by Langley and Cotoni (2004), where the authors have demonstrated that a sufficiently random ensemble can be found to accurately model these two plates with a rigid point connection by a pure SEA approach. The parameters are given in table 5.1.

Table 5.1 Parameters of the statistical components of the statistical-deterministic system.

Subsystem	Thickness [mm]	Dimensions [m × m]	ρ [kg/m^3]	E [GPa]	ν	η
Plate 1	5	1.35×1.2	2800	72	0.3	0.02
Plate 2	15	1.05×1.2				

The deterministic subsystem is represented by an axial spring with constant stiffness, $k = 100$ [kN/m], that interconnects the two statistical subsystems at two degrees of freedom, as only out-of-plane motion is considered. This value is selected to clearly differentiate the motion between the points q_2 and q_3, i.e. the plate-spring interfaces. It was demonstrated that a spring with a stiffness of one hundred times higher than the value here adopted can be assumed to be a rigid connection below 1 [kHz], meaning that no relative motion between the spring ending points would have been expected in the frequency range of interest.

5.4.2 FE-SEA Model of the Case Study System

Modelling the system consists in constructing the total dynamic stiffness matrix from the material properties, geometric parameters, type of connections, etc; as well as the estimation of the total power input from prescribed forces and/or displacements. Analytical or asymptotic expressions are available to quantify the deterministic and direct field matrices, but they are often applicable to simple systems only. Data from simulations or experiments can be also employed to extract information to construct a total dynamic stiffness matrix. Nevertheless, as the system in the present case study is simple in terms of geometry, number of subsystems, and connection type; the modelling is performed from analytical and asymptotic expressions.

Deterministic dynamic stiffness matrix $\mathbf{D_d}$

Even though the number of degrees of freedom are significantly reduced when statistical systems within the structure are described by energy methods, it is often necessary to adopt a

BE or FE analysis to determine the dynamic matrix of the deterministic system of a complex structure. In this case study, however, the deterministic spring has two degrees of freedom, i.e. the axial displacement of the coordinates q_2 and q_3. For a massless and undamped spring, the equations of motion of the deterministic subsystem here considered can be written as

$$k(q_2 - q_3) = F_2 \tag{5.42}$$

$$k(q_3 - q_2) = F_3, \tag{5.43}$$

that can be expressed in matrix form $\mathbf{D}_\mathrm{d}\mathbf{q} = \mathbf{f}_\mathrm{d}$, where the Dynamic stiffness matrix in terms of the spring stiffness is given by

$$\mathbf{D}_\mathrm{d} = \begin{pmatrix} 0 & 0 & 0 & 0 & 0 \\ 0 & 0 & 0 & 0 & 0 \\ 0 & 0 & k & -k & 0 \\ 0 & 0 & -k & k & 0 \\ 0 & 0 & 0 & 0 & 0 \end{pmatrix} \tag{5.44}$$

In general, the size of the deterministic dynamic stiffness matrix is consistent with the number of degrees of freedom of the coordinates of the deterministic subsystem only, however, it is useful to expand the size to the total number of degrees of freedom of the system by completing with rows and columns of zeros, to facilitate the assembly of the total matrix $\mathbf{D}_\mathrm{tot}$.

Direct field matrix $\mathbf{D}_\mathbf{dir}^{(j)}$

As the deterministic structure that connects one o more statistical subsystems can be discretised, it can be assumed that the connection is achieved by multiple points. For the particular case where the separation between two consecutive points is much larger than the wavelength, the direct field matrix can be obtained for each point connection "in isolation" (Cotoni et al., 2007). This condition is assumed as valid for the position of the coordinates q_0 to q_4 within the statistical subsystems of the present case study. Therefore, the analytical expressions for point-type connections developed by Langley and Shorter (2003) are here employed to express the Direct field matrix of each plate, where it is assumed that each point connection is achieved at an embedded rigid disc in the plate, whose radius is the same as the connection element, such as a bolt, as shown in figure 5.3.

In general, the direct field matrix of each point connection is a 6×6 diagonal matrix, as six degrees of freedom can describe the embedded disc motion, and the entries of this matrix are Hankel functions of the wavenumber at a given frequency. As only out-of-plane bending

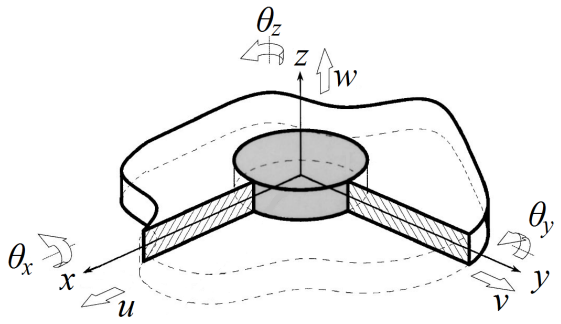

Fig. 5.3 Coordinate system to describe the motion of the embedded disk at the connection point of the flat thin plate. [Adapted from Langley, R. and Shorter, P. (2003). The wave transmission coefficients and coupling loss factors of point connected structures. *The Journal of the Acoustical Society of America*, 113(4):1947–1964.]

motion is considered in the current analysis, the displacement w in the coordinate axis z, shown in figure 5.3, is the only degree of freedom for each point connection, and, therefore, the uncoupled equations for each connection can be written as

$$D_{\text{dir}}^{(1)} q_0 = F_{z_0}^{(1)} \tag{5.45}$$

$$D_{\text{dir}}^{(1)} q_1 = F_{z_1}^{(1)} \tag{5.46}$$

$$D_{\text{dir}}^{(1)} q_2 = F_{z_2}^{(1)} \tag{5.47}$$

$$D_{\text{dir}}^{(1)} q_3 = F_{z_3}^{(2)} \tag{5.48}$$

$$D_{\text{dir}}^{(1)} q_4 = F_{z_4}^{(2)}, \tag{5.49}$$

where the matrix form for the two statistical subsystems is given by the sum

$$\sum_{j}^{2} \mathbf{D}_{\text{dir}}^{(j)} = \begin{pmatrix} D_{\text{dir}}^{(1)} & 0 & 0 & 0 & 0 \\ 0 & D_{\text{dir}}^{(1)} & 0 & 0 & 0 \\ 0 & 0 & D_{\text{dir}}^{(1)} & 0 & 0 \\ 0 & 0 & 0 & D_{\text{dir}}^{(2)} & 0 \\ 0 & 0 & 0 & 0 & D_{\text{dir}}^{(2)} \end{pmatrix} \tag{5.50}$$

The entries of the direct stiffness matrix, are functions of the wavenumber at a given frequency, and in turn, they are dependent on the geometry and material properties of each subsystem. Langley and Shorter (2003) have developed the expression that allows to compute such entries for the the j$^{\text{th}}$ subsystem. For out-of-plane bending motion, each entry is given

by

$$D_{\mathrm{dir}}^{(j)} = X_1 A_1 + X_{1n} A1n \tag{5.51}$$

where

$$X_1 = 2\pi D {\mathrm{k_b}}^3 a \left[-\frac{1}{{\mathrm{k_b}}^2 a^2} H_0^{(2)'}(\mathrm{k_b}a) + \frac{1}{\mathrm{k_b}a} H_0^{(2)''}(\mathrm{k_b}a) + H_0^{(2)'''}(\mathrm{k_b}a) \right] \tag{5.52}$$

$$X_{1n} = 2\pi D {\mathrm{k_b}}^3 a \left[\frac{i}{{\mathrm{k_b}}^2 a^2} H_0^{(2)'}(-i\mathrm{k_b}a) - \frac{1}{\mathrm{k_b}a} H_0^{(2)''}(-i\mathrm{k_b}a) + iH_0^{(2)'''}(-i\mathrm{k_b}a) \right] \tag{5.53}$$

$$A_1 = \frac{H_0^{(2)'}(-i\mathrm{k_b}a)}{H_0^{(2)}(\mathrm{k_b}a) H_0^{(2)'}(-i\mathrm{k_b}a) - iH_0^{(2)}(-i\mathrm{k_b}a) H_0^{(2)'}(\mathrm{k_b}a)} \tag{5.54}$$

$$A_{1n} = \frac{-H_0^{(2)'}(\mathrm{k_b}a)}{H_0^{(2)}(\mathrm{k_b}a) H_0^{(2)'}(-i\mathrm{k_b}a) - iH_0^{(2)}(-i\mathrm{k_b}a) H_0^{(2)'}(\mathrm{k_b}a)}. \tag{5.55}$$

Here $H_0^{(2)^n}$ is the nomenclature used to describe the $\mathrm{n^{th}}$ derivative of the Hankel function of second kind of zero-order, with respect to the complex argument, i.e. $(-i\mathrm{k_b}a)$ or $(\mathrm{k_b}a)$, where a is the radius of the attachment element, and $\mathrm{k_b}$ is the wavenumber for bending waves, which is a function of the radial frequency ω given by

$$\mathrm{k_b} = \left(\frac{m''}{D} \right)^{1/4} \omega^{1/2}, \tag{5.56}$$

where m'' is the mass per unit of area and D is the flexural rigidity of the plate, which is equivalent to $Eh^3/12(1-\nu^2)$ for a flat thin plate.

Alternatively, for the particular case out-of-plane motion and isolated "generalised" coordinates, the entries of the direct field field matrix can be directly estimated from the point impedance Z_p in the form

$$D_{\mathrm{dir}}^{(j)} = i\omega Z_p^{(j)}, \tag{5.57}$$

which is equivalent to the imaginary part of the complex entry computed from equation 5.51.

Since for the current case study the deterministic and the direct field matrices can be computed from known parameters such as material properties, spring stiffness and geometry,

the total FE-SEA dynamic stiffness matrix given by

$$\mathbf{D}_{\text{tot}} = \mathbf{D}_{\text{d}} + \sum_{j}^{2} \mathbf{D}_{\text{dir}}^{(j)} = \begin{pmatrix} D_{\text{dir}}^{(1)} & 0 & 0 & 0 & 0 \\ 0 & D_{\text{dir}}^{(1)} & 0 & 0 & 0 \\ 0 & 0 & D_{\text{dir}}^{(1)} + k & -k & 0 \\ 0 & 0 & -k & D_{\text{dir}}^{(2)} + k & 0 \\ 0 & 0 & 0 & 0 & D_{\text{dir}}^{(2)} \end{pmatrix}, \tag{5.58}$$

can be analytically estimated for each frequency within the frequency range of interest. This total dynamic stiffness matrix must be split in a set of submatrices for autocorrelation of the prescribed and the free/forced degrees of freedom, as well as the crosscorrelation between them. In this case study, as the input is given in the first term, there is no need to rearrange such matrix to differentiate prescribed and non-prescribed coordinates, and the autocorrelating submatrices are given by

$$\mathbf{D}_{\text{pp}} = \begin{pmatrix} D_{\text{dir}}^{(1)} \end{pmatrix} \tag{5.59}$$

$$\mathbf{D}_{\text{ff}} = \begin{pmatrix} D_{\text{dir}}^{(1)} & 0 & 0 & 0 \\ 0 & D_{\text{dir}}^{(1)} + k & -k & 0 \\ 0 & -k & D_{\text{dir}}^{(2)} + k & 0 \\ 0 & 0 & 0 & D_{\text{dir}}^{(2)} \end{pmatrix}, \tag{5.60}$$

whereas the crosscorrelating submatrices are completed by zeros, as there is no correlation between prescribed and free/forced coordinates in this particular system, therefore

$$\mathbf{D}_{\text{pf}} = \begin{pmatrix} 0 & 0 & 0 & 0 \end{pmatrix} \tag{5.61}$$

$$\mathbf{D}_{\text{fp}} = \begin{pmatrix} 0 \\ 0 \\ 0 \\ 0 \end{pmatrix}. \tag{5.62}$$

The FE-SEA model of the system is now complete, and the response in terms of displacement power spectrum can be estimated by firstly estimating the averaged energy of the statistical systems, equation 5.41, and then computing the averaged power spectrum of the unknown coordinates given by equation 5.17.

5.4.3 Numerical Results and FE-SEA Estimation

Numerical data of the displacement response of the coordinates $\mathbf{q} = (q_0\ q_1\ q_2\ q_3\ q_4)^{\mathrm{T}}$ has been collected from a total of 200 FE simulations in the frequency domain for a unit force as input in q_0. Each simulation (realisation) was performed for a particular random distribution of the small masses on each plate. The displacement response at the coordinate q_0, i.e. input point, for each simulation as well as the ensemble average are plotted in figure 5.4, where it is also shown the corresponding FE-SEA estimation computed from the initial formulation of the method for prescribed forces.

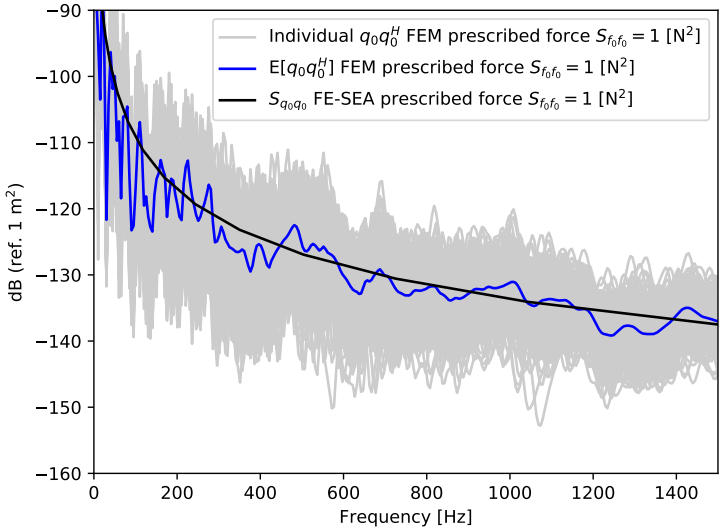

Fig. 5.4 Power spectrum of the displacement response at the degree of freedom q_0 that receives a prescribed unit input force. Grey: each of the 200 individual FE realisations; fluctuating blue: ensemble averaged data from FE simulations; smooth black: FE-SEA estimation.

The averaged response displacement at q_0 from the FE simulations, represented by the blue curve in figure 5.4, was employed as a new input to the FE model, to gather a further ensemble of 200 simulations of the randomised structure. Analogously, the estimated mean displacement at the same coordinate, represented by the black curve in figure 5.4, was given as prescribed displacement to the generalised FE-SEA model, i.e. $\mathbf{q}_{\mathrm{p}} = (q_0)$, to estimate the mean response of the set of coordinates $\mathbf{q}_{\mathrm{f}} = (q_1\ q_2\ q_3\ q_4)^{\mathrm{T}}$.

The averaged response displacement from the FE Monte Carlo simulations, and the corresponding FE-SEA estimation, are plotted as power spectrum for the case where the deterministic force is given as an input, and for the corresponding case where the displacement at q_0 is prescribed. Results for the coordinates q_1 and q_2 of the subsystem that receives the input, and the corresponding q_3 and q_4 of the coupled subsystem, are shown in figure 5.5

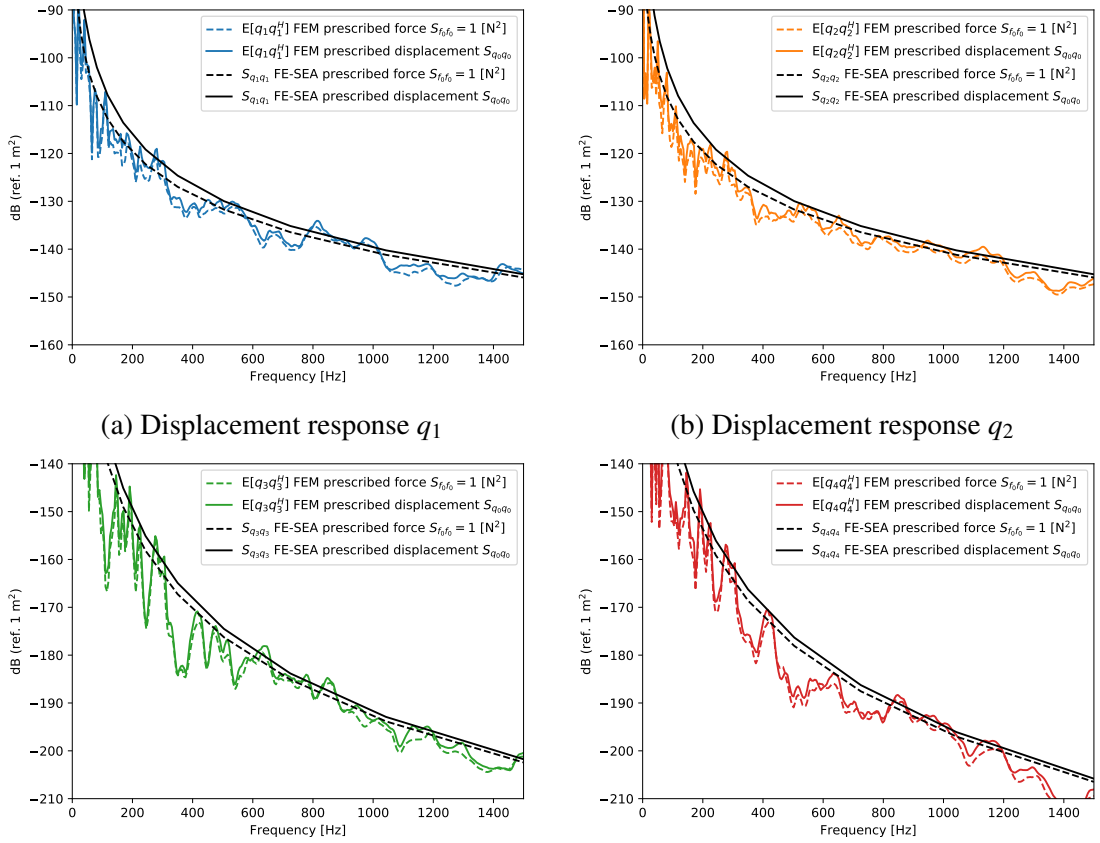

(a) Displacement response q_1

(b) Displacement response q_2

(c) Displacement response q_3

(d) Displacement response q_4

Fig. 5.5 Power spectrum of the displacement response of the interconnected statistical subsystems. Fluctuating curves: averaged data from FE simulations for a prescribed force input (dashed) and for a prescribed displacement (continuous). Smooth black curves: FE-SEA estimation for a prescribed force input (dashed) and for a prescribed displacements (continuous).

5.5 Discussion

The generalised formulation of the equations of the FE-SEA approach to allow both forces and displacements as prescribed inputs, has been proven to be capable of estimating the mean response of the deterministic coordinates within a complex structure, with a relatively high degree of accuracy. This can be visualised in figure 5.5, where the ensemble averaged response of a Monte Carlo simulation fluctuates up to ± 3 dB about the estimated FE-SEA mean, respectively represented by the colour and black solid lines. This range of deviation is also expected for pure SEA as well as FE-SEA estimations where the force is prescribed.

Aside from the accuracy of estimation of the method, another important result is that the theorised non-reversibility of the FE-SEA equations has been proven with data from

simulations, where the ensemble average response at the coordinates $\mathbf{q}_\mathrm{f} = (q_1\ q_2\ q_3\ q_4)^\mathrm{T}$ and the corresponding FE-SEA estimation, is visibly higher for the case where the displacement at q_0 is given as input, solid lines, than when the force is prescribed, dashed lines. Such difference has been plotted in logarithmic scale in figure 5.6, where, except of few regions in the frequency range, it has a positive value and agrees well with the FE-SEA estimation.

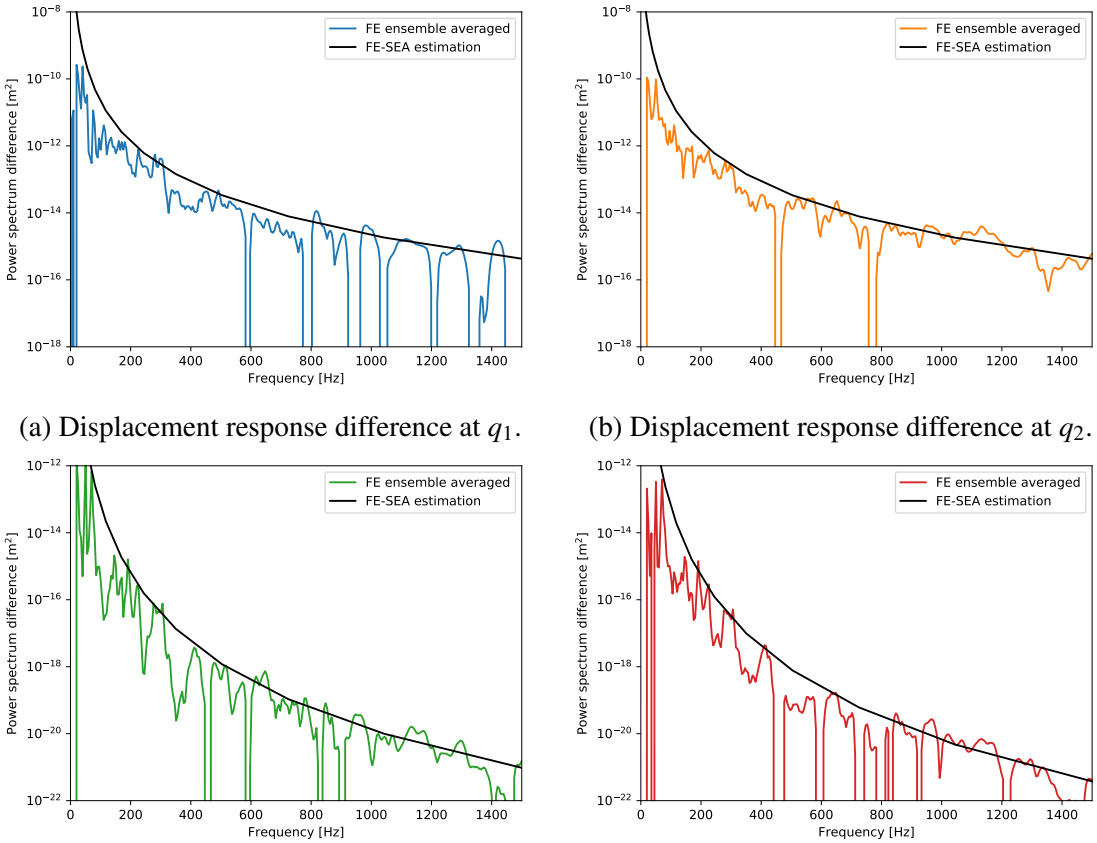

(a) Displacement response difference at q_1.

(b) Displacement response difference at q_2.

(c) Displacement response difference at q_3.

(d) Displacement response difference at q_4.

Fig. 5.6 Response displacement difference between the case of prescribed forces and prescribed displacements at q_0. Fluctuating: from the ensemble averages of FE simulations; continuous: from the FE-SEA estimations.

The generalised hybrid FE-SEA equations developed here have addressed to one of the requirements needed to model the structural-acoustic system that is being an experimental case study in this research project. It is possible now to estimate the mean response of each of the subsystems if the power spectrum of the input is known, which can be calculated from the time history of *in-situ* measurements. However, the present form is limited to linear systems, with constant stiffness, where, in absence of damping of the deterministic system, the deterministic matrix is invariable in the frequency range. Therefore, the following chapter

is concerned in investigating an approach to include the nonlinear behaviour in the vibration transmission path.

Chapter 6

Hybrid FE-SEA Method: Equivalent Linearisation Applied to Nonlinear Modelling

6.1 Introduction

The equations of the Hybrid FE-SEA developed in the previous chapter are valid for linear systems, where the stiffness of each of the deterministic components of the built-up system is constant. In order to make the method applicable to systems with deterministic components that present a nonlinear behaviour, an approach known as equivalent linearisation has been adopted.

Equivalent linearisation techniques are well known since about the end of the the first half of the twentieth century, and are based on the idea that a weak nonlinear system can be approximated to a linear system provided that the error is minimised. This aproach has been initially developed by Krylov and Bogoliubov (1949) to model oscillators with nonlinear stiffness subjected to harmonic inputs. The approach has been extended by Caughey (1963) to model systems with displacement-dependent and velocity-dependent nonlinearities, i.e. nonlinear stiffness and damping, respectively, excited with random inputs, where the criteria of optimisation is the minimisation of the mean-squared error.

In this chapter, the equivalent linearisation described by Caughey (1963) is followed to estimate an equivalent linear stiffness that can be used in the hybrid FE-SEA equations. The method here developed is iterative, as it was found that the optimised constants of the equivalent linear equation are dependent on the response of the system. The estimation of

the response of both the structural and acoustic subsystems of the proposed case study are validated against the experimental data collected from the rig.

6.2 Equivalent Linearisation

The axial force transmitted through a spring is usually defined as displacement-dependent $F(y)$. If the spring stiffness does also dependent on the displacement, the force can then be regarded as a nonlinear function $F_{nl}(y)$, as is the case of a couple of magnets that obeys a nonlinear law, approximated by equation 3.1 presented on chapter 3. Assuming that the nonlinearity is weak, there can be estimated an equivalent linear function in the form of $F_{eq}(y) = k_{eq}y + \mu_{eq}$, where the constants k_{eq} and μ_{eq} are the equivalent coefficients that can be found by optimising the error, expressed as the difference between the nonlinear and the equivalent linear functions, i.e.

$$\varepsilon = F_{nl}(y) - k_{eq}y - \mu_{eq}. \tag{6.1}$$

As recommended by Caughey (1963), for random processes, the optimisation procedure to determine the constants k_{eq} and μ_{eq} can be performed by minimising the mean-squared error. For an ergodic process, the ensemble average error is equivalent to the temporal average given by

$$\mathrm{E}\left[\varepsilon^2\right] = \lim_{T\to\infty} \frac{1}{T} \int_{-T/2}^{T/2} \varepsilon^2 \mathrm{d}t, \tag{6.2}$$

and therefore, the optimum equivalent linear stiffness and mean are found by solving the equations

$$\frac{\partial}{\partial k_{eq}} \mathrm{E}\left[\varepsilon^2\right] = 0 \qquad \text{and} \tag{6.3}$$

$$\frac{\partial}{\partial \mu_{eq}} \mathrm{E}\left[\varepsilon^2\right] = 0, \tag{6.4}$$

respectively. The coefficients of the equivalent linear function are expected to be functions of the response of the system y, and therefore, the procedure to find such coefficients becomes iterative.

6.3 Linearisation of Symmetric and Asymmetric Nonlinear Functions

A weak nonlinear function continuous about a mean value can be represented as a polynomial function by adopting a Taylor expansion, i.e.

$$F_{nl}(y) \approx k_0 + k_1 y + k_2 y^2 + \ldots + k_n y^n, \tag{6.5}$$

where usually the terms up to the third order contribute significantly to the polinomial approximation of a weak nonlinear function. If the force-displacement relation can be approximated with terms of odd order only, the nonlinear function can be considered to be symmetric about the mean, in the sense that $F(y) = -F(-y)$. For zero-mean inputs, the response of a system with symmetric nonlinear restoring force will also have a zero mean. On the other hand, the even terms are related to asymmetric nonlinearities, where there must be a DC offset to avoid negative stiffnesses, and therefore instability. A case of such asymmetric nonlinearities is presented by Demetriou (2018), where the author indicates that a quadratic term of a nonlinear function in a Duffing oscillator incorporates the asymmetry in the restoring force with a positive offset (mean force). The symmetric and asymmetric nonlinear relation between force and displacement are illustrated in figure 6.1.

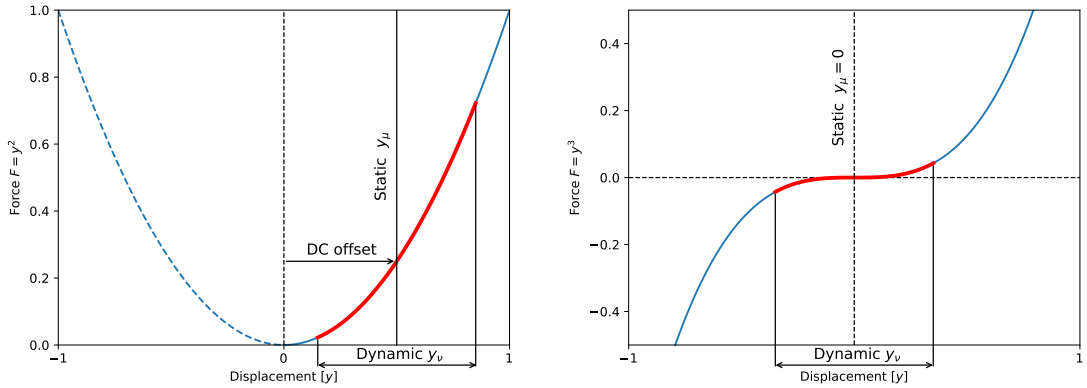

(a) Asymmetric nonlinearity about a mean value $F = k_2 y^2$.

(b) Symmetric nonlinearity about the mean $F = k_3 y^3$.

Fig. 6.1 Nonlinearities of second and third order. Blue: function force vs displacement; red: region of dynamic response.

In order to take into account the mean response due to asymmetries in the nonlinear function, the displacement variable in the equivalent linearised function is required to be explicitly expressed in terms of its dynamic and static components, i.e. $y = y_\nu + y_\mu$, where

y_v is the dynamic variable with zero mean, i.e. $\mathrm{E}[y_v] = 0$, and y_μ is the static mean value. With this convention, the optimum equivalent coefficients estimated from equations 6.3 and 6.4 are found to be

$$k_{eq} = \frac{\mathrm{E}[F_{nl}(y)\, y_v]}{\sigma_v^2} \qquad \text{and} \tag{6.6}$$

$$\mu_{eq} = \mathrm{E}[F_{nl}(y)], \tag{6.7}$$

respectively, where σ_v^2 is the mean square dynamic response, i.e. $\mathrm{E}\left[y_v^2\right]$. In general, the equivalent spring stiffness and mean of the linearised function can be determined by the moments of the response, i.e. the mean and variance of the response. The capability and accuracy of the approach is illustrated by contrasting the response of the nonlinear system and its equivalent linearised system from data gathered from numerical simulations of systems with quadratic and cubic nonlinearities.

6.3.1 Quadratic Nonlinearity

Considering a lightly damped single degree of freedom mass-damper-spring system, where the elastic transmitted force can be modelled by a quadratic function, i.e. $F_{nl}(y) = k_2 y^2$, the equation of motion of such system can be written as

$$\ddot{y} + \lambda \dot{y} + k_2 y^2 = f(t), \tag{6.8}$$

where the λ and k_2 are constants and $f(t)$ is a random input force per unit of mass; provided that the displacements y do not take negative values, otherwise, the nonlinear equation becomes unstable. The coefficients of the equivalent linearised function of a quadratic

nonlinear function are found from equations 6.6 and 6.7, respectively:

$$\begin{aligned} k_{eq} &= \frac{\mathrm{E}\left[k_2\left(y_v + y_\mu\right)^2 y_v\right]}{\sigma_v^2} \\ &= \frac{k_2\mathrm{E}\left[y_v^3\right] + 2k_2 y_\mu \mathrm{E}\left[y_v^2\right] + k_2 y_\mu^2 \mathrm{E}\left[y_v\right]}{\sigma_v^2} \\ &= 2k_2 y_\mu \end{aligned} \tag{6.9}$$

$$\begin{aligned} \mu_{eq} &= \mathrm{E}\left[k_2\left(y_v + y_\mu\right)^2\right] \\ &= k_2\mathrm{E}\left[y_v^2\right] + 2k_2 y_\mu \mathrm{E}\left[y_v\right] + k_2 y_\mu^2 \\ &= k_2\left(\sigma_v^2 + y_\mu^2\right). \end{aligned} \tag{6.10}$$

It is worth noting that it is not possible to derive a equivalent linearised function of a quadratic equation if the variable is not explicitly written in terms of the dynamic and static parts, as it can be seen that the equivalent spring stiffness depends on the mean value of the response.

A numerical simulation has been performed to determine the response of the system with quadratic nonlinearity, i.e. numerical solution to equation 6.8, to a random input with constant spectrum across the frequency range (white noise). The parameters of the equivalent linearised equation of motion are hence computed from the numerical response of the linear system, and a numerical simulation has been also performed to solve the equivalent linear system. Results in the time domain are shown in figure 6.2.

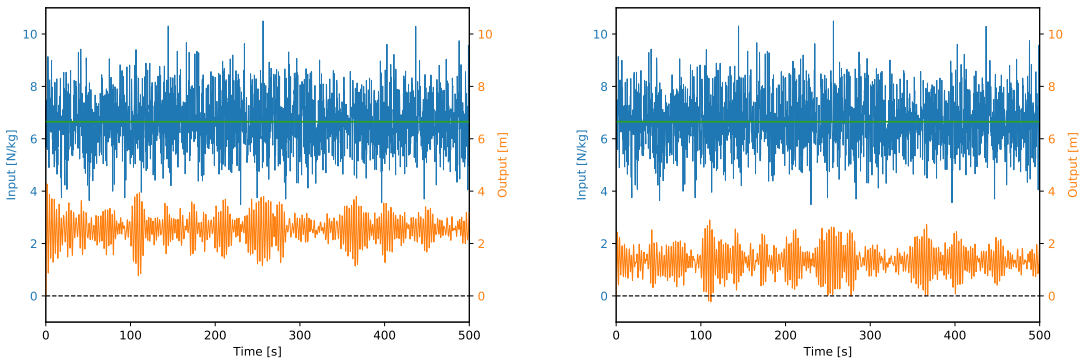

(a) Quadratic $\ddot{y} + \lambda\dot{y} + k_2 y^2 = f(t) + F_S$ (b) Linearised $\ddot{y} + \lambda\dot{y} + k_{eq} y_v + \mu_{eq} = f(t) + F_S$

Fig. 6.2 Response in the time domain of a system with a quadratic order and the corresponding equivalent linearised system. Blue: white noise input; orange: response.

The force-displacement function for the quadratic and the equivalent linearised system are plotted in figure 6.3, where there has also been plotted a linearised function with an offset of $\mu_{eq} - k_{eq} y_\mu$ to visualise the approximation of the quadratic function to a linear about the mean for small displacements.

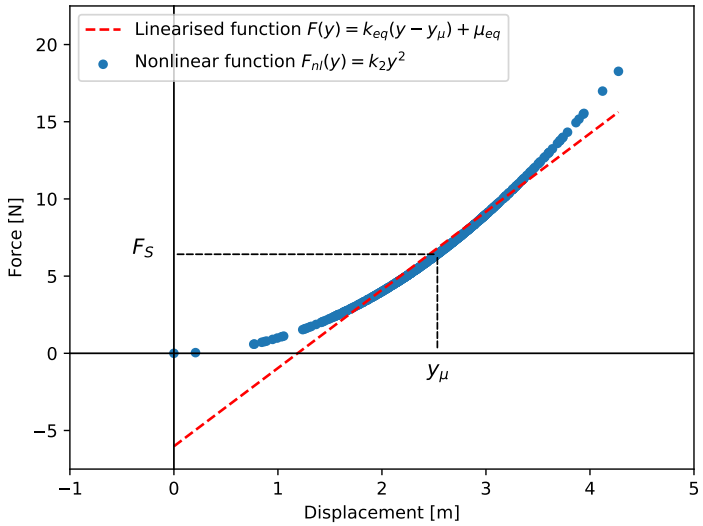

Fig. 6.3 Elastic force vs displacement of the asymmetric nonlinear function. Blue: nonlinear quadratic function; orange: equivalent linearisation; dashed red: linearised function with a vertical offset of $\mu_{eq} - k_{eq} y_\mu$

.

The parameters of the quadratic function and the corresponding linearised function, as well as the mean squared dynamic response and the mean, are shown in table 6.1.

Table 6.1 Parameters and response of a system with quadratic nonlinearity and the corresponding equivalent linearisation.

Function	Stiffness parameters	Mean force [N/kg]	y_μ [m]	σ_v^2 [m^2]	Relative error %
Quadratic	$k_2 = 1$ [N/m^2]	$F_S = 6.65$	2.54	0.234	2.95
Linearised	$k_{eq} = 5.06$ [N/m]	$\mu_{eq} = 6.65$	1.31	0.227	

Even though the estimated mean response of the equivalent linearised system is lower than the nonlinear, the mean square response is about the same order of magnitude, with an underestimation of less than 3%. The error is expected to reduce if the amplitude of the input is lower, as the nonlinearity becomes weaker.

The capability of the equivalent linearisation can be analysed also in the frequency domain. Figure 6.4 shows the half-sided power spectral density of the responses of the nonlinear system and the corresponding linearised system.

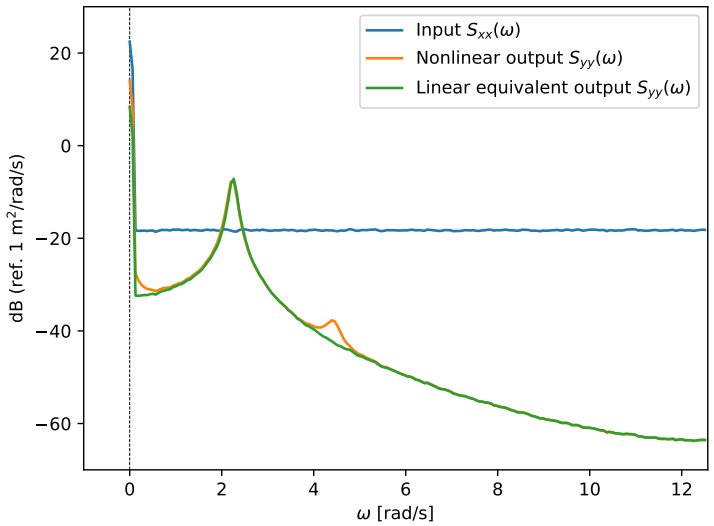

Fig. 6.4 Power spectral density of the second order nonlinear system and the corresponding equivalent linearised. Blue: input; orange: response of the nonlinear system; green: response of the equivalent linearised system.

It can be concluded that the equivalent linearisation estimates the response up to the first harmonic with high accuracy, depending on how weak the nonlinearity is, however further harmonics are dismissed. Nevertheless, the mean square response, represented by the area under the curves of the power spectral density, is well estimated.

6.3.2 Cubic Nonlinearity

It has been stated that a cubic nonlinearity can be regarded as symmetric if the input to the system has a zero mean. If the input oscillates about a static force, i.e. mean input force, the relation between the elastic force and the displacement can be asymmetric and, therefore, the equivalent linearised function of the cubic nonlinear force must have a mean component μ_{eq}. The equation of motion of a system with such cubic nonlinearity can be written as

$$\ddot{y} + \lambda \dot{y} + k_3 y^3 = f(t), \tag{6.11}$$

where there is no risk of instability due to negative values of the response. The random input, therefore, might or might not have a static component. From equations 6.6 and 6.7, the

coefficients of the equivalent linearised function can be calculates, respectively, as

$$\begin{aligned} k_{eq} &= \frac{\mathrm{E}\left[k_3\left(y_\nu + y_\mu\right)^3 y_\nu\right]}{\sigma_\nu^2} \\ &= \frac{k_3\mathrm{E}\left[y_\nu^4\right] + 3k_3 y_\mu \mathrm{E}\left[y_\nu^3\right] + 3k_3 y_\mu^2 \mathrm{E}\left[y_\nu^2\right] + k_3 y_\mu^3 \mathrm{E}\left[y_\nu\right]}{\sigma_\nu^2} \\ &= \frac{3k_3\mathrm{E}\left[y_\nu^2\right]\mathrm{E}\left[y_\nu^2\right] + 3k_3 y_\mu^2 \mathrm{E}\left[y_\nu^2\right]}{\sigma_\nu^2} \\ &= 3k_3\left(\sigma_\nu^2 + y_\mu^2\right) \end{aligned} \tag{6.12}$$

$$\begin{aligned} \mu_{eq} &= \mathrm{E}\left[k_3\left(y_\nu + y_\mu\right)^3\right] \\ &= k_3\mathrm{E}\left[y_\nu^3\right] + 3k_3 y_\mu \mathrm{E}\left[y_\nu^2\right] + 3k_3 y_\mu^2 \mathrm{E}\left[y_\nu\right] + k_3 y_\mu^3 \\ &= k_3\left(3y_\mu\sigma_\nu^2 + y_\mu^3\right) \end{aligned} \tag{6.13}$$

The equivalent stiffness k_{eq} for the linearised function of third order, does exist whether there is or not a mean force in the input, whereas the equivalent mean, as expected, does not exist for zero-mean inputs.

Equation 6.11 has been numerically solved for a zero-mean force input and a non zero-mean input with a positive static force. Similarly to the analysis of the case of quadratic nonlinearity, the corresponding coefficients of the linearised equation were computed by using the data gathered from simulations in the time domain. Results for the cases of the zero-mean and non zero-mean inputs are plotted in figures 6.5 and 6.6.

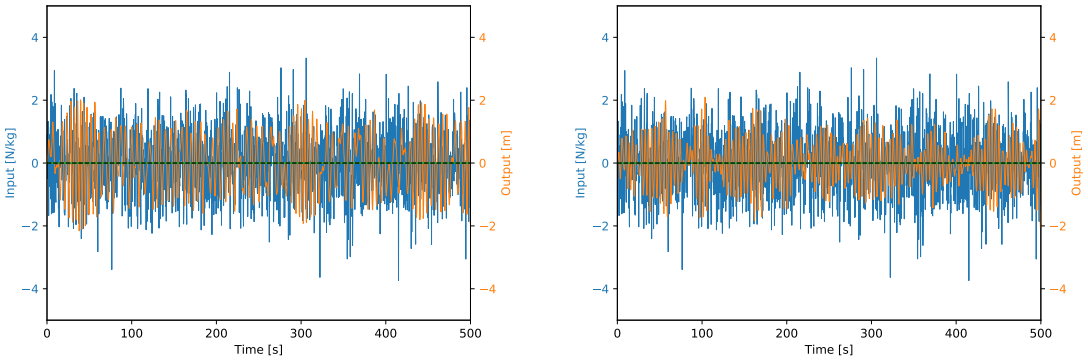

(a) Cubic $\ddot{y} + \lambda\dot{y} + k_3 y^3 = f(t)$ (b) Linearised $\ddot{y} + \lambda\dot{y} + k_{eq} y_\nu = f(t)$

Fig. 6.5 Zero-mean input and time domain response of a system with a cubic nonlinearity and the corresponding equivalent linearised system. Blue: white noise input; orange: response.

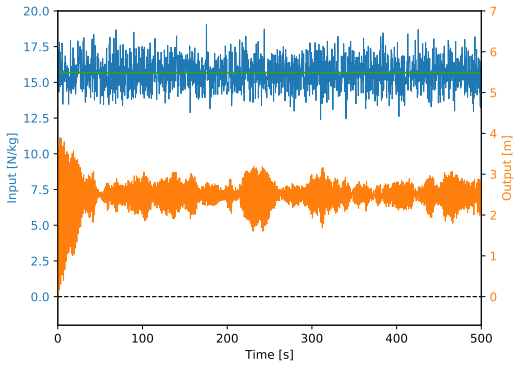

(a) Cubic $\ddot{y}+\lambda\dot{y}+k_3y^3=f(t)+F_S$

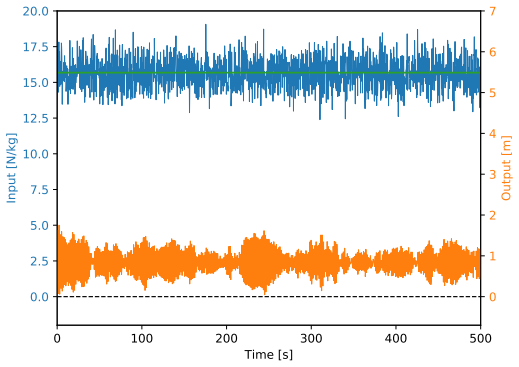

(b) Linearised $\ddot{y}+\lambda\dot{y}+k_{eq}y_v+\mu_{eq}=f(t)+F_S$

Fig. 6.6 Non zero-mean input and time domain response of a system with a cubic nonlinearity and the corresponding equivalent linearised system. Blue: white noise input; orange: response.

The relations force vs displacement are plotted in figure 6.7 for the cases of zero-mean and non zero-mean inputs, i.e. symmetric and nonsymmetric nonlinear relation, respectively.

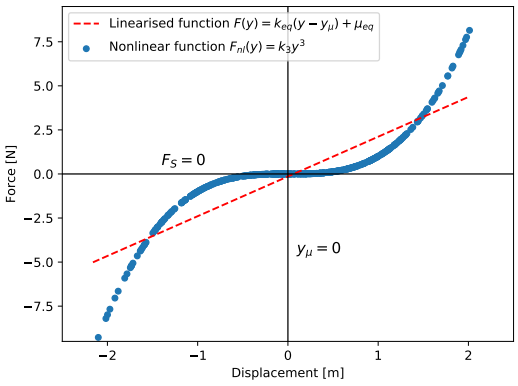

(a) Zero-mean input.

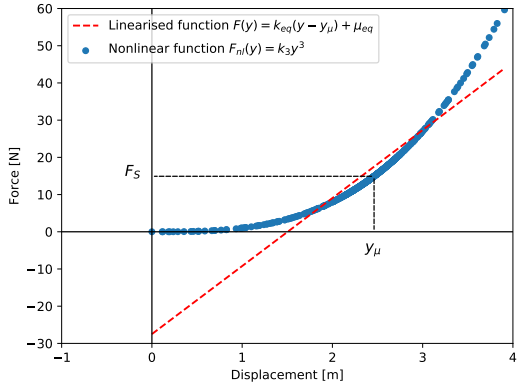

(b) Non zero-mean input

Fig. 6.7 Elastic force vs displacement of the symmetric and asymmetric nonlinear functions. Blue: nonlinear cubic function; orange: equivalent linearisation; dashed red: linearised function with a vertical offset of $\mu_{eq}-k_{eq}y_\mu$

.

The parameters of the equivalent linear functions for the cases of zero-mean and non zero-mean inputs have been computed from the results after numerical simulations, and are presented with the corresponding dynamic and static components of the response for each case of nonlinear and linearised functions in table 6.2.

Table 6.2 Parameters and response of a system with cubic nonlinearity and the corresponding equivalent linearised.

Function	Stiffness parameters	Mean force [N/kg]	y_μ [m]	σ_v^2 [m^2]	Relative error %
Zero-mean cubic	$k_3 = 1$ [N/m^3]	$F_S = 0$	0	0.751	27.3
Linearised	$k_{eq} = 2.25$ [N/m]	$\mu_{eq} = 0$	0	0.546	
Non zero-mean cubic	$k_3 = 1$ [N/m^3]	$F_S = 15.68$	2.48	0.0565	2.83
Linearised	$k_{eq} = 2.25$ [N/m]	$\mu_{eq} = 15.68$	0.84	0.0549	

For the case of zero-mean input, the relative error between the mean square response of the nonlinear and the linearised systems is significantly higher than the corresponding error in the case of non zero-mean input. This is expected since for the first case, the nonlinearity is stronger, as can be visualised in the plot force vs displacement in figure 6.7a. For the case of the input oscillating about a static force, the nonlinearity is weaker. This can be seen in figure 6.7b where the the linear function with an offset of $\mu_{eq} - k_{eq} y_\mu$, represented by the red dashed line, captures the approximate linear behaviour for oscillations about the mean y_μ. The relative error between the estimated mean square response of the nonlinear and the linearised systems is hence smaller, less than 3%.

In the frequency domain, the power spectral density of the input and response for each case of input are plotted in figure 6.8.

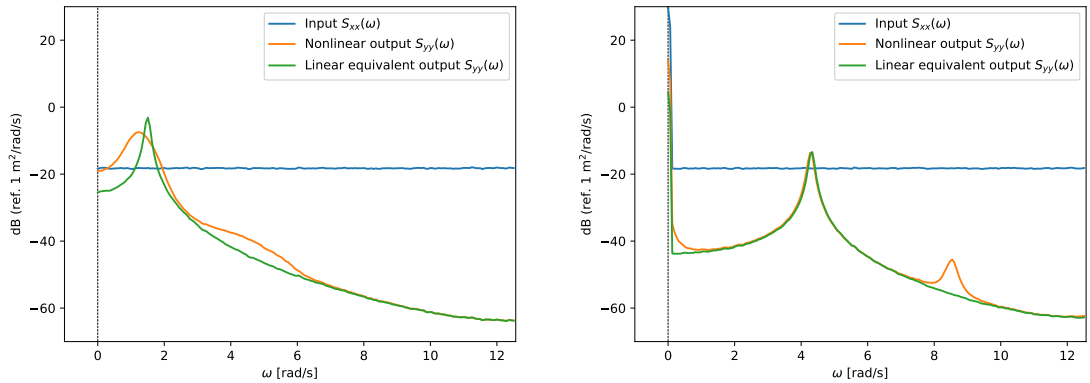

(a) Zero-mean input.

(b) Non zero-mean input.

Fig. 6.8 Power spectral density of the third order nonlinear system and the corresponding equivalent linearised. Blue: input; orange: response of the nonlinear system; green: response of the equivalent linearised system.

For the case of strong nonlinear behaviour, it can be visualised in figure 6.8a, that the equivalent linearised system does not accurately predict the shape of the power spectral density, even though it estimates the position of the first harmonic. Additionally, the third harmonic significantly contributes to the mean square response and hence, since this approach dismisses it, the area under the curve of the linearised system is much lower than the area of the nonlinear system. On the other hand, where the nonlinearity is weaker, the first harmonic is dominant and its shape is accurately predicted by the equivalent linearisation. The second and third harmonics in this case does not contribute substantially and, therefore, the error is smaller than for the symmetric nonlinear system.

6.4 Estimation of the Equivalent Spring Stiffness

In the previous section, it has been demonstrated that the mean square response of a nonlinear system, can be estimated with a high degree of accuracy by an equivalent linear system with optimised coefficients k_{eq} and μ_{eq}. Such coefficients have been computed from numerical simulations in the time domain, as the mean square and mean response need to be known, i.e. σ_y^2 and y_μ, respectively. However, the aim of adopting a equivalent linearisation to analyse systems with nonlinear stiffness is to estimate such coefficients without the need of solving the initial nonlinear equations, as analytical solutions are not always available, and performing numerical simulations in the time domain are computationally expensive, even for simple nonlinear systems.

6.4.1 Equivalent Linearisation of a System with Second and Third Order Nonlinearities

Considering a weakly nonlinear equation of motion of a system with stiffness nonlinearities of second and third order, i.e.

$$m\ddot{y} + \lambda\dot{y} + k_1 y + k_2 y^2 + k_3 y^3 = f(t), \tag{6.14}$$

the equivalent linear equation of motion can be split into a dynamic and a static subequations in the form

$$m\ddot{y}_\nu + \lambda\dot{y}_\nu + \left(k_1 + k_{eq}\right) y_\nu = f_\nu(t) \tag{6.15}$$

$$k_1 y_\mu + \mu_{eq} = F_S, \tag{6.16}$$

where the subindexes "$_v$" denote zero-mean dynamic quantities. The mean square response σ_v^2 can be estimated as the area under the power spectral density curve in the frequency domain. As equation 6.15 is linear, the mean square response is given by

$$\begin{aligned}\sigma_v^2 &= \int_{-\infty}^{\infty} |H(\omega)|^2 S_{ff} \mathrm{d}\omega \\ &= \int_{-\infty}^{\infty} \left| \frac{1}{-m\omega^2 + i\lambda\omega + \left(k_1 + k_{eq}\right)} \right|^2 S_{ff}(\omega)\, \mathrm{d}\omega. \end{aligned} \tag{6.17}$$

For random inputs of white-noise type, i.e. with constant power spectral density S_o, there exist analytical solutions to equations of the the form of equation 6.17 (Crandall and Mark, 2014), and for inputs with $S_{ff} = S_o$ the mean square response of the linearised system is given by

$$\sigma_v^2 = \frac{\pi S_o}{\lambda\left(k_1 + k_{eq}\right)}. \tag{6.18}$$

The parameters σ_v^2 and y_μ needed to estimate the equivalent stiffness of the linearised equation with white-noise inputs, can be directly computed by solving simultaneousley the equations 6.16 and 6.18, where the coefficients k_{eq} and μ and are expressed explicitly in terms of σ_v^2 and y_μ, i.e.

$$\sigma_v^2 = \frac{\pi S_o}{\lambda\left(k_1 + 2k_2 y_\mu + 3k_3\left(\sigma_v^2 + y_\mu^2\right)\right)} \tag{6.19}$$

$$k_1 y_\mu + k_2\left(\sigma_v^2 + y_\mu^2\right) + k_3\left(3y_\mu\sigma_v^2 + y_\mu^3\right) = F_S. \tag{6.20}$$

The total equivalent spring stiffness is then found by adding the linearised stiffness to the linear component, i.e. $k = k_1 + k_{eq}$.

As the direct approach to estimate the equivalent spring stiffness is straightforward, it is restricted to inputs with constant power spectral density over the frequency range of interest. For random non-white inputs, the solution to equation 6.17 is not always available, hence an iterative approach is adopted as follows:

1. Neglect the nonlinear components and solve equation 6.17 with the spring stiffnes k_1 only to estimate an initial mean square response σ_v^2.

2. As an initial σ_v^2 is now know, solve equation 6.20 to find the mean value of the response y_μ.

3. With the initially estimated σ_v^2 and y_μ, compute the equivalent linear stiffness k_{eq}.
4. Use the equivalent linear stiffness k_{eq} to solve equation 6.17 to find a new value of σ_v^2.
5. Repeat the procedure until the estimated k_{eq} converges to a value.
6. The equivalent linearised spring stiffness is then given by $k_1 + k_{eq}$.

6.4.2 Numerical Simulations in the Time Domain

As a case study to illustrate the iterative approach and the computation of the equivalent spring stiffness, numerical simulations have been performed to a system with nonlinear stiffness described by equation 6.14, with parameters given in table 6.3.

Table 6.3 Parameters of the weak nonlinear system with second and third order stiffness nonlinearities.

m [kg]	λ [N-s/m]	k_1 [N/m]	k_2 [N/m^2]	k_3 [N/m^3]	S_o [N-s/rad]
1	0.1	9	4	6	$1/(8\pi)$

The equivalent spring stiffness of the linearised system with white noise input has been estimated following both the direct and iterative approaches. Results are plotted in figure 6.9, where it can be seen that the total equivalent stiffness converges to the value obtained by solving simultaneously equations 6.19 and 6.20 (direct approach). Numerical values are presented in table 6.4.

Table 6.4 Equivalent spring stiffness computed from direct and iterative approaches.

Function	y_μ [m]	σ_v^2 [m^2]	$k_1 + k_{eq}$ [N/m]
Nonlinear	-0.03708	0.1082	–
Linear component only	0	0.1259	9
Direct linearisation	-0.03960	0.1066	10.6311
Iterative linearisation	-0.03979	0.1072	10.6406

It is worth noting that, even though the input has zero mean, the response has a negative mean. This negative offset is expected since the system has a quadratic nonlinearity, hence there is a set-down due to the asymmetry.

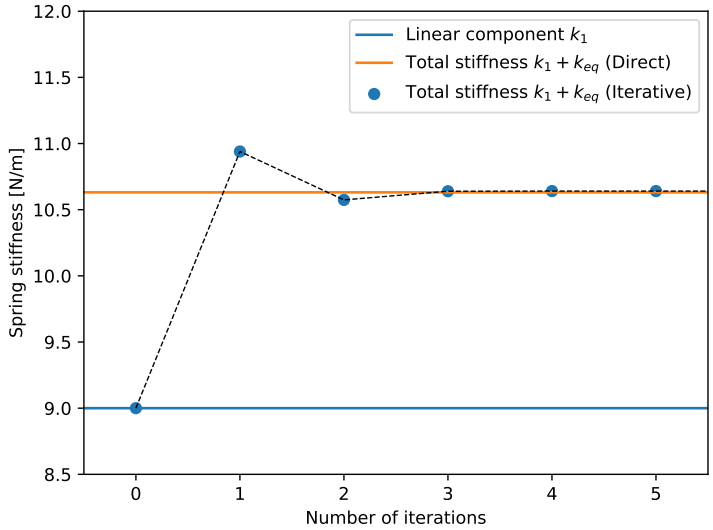

Fig. 6.9 Equivalent spring stiffness. Blue: linear component k_1 only; orange: direct estimation; blue dots: iterations.

In the frequency domain, the harmonics corresponding to the quadratic and cubic nonlinearities can be visualised in the power spectral density plot of the response of the nonlinear system. Figure 6.10 shows additionally the corresponding power spectral densities of the response of a linear system with stiffness k_1 only, and the equivalent linearised with stiffness $k_1 + k_{eq}$.

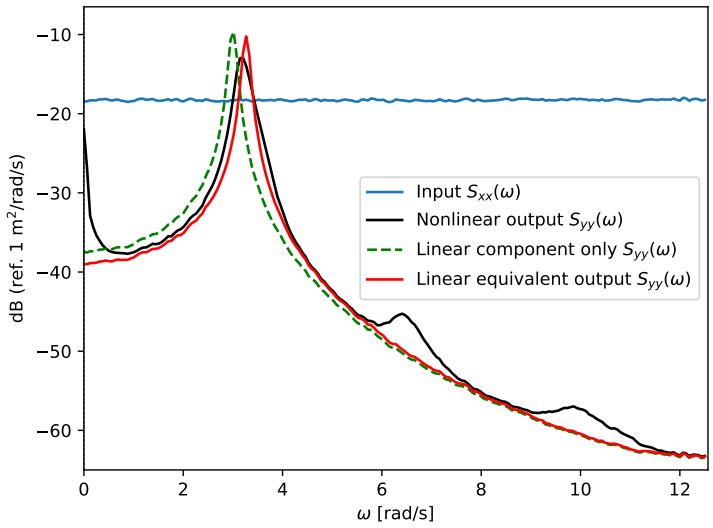

Fig. 6.10 Power spectral density of the response of system with weak second and third order nonlinearities. Blue: input; black: nonlinear system; dashed green: linear system with spring stiffness k_1 only; red: equivalent linear system with spring stiffness $k_1 + k_{eq}$.

As expected, the equivalent linearised system estimates, with relatively high accuracy, the dominant first harmonic of the system, as well as the mean squared response of the system, reducing the error if the nonlinear components are neglected. For the case study here presented, the relative error in the mean square response when neglecting the nonlinear terms is 16.35%, whereas the corresponding error when adopting the equivalent linear system is found to be 0.92%, significantly lower.

6.5 Equivalent Linearisation in the Hybrid FE-SEA

With the aim of modelling a nonlinear complex system to estimate the mean response of the statistical subsystems, structural and/or acoustic, the equivalent linearisation methodology can be implemented to the generalised hybrid FE-SEA equations, developed in chapter 5. The application of the equivalent linearisation in the hybrid FE-SEA approach focuses in linearising the deterministic matrix, $\mathbf{D}_{\mathrm{d}}$, by finding a equivalent linearised matrix of the deterministic subsystems that comprise the complex structure. The equations of the equivalent coefficients of the linearised equation for the symmetric and asymmetric nonlinearities, as well as the iterative approach, are adopted to determine the equivalent entries of such linearised deterministic matrix.

In this section, the application of the method is illustrated with the analysis of the case study described by a structural-acoustic system excited through a nonlinear interface, represented by the couple of magnets. The capability and validation are analysed by contrasting the estimations against dynamic data obtained from the experimental setup.

6.5.1 Application to the Structural-Acoustic System

A simplified model that isolates key features to be analysed in the structural-acoustic system that is being object of study can be described as a set two coupled subsystems, i.e. a statistic system comprised by a flat thin plate coupled to an acoustic cavity, connected to a deterministic nonlinear spring through which the excitation force is transmitted to the flat plate at a deterministic point. A schematic representation of the simplified system can be viewed in figure 6.11.

Two deterministic degrees of freedom are required in this simplified model:

- q_1: Axial displacement at the input.
- q_2: Axial displacement at the interface between the nonlinear spring and the flat thin plate.

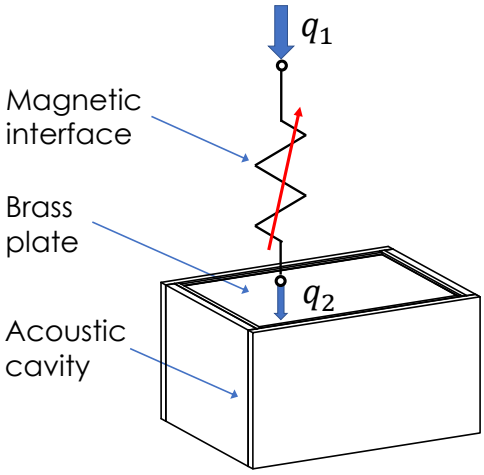

Fig. 6.11 Simplified deterministic-statistic structural-acoustic system.

As the input at q_1 is known and given as a prescribed displacement, the generalised hybrid FE-SEA approach can be employed to determine the mean response of the the flat thin plate, as well as the mean sound pressure levels inside the cavity, provided that the deterministic matrix has been linearised. The total matrix of the system given by the deterministic matrix of the nonlinear interface and the direct field matrix of the plate is given by

$$\mathbf{D}_{\text{tot}} = \begin{pmatrix} k_{eq} & -k_{eq} \\ -k_{eq} & k_{eq} \end{pmatrix} + \begin{pmatrix} 0 & 0 \\ 0 & D_{\text{dir}} \end{pmatrix}, \tag{6.21}$$

where the coefficients k_{eq} can be found from the equivalent linearisation approach. The interface between the plate and the acoustic cavity is assumed to be linear, and the coupling loss factors, as well as the acoustic response can be estimated by solving the SEA problem described in chapter 2, where the power input depends on the nature of the deterministic spring, characterised by the equivalent stiffness k_{eq}.

The equivalent linearisation of the spring force-displacement function can be performed from the nonlinear function of the relative displacement between the output q_2 and the input q_1, i.e. $F(r) = F(q_1 - q_2)$. With this notation, an equivalent linear function the total force, i.e. dynamic and static components, can be found from the equivalent linearisation approach described in the previous section. The main advantage of expressing the response in terms of relative displacement, r, is that the mean square response needed to estimate the equivalent spring stiffness can be found directly by integrating

$$\sigma_r^2 = \int_{-\infty}^{\infty} S_{rr}(\omega)\, \mathrm{d}\omega, \tag{6.22}$$

where the power spectral density of the relative displacement $S_{rr}(\omega)$ can be related to the power spectrum of the displacements $\mathrm{E}\left[\mathbf{q}_r\mathbf{q}_r^{\mathrm{H}}\right]$ calculated from the hybrid FE-SEA method. Expressing the displacements in vectorial form

$$\mathbf{q}_r = \mathbf{q}_1 - \mathbf{q}_2 \tag{6.23}$$

$$\mathbf{q}_r^{\mathrm{H}} = \mathbf{q}_1^{\mathrm{H}} - \mathbf{q}_2^{\mathrm{H}}, \tag{6.24}$$

the averaged power spectrum of the relative response can be then expressed as

$$\mathrm{E}\left[\mathbf{q}_r\mathbf{q}_r^{\mathrm{H}}\right] = \mathrm{E}\left[\mathbf{q}_1\mathbf{q}_1^{\mathrm{H}}\right] - \mathrm{E}\left[\mathbf{q}_1\mathbf{q}_2^{\mathrm{H}}\right] - \mathrm{E}\left[\mathbf{q}_2\mathbf{q}_1^{\mathrm{H}}\right] + \mathrm{E}\left[\mathbf{q}_2\mathbf{q}_2^{\mathrm{H}}\right], \tag{6.25}$$

where, considering the coordinate "$_1$" the prescribed displacement and "$_2$" the free/forced coordinate, the terms of the right-hand-side of equation 6.25 are computed from the set of equations 5.32 to 5.35 derived for the generalised FE-SEA approach in chapter 5, and for the case of prescribed forces only, these expressions take the form

$$\mathrm{E}\left[\mathbf{q}_1\mathbf{q}_1^{\mathrm{H}}\right] = \mathbf{S}_{\mathbf{q}_1\mathbf{q}_1} \tag{6.26}$$

$$\mathrm{E}\left[\mathbf{q}_1\mathbf{q}_2^{\mathrm{H}}\right] = -\mathbf{S}_{\mathbf{q}_1\mathbf{q}_1}\mathbf{D}_{21}^{\mathrm{H}}\mathbf{D}_{22}^{-\mathrm{H}} \tag{6.27}$$

$$\mathrm{E}\left[\mathbf{q}_2\mathbf{q}_1^{\mathrm{H}}\right] = \mathrm{E}\left[\mathbf{q}_1\mathbf{q}_2^{\mathrm{H}}\right]^{\mathrm{H}} \tag{6.28}$$

$$\mathrm{E}\left[\mathbf{q}_2\mathbf{q}_2^{\mathrm{H}}\right] = \mathbf{D}_{22}^{-1}\left(\mathbf{S}_{\mathrm{FF}} + \sum_j \frac{4E_j}{\pi\omega \mathrm{n}_j}\mathrm{Im}\left\{\mathbf{D}_{\mathrm{dir},\,22}^{(j)}\right\}\right)\mathbf{D}_{22}^{-\mathrm{H}}, \tag{6.29}$$

and the submatrices of the total dynamic matrix of the model, expressed by equation 6.21 are

$$\mathbf{D}_{11} = \left(k_{eq}\right),\ \mathbf{D}_{12} = \left(-k_{eq}\right),\ \mathbf{D}_{21} = \left(-k_{eq}\right) \text{ and } \mathbf{D}_{22} = \left(k_{eq} + D_{\mathrm{dir}}\right). \tag{6.30}$$

The energy E_j in equation 5.35 corresponds to the ensemble averaged energy of the plate estimated with the SEA equation matrix form of the SEA equation for two subsystems, i.e. the plate and the acoustic cavity, given by

$$P_o^{(j)} = \omega\eta_j E_j + \sum_k \omega\eta_{jk} n_j \left(\frac{E_j}{n_j} - \frac{E_k}{n_k}\right), \tag{6.31}$$

where the power input due to prescribed displacements, given by equation 5.40, for the spring and structural-acoustic system is reduced to

$$P_o^{(j)} = \frac{\omega}{2}\sum_{r,s}\mathrm{Im}\left\{D_{\mathrm{dir\ ff},\ rs}^{(j)}\right\}\left[\mathbf{D}_{\mathrm{ff}}^{-1}\mathbf{S}_{\mathrm{FF}}\mathbf{D}_{\mathrm{ff}}^{-\mathrm{H}}\right]_{r,s}, \tag{6.32}$$

and the total input $\mathbf{S}_{\mathrm{FF}}$ due to prescribed displacements, that appears in equations 6.29 and 6.33, is given by

$$\mathbf{S}_{\mathrm{FF}} = \mathbf{D}_{21}\mathbf{S}_{\mathbf{q}_1\mathbf{q}_1}\mathbf{D}_{21}^{\mathrm{H}} \tag{6.33}$$

Due to the dependency of the equivalent spring stiffness on the squared response σ_r^2, the approach is iterative:

- Assume a constant spring stiffness to determine an initial total matrix $\mathbf{D}_{\mathrm{tot}}$
- Estimate the external power input to the system P_o given by the external known displacements $S_{q_p q_p}$
- Solve the SEA matrix equation to estimate the averaged energy at each subsystem, i.e. the flat thin plate and the acoustic cavity.
- Recover the components of displacement $\mathbf{q}$
- Estimate the squared response of the relative displacements σ_r^2
- Compute the equivalent spring stiffness from using the σ_r^2 and the static external force, depending on the nature of the nonlinear equation.
- With the computed spring stiffness k_{eq} repeat the procedure until the value for k_{eq} has converged.
- Estimate the dynamic quantities of the response of the structural and acoustic subsystems.

It is worth noting that if the force input were known rather than the displacement, the nonlinear nature of a massless undamped transmission path would not have any influence in the response of the system with respect to the input, both structural and acoustic, since the force at the input coordinate q_1 is the same as the force as in q_2.

6.5.2 Equivalent Linearisation of the Magnets Law

The total force between two magnets, as described in chapter 3, has a nonlinear nature and depends on the separation between the magnets r. Applying the adjusted magnets law, the total force including the static and dynamic parts can be written in the form

$$F_T(r) = -A(r) + \frac{B}{(r+C)^2}, \tag{6.34}$$

where the parameters have been described in chapter 3. This force has a static component due to a preload applied to maintain the septation in equilibrium r_o in the no-motion state, as well as a dynamic component due to the relative motion between the magnets given by the difference between the input and output. As a convention, the dynamic relative displacement is given by $r_v = x(t) - y(t)$, where $x(t)$ is the input and $y(t)$ the output, and the total separation between the magnets in motion is given by $r = r_o - r_v$

The total force then can be expressed as a function of the positive relative dynamic displacement r_v, and subsequently expanded to a polynomial function about $r_v = 0$, in the form of the equation 6.5, i.e.

$$F_T(r) \approx k_0 + k_1 r_v + k_2 r_v^2 + \ldots + k_n r_v^n, \tag{6.35}$$

where the Taylor coefficients are found to be

$$k_0 = -A r_o + \frac{B}{(r_o + C)^2} \tag{6.36}$$

$$k_1 = A + \frac{2B}{(r_o + C)^3} \tag{6.37}$$

$$k_n = \frac{(n+1)B}{(r_o + C)^{(n+2)}}, \qquad \text{for } n \geq 2. \tag{6.38}$$

Alternatively, the magnets law given by equation 6.34 can be also expanded about the separation in equilibrium $r = r_o$, where the coefficients of equation 6.38 with odd subindexes are negative. A comparison between the magnets law and the approximation of the total force to a polynomial function up to third order are shown in figure 6.12, where the shadowed areas indicate the dynamic range at which the approximation is acceptable.

From figure 6.12, it can be noted that the total nonlinear force between two magnets can be approximated to a polynomial function with a good degree of accuracy in the range of relative displacements -2.5 mm $< r < 2.5$ mm. The expected dynamic range in the experimental rig is within such range, and therefore, the polynomial form of the total force up to the third order is used in this model, which can be linearised by adopting the equivalent linearisation approach for quadratic and cubic nonlinearities.

6.5.3 Experimental Data and Equivalent Linear FE-SEA Estimations

The FE-SEA model of the structural-acoustic system has been validated against experimental data that was presented in chapter 3, where a signal with high content of energy around 210 [Hz] was given as input to excite the corresponding harmonics in the response of the

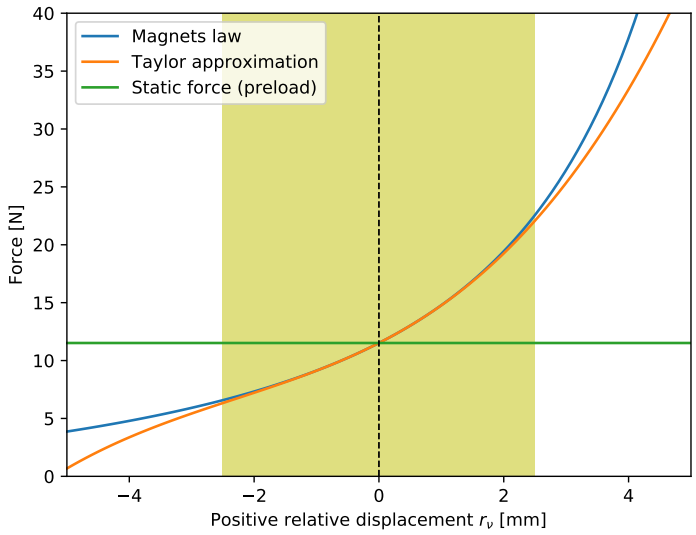

Fig. 6.12 Repulsive force between two magnets from the magnets law and the Taylor expansion up to the third order.

system. Additionally, the acoustic response has been also measured using a microphone placed inside the acoustic cavity. Two cases have been considered: low and higher amplitude inputs. The spectrum of the measured input has been used as the prescribed displacements for the FE-SEA model of the system. The experimental measurements and the FE-SEA estimations of the displacement response at q_2 and the acoustic data are plotted in figure 6.13 for the low input case, and in figure 6.14 for the higher input case

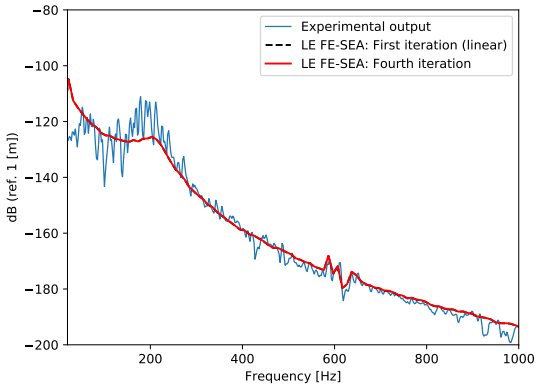

(a) Displacement response at q_2.

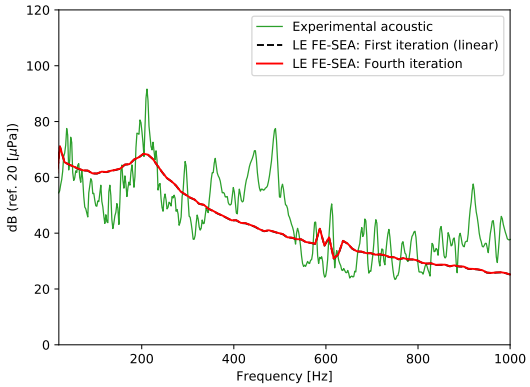

(b) Sound pressure levels.

Fig. 6.13 Power spectral density of the response of the system to a low input. Fluctuating: experimental measurements; dashed black: first iteration (linear); red: fourth iteration (converged). Results from the first and fourth iterations are practically overlapped.

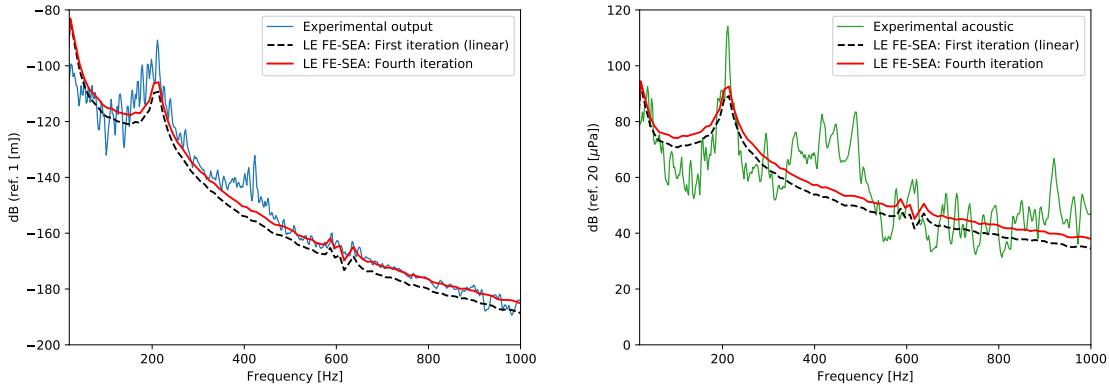

(a) Displacement response at q_2.

(b) Sound pressure levels.

Fig. 6.14 Power spectral density of the response of the system to a higher input. Fluctuating: experimental measurements; dashed black: first iteration (linear); red: fourth iteration (converged).

It was found that a value for the equivalent linearised spring stiffness k_{eq} converges after the fourth iteration. It can be seen that in figures 6.13 and 6.14 that the spectrum of the mean response, structural and acoustic, estimated with the equivalent linear FE-SEA model agrees with the experimental data for both cases of the input amplitude. For low input, the response is well estimated with the first iteration, as the equivalent spring stiffness is nearly the same as the linear component of the Taylor approximation of the magnets law, i.e. $k_{eq} \approx k_1$. On the other hand, for the higher amplitude case the equivalent spring stiffness is increased, and hence the estimated response after the fourth iteration is higher than the first iteration with the linear component only, improving the estimation of the experimental measurements. The mean square response, calculated as the area under the Power Spectral Density curve, which is found from the response spectrum and depends on the sampling rate of the signal for the experimental cases and the FE-SEA estimation are presented in table 6.5.

Table 6.5 Mean square response from experimental data and the FE-SEA estimation.

Input	k_1	k_{eq}	Structural σ^2			Acoustic σ^2		
			Experimental	FE-SEA	$\%\varepsilon$	Experimental	FE-SEA	$\%\varepsilon$
	[N/m]	[N/m]	10^{-10} [m^2]	10^{-10} [m^2]		[Pa^2]	[Pa^2]	
Low	2057	k_1+18	1.52	1.37	9.8	2.54	1.77	30.3
High		k_1+991	11.2	9.97	10.9	73.02	24.26	67.1

The mean response σ^2 across the frequency band of 20 to 1000 [Hz] is significantly higher at the high input case than for the the nearly linear case. The acoustic and structural mean

response estimated with the equivalent linear FE-SEA model is lower than the experimental in both low and input cases. This issue can be also observed in the spectrum plots of the structural response where the experimental response is significantly higher about 210 and 420 [Hz]. Regarding to the acoustic spectrum, as the acoustic cavity is deterministic at frequencies lower than 600 [Hz], the peaks at the natural frequencies will not become smoother when the system is randomised, and therefore, a lack of agreement is expected between the estimations and the experimental measurements

6.6 Discussion

The equivalent linearisation allows one to develop an equivalent linearised FE-SEA model of a complex system that estimates the mean squared response of each subsystem that comprise a complex structure. In general, a good agreement is found between the FE-SEA estimation and the experimental data measured at each individual subsystem of the structural-acoustic subsystem that has been the study case in this research.

The main advantage of the equivalent linearisation is that the mean squared response is readily estimated from simple models of each structure. However, the method has the limitation that the harmonics are not predicted due to nonlinearities. Nevertheless, the effect of the nonlinear transmission path is characterised in the change of the overall amplitude levels of the response. For the study case, as the positive relative displacement increases, i.e. $x(t) - y(t)$, the deterministic system becomes stiffer, and the response of the coupled subsystems are expected to have a higher amplitude than if the linear component of the transmission path is only considered. For low amplitude inputs, however, the nonlinearity has a negligible effect and the equivalent linearised spring stiffness is almost the same as the linear component with no noticeable effects in the response of the system.

The method is applicable for weak nonlinear deterministic systems, where the nonlinear function of force vs displacement can be expanded to a polynomial expression, and hence the equivalent linear stiffness can be found for n orders, usually quadratic and cubic orders. The analysis complicates when such nonlinear function cannot be expanded to a polynomial expression as the optimised equivalent spring stiffness is found from the average of the nonlinear function which in turn depends on the static and dynamic components of the response that need to be known in the time domain, which is beyond of the capability of the FE-SEA method.

Chapter 7

Conclusions and Further Work

7.1 Conclusions

The main aim of this research project has been to develop a framework to investigate and characterise the effect, or otherwise, that nonlinear behaviour in the transmission path affects the structural and acoustic response of a system, in a range of frequencies at which the response has statistical nature. The work is addresses to the analysis of interior noise in vehicles generated by the road-vehicle interaction, known as road noise, and key aspects on the structure-borne noise generation phenomenon in a system with uncertainties and the effect of stiffness nonlinearities of several components in the transmission path, mainly in the components of the suspension system, have been analysed by scaling the problem to a simplified structural-acoustic system, excited through a nonlinear device with known power spectral density of a known random input.

7.1.1 Physical Statistical Structural-Acoustic System

The phenomenon of sound radiation to an acoustic volume, such as a car cabin, from the induced vibrations of flexible structures like the thin panels that enclose such volume, has been isolated from the more broad problem of road-noise generation in a complete model of a car. This structural-acoustic system has been the base of study to contrast experimental data with numerical models with the developed theory for modelling in time and frequency domain. The design of this scaled model is based in the mode count of a full scale car cabin and a large thin flexural subsystem such as the roof panel, up to 500 [Hz]. Therefore, the range of frequency analysis of the scaled experimental setup is found to be increased up to about 1100 [Hz], within which both the structural and acoustic subsystems have a statistical rather than deterministic nature. As the structural-acoustic system and the radiation

phenomenon is linear, a Statistical Energy Analysis approach (SEA) has been adopted to model the system to estimate the mean response of the structural subsystem and the acoustic cavity with a known power input. The findings in the first part of this research, presented in chapter 2, are

(1) Besides of the capability of the Statistical Energy Analysis to estimate the mean response of a structural-acoustic system, the experimental data of the dynamic responses of each subsystem within the built-up system, i.e. a flexible panel coupled to an acoustic cavity, constitute a supporting evidence that the extended theory presented by Langley and Cotoni (2004) to estimate the variance response based on the statistics of the Gaussian Orthogonal Ensemble (GOE), is applicable to coupled structural-acoustic systems. This experimental validation is published in Andrade et al. (2019).

(2) For the case of a randomised structure coupled to a deterministic cavity, the variance of the acoustic response predicted by the GOE statistics is governed by the random power input, and therefore, the relative variance of the acoustic response is coincident with the relative variance of the response of the sound radiating structural system. On the other hand, the variance of the response of a random acoustic cavity coupled to a random flexible plate reaches a higher value, as expected, since the estimation of the variance with the GOE statistics considers also the random SEA matrix of the built-up system. These two cases were demonstrated with experimental data from the structural-acoustic rig, where the randomisation of the flat thin plate was done by placing small masses on the plate at random locations for each different realisation, whereas the acoustic cavity was randomised by changing the position of randomly distributed rigid baffles inside the volume.

7.1.2 SEA Nonlinear Analysis in the Time Domain

As it is not usually possible to find a solution to a nonlinear equation of motion, as is the case of systems with nonlinear stiffness, it is not directly possible to extend the SEA approach, to the nonlinear analysis in the frequency domain from the framework developed for the structural-acoustic system, and therefore numerical approaches can be adopted to solve the nonlinear equations of motion in the time domain when the time history of the input signal is known. However, even though the problem of road-noise in vehicles has been isolated to a simple structural-acoustic system, there are still a vast number of degrees of freedom in the system making it a prohibitively expensive procedure to find a numerical solution, in terms of computation cost. Hence the size of the problem has been further reduced by adopting the concepts of infinite plate and weakly structural-acoustic coupling presented on chapter 3, that

allowed to develop an equivalent nonlinear single degree-of-freedom system. In this sense, the the effect of the nonlinear transmission path is observed and analysed on the response of the structural system only, and the effect can be extrapolated to the acoustic response due to the linear nature of the structural-acoustic system. In this part of the research, the main findings are:

(3) The equivalent damper model of the flat thin plate, with the nonlinear stiffness characteristics of a couple of magnets in the experimental setup, results in an overdamped single-degree-of-freedom system, and therefore, no resonant modes were observed, neither from experimental data nor from numerical simulations of the model in the time domain, for nearly flat power spectral densities of the input in the frequency band of 20 to 2000 [Hz]. Hence, the reduction in coherence between the input and output signals, due to nonlinearities, was non visible at particular frequencies, but rather a constant reduction was observed the whole frequency band from numerical simulations. This constant reduction is increased as the amplitude of input signal increases.

(4) In order to excite harmonics in the response power spectral density, the input to the system has been tailored to have a higher amplitude about 210 [Hz]. Therefore, from numerical simulation, second and third harmonics in the response were observed at 420 and 630 [Hz], respectively, generated as the amplitude of the input signal is increased. The effect of the nonlinearity in the structural response was also observed in the coherence plots, where a reduction of coherence was observed at the corresponding frequencies of the second and third harmonics

(5) Experimental data have validated the findings from numerical simulations in the time domain of the equivalent damper model, for the cases where the input to the system has a nearly flat power spectral density, as well as when the input signal has a higher content of energy about 210 [Hz]. The experimental response power spectral density as well as coherence, are estimated with a high degree of accuracy by the damper model, except at frequencies below 250 [Hz]. This lack of agreement was demonstrated to be caused by external noise sources in the environment, particularly due to the loud low frequency noise produced by the shaker in the experimental setup, as the experimental coherence calculated with an external acoustic signal as an additional input, i.e. multiple coherence, is closer to the predictions by the equivalent damper model.

(6) The equivalent damper model is not only capable to characterise the effects that a nonlinear transmission path has in the dynamic response of the structural component

of the system, but also estimates the averaged response at a high degree of accuracy. As the experimental data was not taken from a randomised structure, as it was for the linear SEA analysis of the structural-acoustic system described in chapter 2, the measured structural response does not represent the ensemble averaged response, but rather the dynamic response of a single system. Nevertheless, the fluctuations of the experimental power spectral density plots are expected to smooth out to agree with the estimations of the model if the system were further randomised. However, the main drawback of this model is that it cannot be extended to analyse more complex structures where coupling effects cannot be neglected. In addition, the time history of the input signal is not always available, but rather its power spectral density might be known, and therefore the the investigation was further addressed to improve the framework to the analysis in the frequency domain.

7.1.3 Nonlinear Analysis in the Frequency Domain

The Wiener series, initially derived in the time domain, have been adopted to develop a set of functions in the frequency domain to estimate the degree of contribution of several orders of nonlinearities to the total power spectral density of the output, as described in chapter 4. The equivalent characteristic input-dependent functions of the system to a n^{th} order of nonlinearity are known as the corresponding Wiener kernels of n^{th} order, and the measurement of such kernels for any Gaussian zero-mean input signal has been also developed in the frequency domain. The applicability of the Wiener theory in the frequency domain was illustrated from numerical simulations of an equivalent damper model as developed in chapter 3 with an SEA approach, for a bilinear stiffness interface between the input and output, as well as from experimental data in the structural-acoustic rig.

One of the major outcomes of this research is the developed theory, and further numerical and experimental validation, that extends the capability of the hybrid FE-SEA approach to include prescribed displacements as input and nonlinear characteristics of the deterministic components of a complex vibro-acoustic system, as presented in chapters 5 and 6, respectively. The main findings regarding to the nonlinear analysis in the frequency domain are:

(7) As the major contribution to the nonlinearity in the transmission path of the present structural-acoustic system is of quadratic order, after measuring the first and second order Wiener kernels of the system from experimental data gathered in the time domain, the contributions of first and second order to the total power spectral density of the response of the system have been estimated with a high degree of accuracy. Additionally, the experimental coherence between the input and output was also

reconstructed, which was expected to be close to one except in the region below 250 [Hz], were such lack of coherence at lower frequencies from experimental data is demonstrated to be caused by external noise sources in the environment. It is found however, that the estimated contribution to the response due to the quadratic nonlinearity converges from above, meaning that, if the averages in the Wiener kernel have not converged to a reliable value, the reconstructed coherence might takes values larger that one at frequencies where the nonlinearity has an effect.

(8) The generalised set of FE-SEA equations to estimate the ensemble averaged displacement cross-spectral matrix of the system have been derived following the diffuse field reciprocity theory developed by Shorter and Langley (2005b). It was found that the equations are nonreversible in the sense that the estimated ensemble averaged displacements calculated with prescribed forces differ to those estimated with a set of prescribed displacements from the previous calculation, as the nature of the input is deterministic and the output is rather statistic. This issue was demonstrated with Monte Carlo simulations performed in a FE software, and the ensemble averaged displacements predicted by the generalised FE-SEA model agrees well with the results from simulations.

(9) The analysis of the effect of nonlinear stiffness characteristics of the transmission path in the response of a complex vibroacoustic system, performed with an equivalent linearised FE-SEA approach, indicates that as the amplitude of the input signal increases, the overall response of both, the structural and acoustic subsystems, increases at higher degree than as if they were estimated with the linear component only, improving the prediction of the mean squared response of the system. This improvement was better visualised in the response of the structural system than in the acoustic response, as for the range of frequencies up to 600 [Hz], the deterministic nature of the acoustic cavity is dominant. A drawback of the FE-SEA analysis with the equivalent linearisation of the nonlinear deterministic dynamic matrix, however, is that the approach is limited to estimate the squared mean response of each subsystem, but it gives no information about harmonics in the response or losses of coherence due to the nonlinear transmission path. Nevertheless, the method gives valuable information about the dimension of the problem for the design of either a passive or active noise control system.

7.2 Suggestions for Further Work

In active noise control applications, it is known that the maximum theoretical levels of noise reduction that can be achieved with a linear scheme are given by the coherence limit as $10\log_{10}\left(1-\gamma_{XY}^2\right)$, therefore the higher the coherence, i.e. the more linear the system is, the more noise levels could be possible reduced. As for the case of nonlinear systems, the Wiener theory in the frequency domain could be in principle applied to reconstruct coherence between the input and output signals in a nonlinear system if the n^{th} Wiener kernels are known. Unfortunately at this stage, the computation of the second order Wiener kernel from data in the time domain, either from experimental measurements or from simulations, is unpractical as a vast number of individual frames of the signal in the frequency domain, i.e. the Fourier transform of the signals, are needed for the average $\mathrm{E}[Y(\omega)X^*(\omega_1)X^*(\omega_2)]$, found in the second order Wiener kernel equation, to converge to a reliable value that can be used in the estimation of the contribution of the power spectral density of second order to the total response of the system, and therefore reconstruct the coherence. Further research needs to be done to improve the measurement of the Wiener kernels of second order, or higher orders if needed, from a significantly lower number of individual frames in order to make the theory applicable to active noise control applications. An initial step has been done in this matter by considering the concept of multiple coherence, where the computation of first and second order Wiener kernels is performed analogously to the estimation of the transfer functions of a linear system with two uncorrelated inputs, and early stage results, not presented in this thesis, have proved that this approach significantly improves the computation performance of the kernels and the corresponding reconstructed coherence.

The equivalent linearisation applied to nonlinear modelling with the generalised hybrid FE-SEA method has been employed to the analysis of a scaled relatively simple system, i.e. the structural-acoustic system with a nonlinear interface, however the method can be applied to more complex structures where the inputs are given by known displacements rather than forces. In fact, for applications in real systems, it is more practical to estimate the input to the structure from measurements taken in the time domain with accelerometers, and then processing the data to recover the displacement power spectral density. Applications include, for example, the analysis of structural vibrations in buildings due to earthquake excitations, where the history of ground displacements can be known rather than forces applied to the structures.

References

Andrade, L., Langley, R. S., Butlin, T., de Brett, M., and Nielsen, O. M. (2019). Experimental validation of variance estimation in the statistical energy analysis of a structural-acoustic system. *Proceedings of the Institution of Mechanical Engineers, Part C: Journal of Mechanical Engineering Science*, 0(0):1–12.

Atalla, N. and Sgard, F. (2015). *Finite element and boundary methods in structural acoustics and vibration*. CRC Press.

Bernhard, R. (1996). The limits of the predictability due to manufacturing and environmentally induced uncertainty. In *Proceedings of InterNOISE*. INCE-USA.

Blevins, R. (2006). Modal density of rectangular volumes, areas, and lines. *The Journal of the Acoustical Society of America*, 119(2):788–791.

Bocquillet, A., Ichchou, M., Moron, P., and Jezequel, L. (1999). On the validity domain of some high frequency energy models. In *IUTAM symposium on Statistical Energy Analysis*, pages 25–36. Springer.

Caughey, T. K. (1963). Equivalent linearization techniques. *The Journal of the Acoustical Society of America*, 35(11):1706–1711.

Chatfield, C. (1996). *The Analysis of Time Series: An Introductionl*. Chapman & Hall/CRC.

Chen, S., Wang, D., and Zan, J. (2011). Interior noise prediction of the automobile based on hybrid fe-sea method. *Mathematical Problems in Engineering*, 2011.

Cicirello, A., Langley, R., Kovalevsky, L., and Woodhouse, J. (2012). The hybrid finite element / statistical energy analysis method. In Desmet, W., Okuyners, B., and Atak, O., editors, *CAE methodologies for mid-frequency analysis in vibration and acoustics*, chapter 7. Katholieke Universiteit Leuven.

Cotoni, V., Langley, R., and Kidner, M. (2005). Numerical and experimental validation of variance prediction in the statistical energy analysis of built-up systems. *Journal of Sound and Vibration*, 288(3):701–728.

Cotoni, V., Shorter, P., and Langley, R. (2007). Numerical and experimental validation of a hybrid finite element-statistical energy analysis method. *The Journal of the Acoustical Society of America*, 122(1):259–270.

Crandall, S. H. and Mark, W. D. (2014). *Random vibration in mechanical systems*. Academic Press.

Cremer, L. and Heckl, M. (2005). *Structure-Borne Sound: Structural Vibrations and Sound Radiation at Audio Frequencies*. Springer Science & Business Media.

Demetriou, D. (2018). *An investigation on Nonlinear Random Vibrations based on Wiener series theory*. PhD thesis, University of Cambridge.

Demir, O., Keskin, I., and Cetin, S. (2012). Modeling and control of a nonlinear half-vehicle suspension system: a hybrid fuzzy logic approach. *Nonlinear Dynamics*, 67(3):2139–2151.

Fahy, F. J. (1994). Statistical energy analysis: a critical overview. *Philosophical Transactions of the Royal Society of London A: Mathematical, Physical and Engineering Sciences*, 346(1681):431–447.

Fahy, F. J. and Gardonio, P. (2007). *Sound and structural vibration: radiation, transmission and response*. Academic press.

Fischer, M. (2006). Statistical energy analysis. Seminar: Vibrations and Structure-Borne Sound. TU München.

Fraser, G. (1998). *Structure Borne Sound in Motor-Vehicles Using Statistical Energy Analysis*. PhD thesis, Heriot-Watt University.

Gardiner, C. (1985). *Handbook of stochastic methods*, volume 3. springer Berlin.

Genuit, K. (2004). The sound quality of vehicle interior noise: a challenge for the nvh-engineers. *International journal of vehicle noise and vibration*, 1(1-2):158–168.

Graff, K. F. (2012). *Wave motion in elastic solids*. Courier Corporation.

Hambric, S. A. (2016). Structural vibrations. In Hambric, S. A., Sung, S. H., and Nefske, D. J., editors, *Engineering Vibroacoustic Analysis: Methods and Applications*, chapter 2, pages 10–51. John Wiley & Sons.

Hambric, S. A., Sung, S. H., and Nefske, D. J. (2016). *Engineering Vibroacoustic Analysis: Methods and Applications*. John Wiley & Sons.

Hansen, C., Snyder, S., Qiu, X., Brooks, L., and Moreau, D. (2012). *Active control of noise and vibration*. CRC Press.

Hawes, D. (2016). *Nonlinear Stochastic Vibration Analysis for Energy Harvesting and Other Applications*. PhD thesis, University of Cambridge.

Jacobsen, F. (2011). The sound field in a reverberation room. Technical report, Technical University of Denmark, Lyngby, Denmark.

Jacobsen, F. and Rodríguez Molares, A. (2010). The ensemble variance of pure-tone measurements in reverberation rooms. *The Journal of the Acoustical Society of America*, 127(1):233–237.

Kovacic, I. and Brennan, M. J. (2011). *The Duffing equation: nonlinear oscillators and their behaviour*. John Wiley & Sons.

Krylov, N. M. and Bogoliubov, N. N. (1949). *Introduction to non-linear mechanics*. Princeton University Press.

Langley, R. (1989). A general derivation of the statistical energy analysis equations for coupled dynamic systems. *Journal of Sound and Vibration*, 135(3):499–508.

Langley, R. (1990). A derivation of the coupling loss factors used in statistical energy analysis. *Journal of Sound and Vibration*, 141(2):207–219.

Langley, R. (1994). The modal density and mode count of thin cylinders and curved panels. *Journal of Sound and Vibration*, 169(1):43–53.

Langley, R. (2007). On the diffuse field reciprocity relationship and vibrational energy variance in a random subsystem at high frequencies. *The Journal of the Acoustical Society of America*, 121(2):913–921.

Langley, R. (2010). The analysis of random built-up engineering systems. In Wright, M. and Weaver, R., editors, *New directions in linear acoustics and vibration: quantum chaos, random matrix theory and complexity*, chapter 14, pages 231–250. Cambridge University Press.

Langley, R. and Bremner, P. (1999). A hybrid method for the vibration analysis of complex structural-acoustic systems. *The Journal of the Acoustical Society of America*, 105(3):1657–1671.

Langley, R. and Brown, A. (2004a). The ensemble statistics of the band-averaged energy of a random system. *Journal of Sound and Vibration*, 275(3):847–857.

Langley, R. and Brown, A. (2004b). The ensemble statistics of the energy of a random system subjected to harmonic excitation. *Journal of Sound and Vibration*, 275(3):823–846.

Langley, R. and Heron, K. (1990). Elastic wave transmission through plate/beam junctions. *Journal of Sound and Vibration*, 143(2):241–253.

Langley, R. and Shorter, P. (2003). The wave transmission coefficients and coupling loss factors of point connected structures. *The Journal of the Acoustical Society of America*, 113(4):1947–1964.

Langley, R. S. and Cotoni, V. (2004). Response variance prediction in the statistical energy analysis of built-up systems. *The Journal of the Acoustical Society of America*, 115(2):706–718.

Lee, Y. and Schetzen, M. (1965). Measurement of the wiener kernels of a non-linear system by cross-correlation. *International Journal of Control*, 2(3):237–254.

Leppington, F., Broadbent, E. G., and Heron, K. (1984). Acoustic radiation from rectangular panels with constrained edges. *Proceedings of the Royal Society of London. A. Mathematical and Physical Sciences*, 393(1804):67–84.

Leppington, F. G., Broadbent, E. G., and Heron, K. (1982). The acoustic radiation efficiency of rectangular panels. *Proceedings of the Royal Society of London. A. Mathematical and Physical Sciences*, 382(1783):245–271.

Liu, G.-R. and Quek, S. S. (2013). *The finite element method: a practical course*. Butterworth-Heinemann.

Lyon, R. and DeJong, R. (1995). *Theory and application of statistical energy analysis*. Butterworth - Heinemann.

Manohar, C. and Keane, A. (1994). Statistics of energy flows in spring-coupled one-dimensional subsystems. *Philosophical Transactions of the Royal Society of London A: Mathematical, Physical and Engineering Sciences*, 346(1681):525–542.

McGee, C. G., Haroon, M., Adams, D. E., and Luk, Y. W. (2005). A frequency domain technique for characterizing nonlinearities in a tire-vehicle suspension system. *Journal of vibration and acoustics*, 127(1):61–76.

Mehta, M. L. (2004). *Random matrices*. Elsevier.

Meirovitch, L. (1975). *Elements of vibration analysis*. McGraw-Hill.

Möser, M. (2009). *Engineering acoustics: an introduction to noise control*. Springer Science & Business Media.

Musser, C., Manning, J., and Peng, G. C. (2011). Prediction of vehicle interior sound pressure distribution with sea. Technical report, SAE Technical Paper.

Nelson, P. A. and Elliott, S. J. (1991). *Active control of sound*. Academic press.

Newland, D. (2005). *An Introduction to Random Vibrations, Spectral & Wavelet Analysis*. Dover Publications Inc.

Norton, M. P. and Karczub, D. G. (2003). *Fundamentals of Noise and Vibration Analysis for Engineers*. Cambridge University press.

Potter, R. (1977). Matrix formulation of multiple and partial coherence. *The Journal of the Acoustical Society of America*, 61(3):776–781.

Schetzen, M. (2006). *The Volterra & Wiener Theories of Nonlinear Systems*. Krieger Publishing.

Schroeder, M. R. (1962). Frequency-correlation functions of frequency responses in rooms. *The Journal of the Acoustical Society of America*, 34(12):1819–1823.

Shorter, P. and Cotoni, V. (2016). Statistical energy analysis. In Hambric, S. A., Sung, S. H., and Nefske, D. J., editors, *Engineering Vibroacoustic Analysis: Methods and Applications*, chapter 11, pages 339–383. John Wiley & Sons.

Shorter, P. J. and Langley, R. (2005a). Vibro-acoustic analysis of complex systems. *Journal of Sound and Vibration*, 288(3):669–699.

Shorter, P. J. and Langley, R. S. (2005b). On the reciprocity relationship between direct field radiation and diffuse reverberant loading. *The Journal of the Acoustical Society of America*, 117(1):85–95.

Smith, W. F. (2010). *Waves and Oscillations*. Oxford University Press USA.

Soong, T. T. (2004). *Fundamentals of probability and statistics for engineers*. John Wiley & Sons.

Steel, J., Fraser, G., and Sendall, P. (2000). A study of exhaust noise in a motor vehicle using statistical energy analysis. *Proceedings of the Institution of Mechanical Engineers, Part D: Journal of Automobile Engineering*, 214(1):75–83.

Totaro, N., Dodard, C., and Guyader, J.-L. (2009). Sea coupling loss factors of complex vibro-acoustic systems. *Journal of Vibration and Acoustics*, 131(4):041009.

Ver, I. L. and Beranek, L. L. (2006). *Noise and vibration control engineering: principles and applications*. Wiley.

Vokoun, D., Beleggia, M., Heller, L., and Šittner, P. (2009). Magnetostatic interactions and forces between cylindrical permanent magnets. *Journal of magnetism and Magnetic Materials*, 321(22):3758–3763.

Volterra, V. (1887). *Sopra le funzioni che dipendono da altre funzioni*. Tip. della R. Accademia dei Lincei.

Wiener, N. (1958). *Nonlinear problems in random theory*. The Massachusetts Institute of Technology Press.

Woodhouse, J. (1981). An introduction to statistical energy analysis of structural vibration. *Applied Acoustics*, 14(6):455–469.

Yung, V. Y. and Cole, D. J. (2006). Modelling high frequency force behaviour of hydraulic automotive dampers. *Vehicle System Dynamics*, 44(1):1–31.

Zienkiewicz, O. C., Taylor, R. L., Taylor, R. L., and Taylor, R. L. (2000). *The finite element method: solid mechanics*, volume 2. Butterworth-heinemann.

Appendix A

Python Script for Monte Carlo Simulations in an ABAQUS

An FE model can be developed in any FE-related software, where the geometry, material properties, boundary conditions etc., are defined prior running a simulation, and results can be extracted and stored after the computation is complete. To gather data from a randomised structure, the model has to be modified manually for each realisation. As a large ensemble is usually required to calculate the mean response from gathered data, this procedure is time consuming and an automatised method must be adopted.

A script in python has been implemented to automatically randomise the structure, perform the computation and store data for each realisation, from a model constructed in the commercial FE software ABAQUS. Simulations with an Steady State Direct method are performed to the system described in chapter 5. After constructing a model of such system in ABAQUS, the CAE model is converted to a python script, and loaded before running the implemented script here presented:

```
# -*- coding: mbcs -*-
#
# Abaqus/CAE Release 6.14-1 replay file
# Internal Version: 2014_06_04-23.11.02 134264
# Created by lga23

# IMPORT LIBRARIES

from abaqus          import *
from abaqusConstants import *
from caeModules      import *
from driverUtils     import executeOnCaeStartup
from numpy           import *
```

```
14 from random          import randrange, sample
15 import pandas
16 executeOnCaeStartup()
17
18 # OPEN ABQUS MODEL
19
20 execfile('C:/Temp/Model_CoupledPlates.py', __main__.__dict__)
21
22 # LOADING CONDITION: CONCENTRATED FORCE
23
24 a = mdb.models['Model-1'].rootAssembly
25 region = a.instances['Part-1-1'].sets['Set-InForce']
26 mdb.models['Model-1'].ConcentratedForce(name='Load-1', createStepName
       ='Step-1', region=region, cf3=1+0j, distributionType=UNIFORM,
       field='', localCsys=None)
27
28 # DEFINE FUNCTION FOR THE COMPUTATION OF EACH RANDOM REALISATION
29
30 def AutomatisedComputation(obdFileName,resultsFile):
31
32   nTEST = 200
33   for i in arange(nTEST): # 200 individual realisations
34
35     # Random distribution of ten masses on plate 1 (0.3402 [kg] each)
36
37     p = mdb.models['Model-1'].parts['Part-1']
38     n = p.nodes
39
40     listnodes = []
41     for j in sample(range(len(n)), 10):
42       listnodes.append(n[j])
43
44     nodes = mesh.MeshNodeArray(listnodes)
45     p.Set(nodes=nodes, name='Set-SelectedNodes1')
46     #: The set 'Set-SelectedNodes1' has been created (10 nodes).
47     p = mdb.models['Model-1'].parts['Part-1']
48     region=p.sets['Set-SelectedNodes1']
49     mdb.models['Model-1'].parts['Part-1'].engineeringFeatures.
       PointMassInertia(name='Inertia-plate1', region=region, mass
       =0.3402, alpha=0.0, composite=0.0)
50
51     # Random distribution of ten masses on plate 2 (0.7938 [kg] each)
52
53     p = mdb.models['Model-1'].parts['Part-2']
```

```
54      n = p.nodes
55
56      listnodes = []
57      for k in sample(range(len(n)), 10):
58        listnodes.append(n[k])
59
60      nodes = mesh.MeshNodeArray(listnodes)
61      p.Set(nodes=nodes, name='Set-SelectedNodes2')
62      #: The set 'Set-SelectedNodes2' has been created (10 nodes).
63      p = mdb.models['Model-1'].parts['Part-2']
64      region=p.sets['Set-SelectedNodes2']
65      mdb.models['Model-1'].parts['Part-2'].engineeringFeatures.
    PointMassInertia(name='Inertia-plate1', region=region, mass
    =0.7938, alpha=0.0, composite=0.0)
66
67      # Submit model for the computation of the i(th) realisation
68
69      mdb.Job(name=obdFileName, model='Model-1', description='', type=
    ANALYSIS, atTime=None, waitMinutes=0, waitHours=0, queue=None,
    memory=90, memoryUnits=PERCENTAGE, getMemoryFromAnalysis=True,
    explicitPrecision=SINGLE, nodalOutputPrecision=SINGLE, echoPrint=
    OFF, modelPrint=OFF, contactPrint=OFF, historyPrint=OFF,
    userSubroutine='', scratch='', resultsFormat=ODB,
    multiprocessingMode=DEFAULT, numCpus=1, numGPUs=0)
70      mdb.jobs[obdFileName].submit(consistencyChecking=OFF)
71
72      mdb.jobs[obdFileName].waitForCompletion()
73
74      # Visualise results and extract displacements at the set of nodes
75
76      o3 = session.openOdb(name='C:/Temp/'+obdFileName+'.odb')
77      session.viewports['Viewport: 1'].setValues(displayedObject=o3)
78      session.viewports['Viewport: 1'].odbDisplay.basicOptions.
    setValues(numericForm=COMPLEX_MAGNITUDE)
79
80      odb = session.odbs['C:/Temp/'+obdFileName+'.odb']
81      xyList = xyPlot.xyDataListFromField(odb=odb, outputPosition=NODAL
    , variable=(('U', NODAL, ((COMPONENT, 'U3'), )), ), numericForm=
    COMPLEX_MAGNITUDE, nodeSets=('PART-1-1.SET-CONNECTION1', 'PART
    -1-1.SET-INFORCE', 'PART-1-1.SET-RESPONSE1', 'PART-2-1.SET-
    CONECTION2', 'PART-2-1.SET-RESPONSE2', ))
82      xyp = session.xyPlots['XYPlot-'+str(i)]
83      chartName = xyp.charts.keys()[0]
84      chart = xyp.charts[chartName]
```

```
85      x0 = chart.curves['U:U3 Magnitude: PART-1-1 N: 1']
86      x1 = chart.curves['U:U3 Magnitude: PART-1-1 N: 18']
87      x2 = chart.curves['U:U3 Magnitude: PART-1-1 N: 24']
88      x3 = chart.curves['U:U3 Magnitude: PART-2-1 N: 6']
89      x4 = chart.curves['U:U3 Magnitude: PART-2-1 N: 10']
90
91      # Save data and close session for the next computation
92      session.writeXYReport(fileName=resultsFile+str(i)+'.rpt', xyData
        =(x0, x1, x2, x3, x4))
93      del session.xyDataObjects['U:U3 Magnitude: PART-1-1 N: 1']
94      del session.xyDataObjects['U:U3 Magnitude: PART-1-1 N: 18']
95      del session.xyDataObjects['U:U3 Magnitude: PART-1-1 N: 24']
96      del session.xyDataObjects['U:U3 Magnitude: PART-2-1 N: 6']
97      del session.xyDataObjects['U:U3 Magnitude: PART-2-1 N: 10']
98      session.odbs['C:/Temp/'+obdFileName+'.odb'].close()
99
100   print(str(nTEST),' REALISATIONS HAVE BEEN COMPUTED!')
101
102 # PERFORM COMPUTATION FOR THE PRESCRIBED FORCE
103
104 AutomatisedComputation('Job-Prescribed_f0','results_f0_')
105
106 # COMPUTE MEAN RESPONSE q0 FROM RESULTS
107
108 frequencyABQ = linspace(0.1,1500,300)
109 InForce      = zeros((300,nTEST))
110
111 for i in arange(nTEST):
112     df = pandas.read_fwf('results_f0_'+str(i)+'.rpt',skiprows
        =[0,1,2,3],nrows=300).values[:,1:]
113
114     InForce[:,i]= df[:,2]  # N: 24 (desplacement q0)
115
116 mInForce      = mean(InForce,axis=1)    # mean desplacement q0
117
118 # APPLY PRESCRIBED DISPLACEMENT
119
120   # Express data of q0 vs. frequency in a 'tuple' form
121
122 tabular_input = []
123 for j in arange(nTEST):
124   tabular_input.append((frequencyABQ[j],mInForce[j]))
125
126   # Delete the previously prescribed force in the model
```

```
127
128 del mdb.models['Model-1'].loads['Load-1']
129
130   # Define the prescribed displacement as an input
131
132 mdb.models['Model-1'].TabularAmplitude(name='mean_q0', timeSpan=STEP,
      smooth=SOLVER_DEFAULT, data=tabular_input)
133 a = mdb.models['Model-1'].rootAssembly
134 region = a.instances['Part-1-1'].sets['Set-InForce']
135 mdb.models['Model-1'].DisplacementBC(name='BC-1', createStepName='
    Step-1', region=region, u1=UNSET, u2=UNSET, u3=1+0j, ur1=UNSET,
    ur2=UNSET, ur3=UNSET, amplitude='mean_q0', fixed=OFF,
    distributionType=UNIFORM, fieldName='', localCsys=None)
136
137 # PERFORM COMPUTATION FOR THE PRESCRIBED DISPLACEMENT
138
139 AutomatisedComputation('Job-Prescribed_q0','results_q0_')
140
141 # -*- end -*-
```

The complex magnitude of displacements at q_1, q_2, q_3, q_4, for the cases where the force and displacement at q_0 are prescribed, can be extracted and processed from the '.rpt' stored files. The python code to process these files is given by lines 108 to 116 in this script.